COMPUTATIONAL STUDIES ON THE EFFECT OF COMPOSITION AND INTERACTIONS ON STRUCTURE, DYNAMICS AND GAS ADSORPTION PROPERTIES OF POLYMERIC MATERIALS

Thesis Submitted to AcSIR for the Award

of the Degree of

Doctor of Philosophy

in Chemical Sciences

By

Pragati Sharma

Registration Number: 10CC13A26029

Under the guidance of

Dr. Rajnish Kumar & Dr. Suman Chakrabarty

Physical & Material Chemistry Division

CSIR-National Chemical Laboratory, Pune, India- 411008

Declaration

I hereby declare that the thesis entitled "**Computational studies on the effect of composition and interactions on structure, dynamics and gas adsorption properties of polymeric materials**" submitted for the degree of Doctor of Philosophy in Chemical Sciences to the Academy of Scientific & Innovative Research (AcSIR), has been carried out by me at the Physical and Material Chemistry Division of CSIR-National Chemical Laboratory, Pune, India-411008, under the supervision of Dr. Rajnish Kumar and Dr. Suman Chakrabarty. Research material obtained from other sources has been duly acknowledged in the thesis. The work is original and has not been submitted in part or full by me for any other degree or diploma to any other Institution or University.

Date**:**

Place:

_____

Pragati Sharma
Senior Research Fellow,
Physical and Material Chemistry Division,
CSIR-National Chemical Laboratory,
Dr. Homi Bhabha Road, Pune-411 008, Maharashtra, India
& Academy of Scientific & Innovative Research (AcSIR)-CSIR, India

Certificate

This is to certify that the work incorporated in this Ph.D. thesis entitled "**Computational studies on the effect of composition and interactions on structure, dynamics and gas adsorption properties of polymeric materials"** submitted by **Ms. Pragati Sharma** to Academy of Scientific and Innovative Research (AcSIR) in fulfillment of the requirements for the award of the **Degree of Philosophy in Chemical Sciences,** embodies original research work under our supervision. We further certify that this work has not been submitted to any other University or Institution in part or full for the award of any degree or diploma. Research material obtained from other sources has been duly acknowledged in the thesis. Any text, illustration, table etc., used in the thesis from other sources, have been duly cited and acknowledged.

(Student)	(Supervisor)	(Co-supervisor)
Ms. Pragati Sharma	Dr. Rajnish Kumar	Dr. Suman Chakrabarty
Ph.D. Student	Senior Scientist	Ramanujan Fellow
PMC Division	CEPD Division	PMC Division
CSIR -NCL, Pune	CSIR-NCL, Pune	CSIR-NCL, Pune

Dedicated to my parents ...

Acknowledgement

The research work presented in this thesis was kept on track and seen through completion with the motivation and inspiration of numerous people. It gives me immense pleasure to express my warm appreciation and heartfelt gratitude towards all those people who helped and supported me during my Ph.D.

I extend my deepest gratitude to my advisors: Dr. Rajnish Kumar and Dr. Suman Chakrabarty and also to Dr. Sudip Roy for their excellent supervision, guidance and encouragement through my research career. I am thankful to Dr. Sudip Roy for introducing me to the exciting field of computational chemistry and Dr. Suman Chakrabarty for providing me novel ideas, valuable suggestions for the projects and insightful discussions. I would like to thank them for providing me opportunities to interact and collaborate with experimentalists and distinguished scientists of the field which enriched my knowledge and research account in a great way.

I wish I would have had more time to work with Dr. Suman Chakrabarty. His dynamic personality, dedicated working style and scientific outlook has always amazed and inspired me.

I thank my collaborators across the globe: Dr. Ashish Lele, Dr. Prakash Wadgaonkar, Dr. Swaminathan Shivaram and Dr. C.V Avadhani for giving me opportunities to work on various projects with them. A special mention to Dr. Ali Karimi, Continental tires, Germany for the various scientific discussions and innovative ideas that have contributed to this thesis a lot.

I would like to acknowledge the members of my doctoral advisory committee (DAC), Dr. Arun Venkatnathan, Dr. Kumar Vanka, and Dr. Anu Raghunathan for their fair evaluation and constructive comments and suggestions. Heartfelt thanks to AcSIR and SAC officials for their prompt help in official documentations.

My present and past research group members have always provided a stimulating and fun environment to learn and work. I thank Vrushali Hande, Bappa Ghosh, Nilesh Choudhury, Amit Kumawat, Neharika Chamachi, Swagata Pahari, Chandan Choudhury, Souvik Chakraborty, Subhadip Das, Santu Biswas, Sheelan Sengupta, Prithvi Raj Pandey, Sujit Sarkar, and Anil Mahshal, for being a friendly and cheerful group of colleagues.

A special thanks to Vrushali Hande and Bappa Ghosh for many scientific and non-scientific discussions and for being excellent friends throughout this journey. I would also thank my roommates: Swechchha, Nidhi and Smriti for helping me initially in adjusting to Pune. Thanks for many unforgettable memories and making my stay memorable which I will cherish forever.

I am grateful to Dr. Sourav Pal and Dr. Ashwini Kumar Nangia, Directors, CSIR-NCL, Pune for allowing me to carry out my research work in India's most esteemed, well-equipped and biggest chemical laboratory. I acknowledge Council of Scientific and Industrial Research (CSIR) for providing me funding for the research.

Last but not the least a special thanks to my parents, Arvind Kumar Sharma and Madhu Sharma, my brother Sudhir and sister Kumud for their constant support and encouragement throughout the years. Many a times, it was only because of your unconditional belief and confidence that helped me to overcome hard times and accomplish my dreams. Thanks Papa for the hour long consultations that helped and boosted my confidence many a times and Mom for being patient and supportive. Words can't express the gratitude I feel for both of you and so I dedicate this thesis to you.

Abstract

Properties of functional polymeric materials can be tuned by either varying the composition of a multi-component system, or by chemical modification of the constituents. Thus it is extremely crucial to develop a molecular level understanding of these interactions and the role of composition that manifests into desired functional properties. The present thesis involves computer simulation studies of various polymeric systems investigating the effect of composition and interactions on the polymer properties at a molecular level. The thesis has been classified into three major parts based on the selected polymer or property of interest as follows. In Part A and B, interactions in polymeric systems are modified by changing the compositions, by incorporating additives in part A and altering chemical structure of polymer in part B. Part C investigates the gas adsorption characteristics of a polymeric system and the role of structural and dynamical heterogeneity therein.

In **Chapter 1**, the thesis introduces the systems under consideration and presents a brief review of the literature. Subsequently, a description of applied computational methods and concepts is given in **Chapter 2**. These chapters are common to all parts A, B and C. Separate introductions and computational details relevant to each part are further discussed in individual parts.

Part A

It includes chapter 3, 4 and 5. The systems under study in part A are rubber and rubber-plasticizer mixtures, focusing majorly on deciphering the molecular mechanisms related to glass transition and its impact on structural and dynamic properties of rubbers.

Chapter 3: A brief overview of properties of rubber, rubber composites and rubber blends is presented. Emphasizing the fact that a systematically validated force-field and proper equilibration are the major pre-requisites for any polymer simulation. In the first working chapter of this thesis, we have validated quantum-chemically derived force-fields of rubber by calculating glass transition temperature (T_g), density and local chain characteristics like end-to-end distance and radius of gyration (R_g). All calculated properties have been compared to corresponding experimental results and force fields are also tuned in cases where calculated properties do not match with experiments. A potential energy based

equilibration protocol has been proposed and tested for rubbers under study: cis and trans-Polybutadiene and Polyisoprene.

Chapter 4: Additives are incorporated in rubber-matrix to enhance the mechanical and physico-chemical properties of rubbers for their optimum use in tire and other rubber industries. Plasticizers are the additives which increases the flexibility and processibility of rubbers. This chapter is focused on deducing the molecular mechanisms of plasticizer action in rubbers. Effect of plasticizers on structural and dynamic properties of rubber has been analyzed. Various polymer properties like free volume, end-to-end distance, R_g, autocorrelation functions, mean square diffusion, structural and dynamic heterogeneity have been explored.

Chapter 5: The most common method employed for calculating T_g of polymers from MD simulations involves deducing temperature dependence of properties like density and specific volume. The slope of density-temperature plot gives T_g. However this protocol is computationally expensive involving polymer equilibration at temperatures below T_g. In this chapter, we have proposed a method of calculating T_g from segmental (α) relaxation times at temperatures higher than T_g. Incoherent intermediate scattering function Fs(q,t) are used to calculate relaxation times and then T_g is calculated using Vogel-Fulcher-Tamman equations.

Part B

It includes chapter 6. The system under study is ionomer melt of star telechelic D, L-poly-lactide and the property under investigation is viscosity.

Chapter 6: Star D,L-Poly-lactic acid (PDLLA) shows the typical exponential decrease in viscosity with temperature. However ionomer formed by replacing acid groups of chain ends with sodium carboxylate ions, shows a significant increase in elasticity and non-monotonic temperature dependence of viscosity at temperatures above T_g, which is unusual. The molecular mechanism responsible for the non-monotonic temperature dependence of viscosity has been investigated in this chapter.

Part C

It includes chapter 7. The system under study is Polyethyleneimine (PEI) and its carbon dioxide capture properties have been investigated.

Chapter 7: A brief introduction of existing carbon dioxide capture technologies focusing on the merits and demerits of each method is provided. Characteristics of CO_2 capture through polymeric membranes, especially nitrogen containing polymers is discussed.

The mechanism of CO_2 adsorption in PEI is investigated using Grand Canonical Monte Carlo (GCMC) and Molecular dynamics (MD) simulation studies. A detailed analysis of intermolecular interactions between PEI and CO_2 at the interface, bulk and local structural regions of PEI melt has been performed to assess the adsorption effectiveness. Effect of structural and dynamic heterogeneities on adsorption process has been analyzed.

Chapter 8: A brief summary of the research work and derived conclusions is provided. Scope for the future work has also been discussed.

List of publications

1. **Pragati Sharma,** Suman Chakrabarty*, Sudip Roy*, and Rajnish Kumar*. Molecular View of CO_2 Capture by Polyethylenimine: Role of Structural and Dynamical Heterogeneity. Langmuir, **2018,** *34* (17), 5138–5148

2. Vikas Kumar, Shyambo Chatterjee, **Pragati Sharma**, Suman Chakrabarty, Chilukuri V. Avadhani, Swaminathan Sivaram*. Soluble polybenzimidazoles with intrinsic porosity: Synthesis, structure, properties and processability.
   J. Polym. Sci., Part A: Polym. Chem. **2018,** *56*, 1046–1057

3. Sachin S. Kuhire, **Pragati Sharma**, Suman Chakrabarty, Prakash P. Wadgaonkar*. Partially bio-based poly (amide imide)s by polycondensation of aromatic diacyl hydrazides based on lignin-derived phenolic acids and aromatic dianhydrides: Synthesis, characterization, and computational studies.
   J. Polym. Sci., Part A: Polym. Chem. **2017,** 55, 3636-3645

4. **Pragati Sharma**, Sudip Roy*, Hossein Ali Karimi-Varzaneh. Validation of Force Fields of Rubber through Glass-Transition Temperature calculation by Microsecond Atomic-Scale Molecular Dynamics Simulation.
   The Journal of Physical Chemistry B **2016,** 120(7), 1367-1379

5. Amruta Kulkarni, **Pragati Sharma**, Suman Chakrabarty, Ashish Lele*. Anomalous Rheology of Star Telechelic Polylactide Ionomer. (Under review, ACS Macroletters)

6. **Pragati Sharma,** Sudip Roy, and Hossein Ali Karimi-Varzaneh. Understanding Plasticizer Action from Molecular Perspective: A Case Study of Polybutadiene Rubber-Plasticizer Blend. (Manuscript under preparation)

Contents

List of Figures

CHAPTER– 1

General Introduction and Scope of Thesis

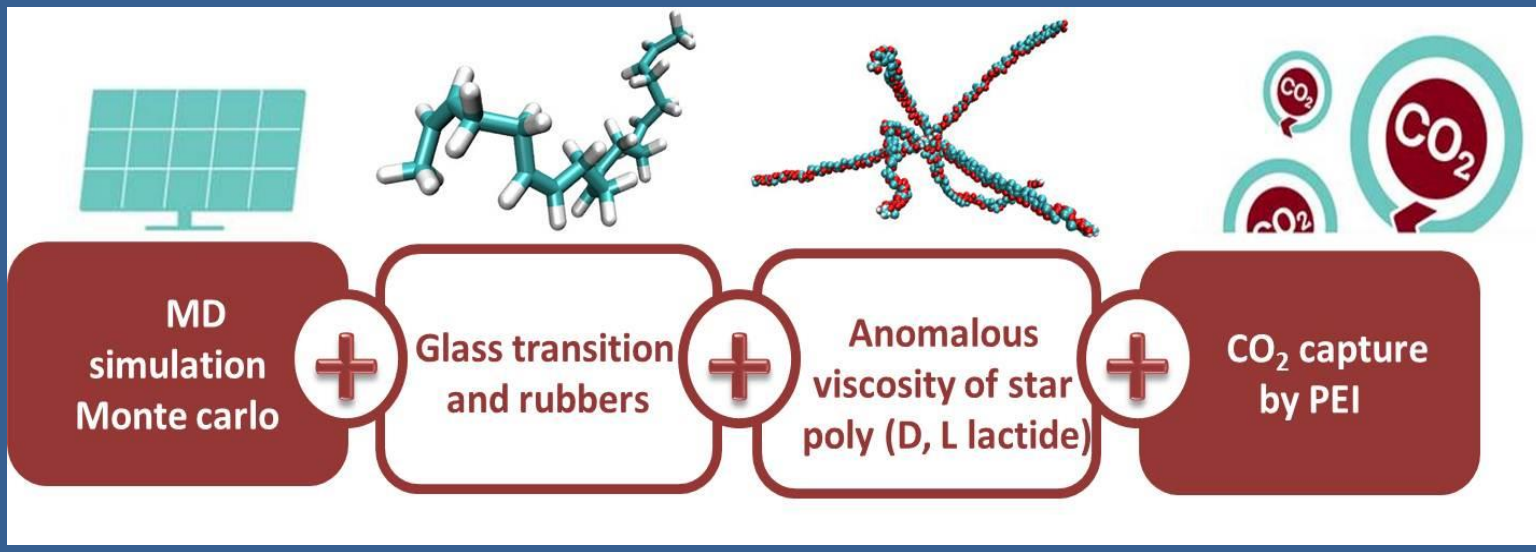

1.1 Historical background

"Materials are creators of human civilization"

The history of modern man is defined by the development of materials. From Stone Age to Copper Age to the Iron Age, new materials have always acted as the breaker of status quo and opened new horizons in human scientific development. The advent of modern age has necessitated the availability of more and more sophisticated and useful materials. This continued strive to find stronger, tougher, lighter and more efficient material led to a new class of wonder material: polymer. Polymers have become ubiquitous and superseded almost all materials. Polymers have revolutionized our day to day lives, exhibiting versatile applications in various fields like automation, electronics, biomedical, gas sequestration, pharmaceutical, textile, rubber, plastic etc[1-4].

The term polymer was coined by Berzelius (1853). Concepts related to polymer chemistry started shaping long back in nineteenth century with the discovery of celluloid and cellulose acetate from natural cellulose followed by the discovery of first fully-synthetic polymer, Bakelite in 1907. However the development of polymer physics started only after the pioneering work of Herman Staudinger in 1922. Staudinger worked on viscoelasticity of polymeric solutions and demonstrated the existence of large macromolecules. He suggested "macromolecular hypothesis" which stated that the large macromolecules are made up of covalently linked repetitive monomeric units and characterized them as polymers. Before Staudinger, polymers were believed to be colloidal in nature, formed of small molecules associating through covalent bonds of mysterious nature[1,5].

Subsequent developments in experimental techniques like scattering, e.g. Small-angle X-ray scattering (SAXS), Small-angle Neutron scattering (SANS), Light scattering (LS) have increased our understanding of polymer physics by probing the atomic/molecular level structure and dynamics. Statistical mechanical tools have always been required for physical interpretation of polymer behavior. Paul Flory is considered one of the pioneers in the area of polymer physics. Kuhn and Flory proposed a method for computing the probable size of polymer chains in good solvents by introducing the concept of Gaussian coils for ideal chains, excluded volume for real chains, scaling theory for semi-dilute solutions and Flory-Huggins theory for concentrated solutions which also explained the thermodynamics of polymers in solution[2,6]. Reptation theory

proposed by De-Gennes[7], Edwards and Doi[8] explains the dependence of chain dynamics on the length or molecular weight of polymer chains in very concentrated solutions and polymer melts. Reptation model is also used as a mechanism to describe viscous flow in amorphous polymers. Theoretical polymer physics is an active area of research wherein new theories related to polymer structure, dynamics, thermodynamics, kinetics etc. have been constantly predicted and old theories are improved.[9-14]

1.2 Computer Simulations

An important aspect of polymer physics involves the validation of these theories by testing on real systems and then applying them for designing newer polymers with improved properties/applications. Exploring structure and dynamics of polymers is a complicated task. Polymers are large molecules, presence of enormous number of degrees of freedom, complex structure, intra and intermolecular interactions pose complications in studying the molecular mechanisms through experiments.

Computer simulation has emerged as a state of the art technique to investigate the structure and dynamics in polymeric systems. In this approach computers can be used as virtual laboratories, where the interaction parameters and composition of the system can be tuned and their effects on the material properties can be examined. Simulations may act as bridge between theory and experiments. They offer valuable test of assumptions and predictions of theoretical model as well as attempt to mimic experimental systems like polymer solutions, melts, self-assemblies, and networks. Computer experiments are now extensively applied to almost all fields of science and technology. In the present thesis, we have also employed molecular dynamics simulations to explore properties of different polymers. A detailed description of the simulation methods used in this thesis is given in Chapter 2.

1.3 Scope of thesis

The complexity of polymeric systems is evident in terms of their molecular architecture: linear, branched, ring; morphology: crystalline, semi-crystalline, amorphous; physical state: rubbery, glassy; material form: melt, solution, films etc. These macroscopic polymer properties are fundamentally linked to molecular level structure and interactions. Changes in the atomic structure, molecular architecture or composition modify the structural and dynamic properties of

polymeric constituents which are then reflected at the macroscopic level[15]. A typical example comes from the tire industry where different types of tires are produced from polymers like polybutadiene, polyisoprene, polystyrene etc., selected on the basis of their glass transition temperature, which originates due to segmental motion of the chains[16]. Thus a structure-property relationship exists in polymeric materials[17]. Every now and then, a new polymer with desired properties is synthesized by changing the structure via chemical constituents, monomeric arrangement (e.g. block co-polymers) and compositions (e.g. polymer composites). Competing with the rapid discovery of new polymers, it becomes vital to increase the comprehension of molecular properties in polymeric systems. Therefore, with an objective to develop further understanding of structural and dynamic polymer properties, with the change in composition and molecular interactions, we have simulated different polymer systems, each involved in a different application in this thesis. The thesis is divided into three parts and in total contains 9 chapters.

Part A investigates the effect of composition on polymer properties. The system under study is a rubber-plasticizer blend: Polybutadiene rubber matrix with different polymers in varied proportions.

Part B deals with the effect of interactions on polymer properties, effect of sticky chain-end interactions on viscoelastic properties of star telechelic Poly-lactic acid ionomer have been explored.

Part C investigates the CO_2 capture characteristics in Polyethyleneimine and the role of molecular thermodynamics and dynamics therein. Different polymers with distinct compositions and interactions have been studied in this thesis. All of these systems are either amorphous in nature or in the melt state. The overall objective of this thesis is to establish a clear correlation between the molecular properties and the bulk properties of the polymers.

References

1. Rubinstein, M.; Colby, R. H., *Polymer physics*. Oxford University Press New York: 2003; Vol. 23.

2. Flory, P. J., *Principles of polymer chemistry*. Cornell University Press: 1953.

3. Rodriguez, F.; Cohen, C.; Ober, C. K.; Archer, L., *Principles of polymer systems*. CRC Press: 2014.

4. Cowie, J. M. G.; Arrighi, V., *Polymers: chemistry and physics of modern materials*. CRC press: 2007.

5. Yamakawa, H., *Modern theory of polymer solutions*. Harper & Row: 1971.

6. Flory, P.; Volkenstein, M., Statistical mechanics of chain molecules. Wiley Online Library: 1969.

7. De Gennes, P.-G., *Scaling concepts in polymer physics*. Cornell university press: 1979.

8. Doi, M.; Edwards, S. F., *The theory of polymer dynamics*. oxford university press: 1988; Vol. 73.

9. Ganesan, V.; Jayaraman, A., Theory and simulation studies of effective interactions, phase behavior and morphology in polymer nanocomposites. *Soft Matter* **2014,** *10* (1), 13-38.

10. Fredrickson, G. H.; Orland, H., Dynamics of polymers: A mean-field theory. *The Journal of chemical physics* **2014,** *140* (8), 084902.

11. Takahashi, K. Z.; Nishimura, R.; Yamato, N.; Yasuoka, K.; Masubuchi, Y., Onset of static and dynamic universality among molecular models of polymers. *Scientific reports* **2017,** *7* (1), 12379.

12. Lang, M.; Rubinstein, M.; Sommer, J.-U., Conformations of a long polymer in a melt of shorter chains: Generalizations of the Flory theorem. *ACS macro letters* **2015,** *4* (2), 177-181.

13. Chremos, A.; Nikoubashman, A.; Panagiotopoulos, A. Z., Flory-Huggins parameter χ, from binary mixtures of Lennard-Jones particles to block copolymer melts. *The Journal of chemical physics* **2014,** *140* (5), 054909.

14. Werner, E.; Mehlig, B., Confined polymers in the extended de Gennes regime. *Physical Review E* **2014,** *90* (6), 062602.

15. Porter, D., *Group interaction modelling of polymer properties*. CRC Press: 1995.

16. Arbe, A.; Alvarez, F.; Colmenero, J., Neutron scattering and molecular dynamics simulations: synergetic tools to unravel structure and dynamics in polymers. *Soft Matter* **2012,** *8* (32), 8257-8270.

17. Mark, J. E.; Erman, B.; Roland, M., *The science and technology of rubber*. Academic press: 2013.

CHAPTER – 2

Computational Methods and Concepts

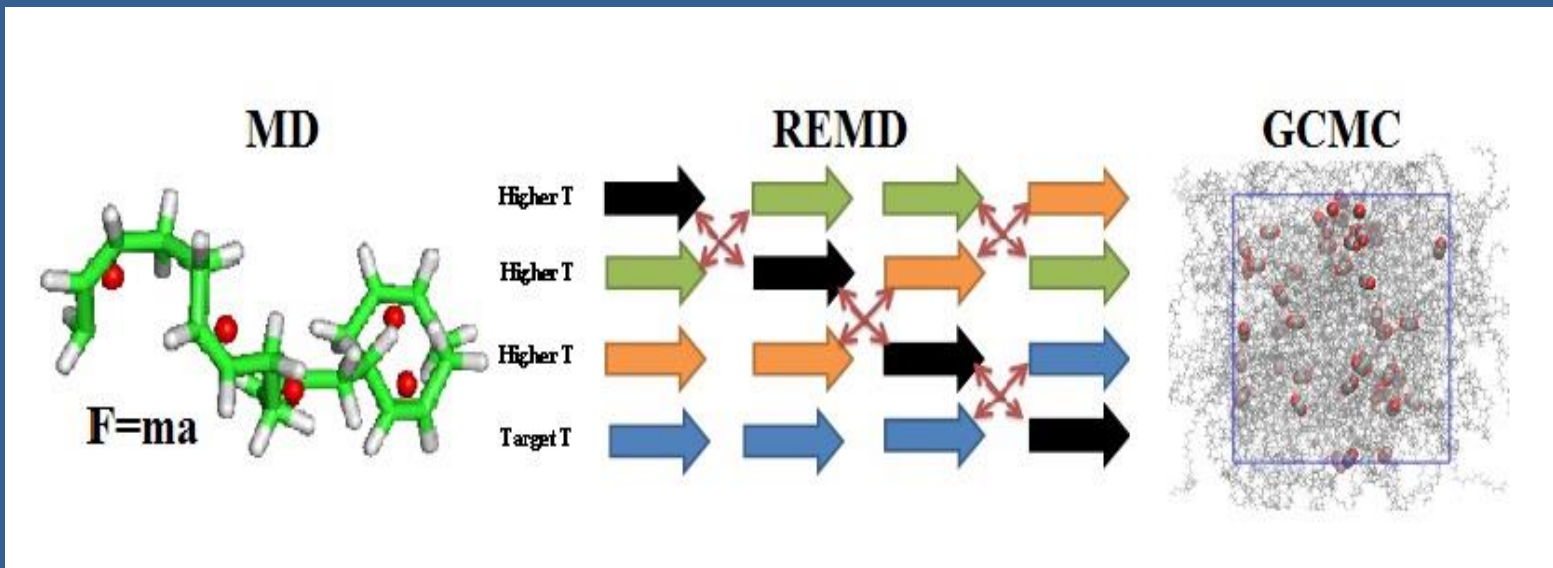

Introduction

Molecular modeling is a powerful tool to investigate the behavior of macroscopic systems using microscopic simulations. Complex chemical structures are modeled with atomistic level details and driving forces responsible for various structural, dynamic, thermodynamic and mechanical properties are analyzed. There are various levels of theories and fundamental equations in different classes of molecular modeling[1-2]. In this thesis, we have used all-atomistic molecular dynamics simulations (MD) to study the properties of rubber-composites and viscosity behavior of PDLLA ionomer. MD simulations and Grand Canonical Monte Carlo (GCMC) techniques are used to study the gas adsorption behavior of Polyethyleneimine (PEI). We have also used Replica exchange molecular dynamics (REMD) technique for efficient sampling of the polymer configurations in the phase space. A brief description of employed simulation methods and some basic concepts are discussed in this chapter.

2.1 Classical Molecular Dynamics

Molecular dynamics is a many body simulation method used for studying the physical motion of atoms and molecules. In classical MD, atoms and molecules are allowed to interact for a fixed period of time exhibiting evolution of properties with time. Motion of particles in the systems is treated by the 'classical' Newton's equation of motion.

$$F_i = m_i \frac{\partial^2 r_i}{\partial t^2}, i = 1..N \qquad \textbf{(2.1)}$$

Here m_i is the mass and r_i is the position of i^{th} particle in a system composed of N number of particles. The force acting on the particle is calculated from the gradient of inter-particle potential, V.

$$F_i = -\frac{\partial V_{(r1,r2....rN)}}{\partial r_i} \qquad \textbf{(2.2)}$$

The inter-particle potential, V is defined as the function of the position of respective particles. These potential functions are called as force fields. Forces derived from these potentials are used to calculate the position and velocities of particles. Total Simulation time is divided into small

time steps and at each time step, new positions and velocities is calculated from the data collected in previous step. Positions and velocities at each time step is written in an output file called as trajectory. Generated trajectory files are then used for visualizing motions of atoms and molecules and calculating microscopic properties of interest.

2.1.1 Force field

Force field consists of a set of empirical parameters and functions which represents systems internal potential energy in terms of atomic positions. The force field parameters are derived either from experiments or quantum chemical calculations. An all-atomistic force field considers every atom including hydrogen as an interacting site; a united atom force field considers a group of atoms like methyl and methylene as one interaction site. Coarse grained simulations consider even cruder representations by averaging over unessential atomic details. Even higher length and time scales can be obtained in continuum simulations. The basic functional form of force fields includes bonded and non-bonded terms as shown in equation 2.3.

$$V = V_{bonded} + V_{nonbonded}$$

$$V_{bonded} = \sum_{bonds} \frac{1}{2} k_b (b - b_0)^2 + \sum_{angles} \frac{1}{2} k_\theta (\theta - \theta_0)^2 + \sum_{dihedrals} k_\varphi (1 + \cos(n\varphi - \lambda))$$

$$V_{nonbonded} = \sum_{LJ} 4\varepsilon_{ij} \left[\left(\frac{\sigma_{ij}}{r_{ij}} \right)^{12} - \left(\frac{\sigma_{ij}}{r_{ij}} \right)^{6} \right] + \sum_{coulomb} \frac{q_i q_j}{4\pi\epsilon_0 r_{ij}} \quad \textbf{(2.3)}$$

Bonded potentials include bonds, angles and dihedral terms; bonds and angles being treated as harmonic potential while dihedrals as cosine periodic functions. The values b_0, θ_0 and Φ_0.denote the equilibrium bond length, angle and dihedral values and b, θ and Φ represents the respective values at a certain time. The harmonic force constants k_b, k_θ, k_Φ gives measure of the energy required for stretching or contracting bonds, bending angles and dihedrals respectively.

Non-bonded potentials include columbic and Lennard-jones 12-6 potential. In the expression for LJ potential, ε_{ij} denotes the strength of interactions between two atoms. r_{ij} denotes the distance between particles and σ_{ij} is the distance where inter-particle potential is zero. The last term

represents coulomb potential as per coulombs law, q_i and q_j are the partial charges on atoms i and j. ε_0 and ε_r represents the dielectric constants in vacuum and medium. Values of bond lengths, angles and dihedrals, corresponding force constants, LJ parameters: σ_{ij}, ε_{ij} and columbic parameters q_i, q_j, r_{ij} are given as input in MD simulations. Some commonly used classical force fields are OPLS[3-4], CHARMM[5-6], AMBER[7], and GROMOS[8]. These are parameterized against different classes of chemical compounds. Primarily, three inputs are required for MD simulations: initial coordinates, force fields and a set of instructions to run the simulation. Initial coordinates are obtained from experiments like NMR or X-ray crystallography or from the building model. Before starting MD simulations, the geometry of these starting structures is optimized because if these are far away from the minima of potential energy surface, forces and potential will become large, steric clashes can occur and the simulation can fail. Thus initial structure is energy minimized a priory to MD simulations. Commonly used algorithms for energy minimization are steepest descent and conjugate gradient methods.

2.1.2 The MD simulation algorithm

A MD simulation method basically covers three steps: Initiation, force calculations and integration of newton's equation of motion. Initiation indicates the selection of initial positions and velocities of particles. Initial positions of particles are assigned in the form of coordinates r_i (x_i, y_i, z_i) and initial velocities are generated using Maxwell-Boltzmann distribution at a particular temperature using formula:

$$p(v_i) = \sqrt{\frac{m_i}{2\pi kT} \exp\left(-\frac{m_i v_i^2}{2kT}\right)} \qquad \textbf{(2.4)}$$

Here distribution of velocities, $p(v_i)$ is generated from random numbers, however all velocities are scaled so that total energy corresponds to temperature T. k is the Boltzmann constant.

After initiation, forces are calculated from the gradient of potentials. These forces are then used to calculate new positions and velocity by integrating equation of motion and thus particles propagates in the system. Among various integration algorithms available, leap frog[9] is widely used. The updated positions and velocities are obtained from forces using following relations:

$$v\left(t + \tfrac{1}{2}\delta t\right) = v\left(t - \tfrac{1}{2}\delta t\right) + \frac{F(t)}{m}\delta t \qquad \textbf{(2.5)}$$

$$r(t + \delta t) = r(t) + v\left(t + \frac{1}{2}\delta t\right)\delta t \quad \textbf{(2.6)}$$

It calculates velocities at time $t + \frac{1}{2}\delta t$ and positions at t + δt. Thus positions and velocities are not calculated at the same time, they leap over each other. The velocities are then approximated using following equation:

$$v(t) = \frac{1}{2}\left[v\left(t - \frac{1}{2}\delta t\right) + v\left(t + \frac{1}{2}\delta t\right)\right] \quad \textbf{(2.7)}$$

Here δt is the time step used in simulations. It is generally taken as 1 femtosecond, selected according to the frequency of bond vibrations. However higher time steps have also been used when bond vibrations are constrained during simulations to enhance computational performance and if it does not affect system dynamics significantly. Several bond constraint algorithms like LINCS[10-11] and SHAKE[12] have been implemented in gromacs package which we have used in this thesis.

Similar to bond constraints, several numerical approximations like cut-off schemes are applied to non-bonded potentials also. Non-bonded potentials are pair additive i.e. calculations are done for each pair of neighbours. Hence the numbers of calculation steps are proportional to square of the number of pairs. Such calculations are computationally intensive; therefore these are restricted within a cut-off radius around each particle. LJ potentials are truncated beyond cut-off radius using shift or switch functions. While Long-range columbic interactions (beyond cut-off) are calculated with methods; reaction-field[13-14], Ewald sum, PME (Particle mesh ewald summation)[15].

2.1.3 Periodic boundary conditions (PBC)

It denotes a periodic array of simulation boxes, where each box is surrounded by its replica in all sides. This condition is used to eliminate finite size effects in simulations as shown in Figure 2.1

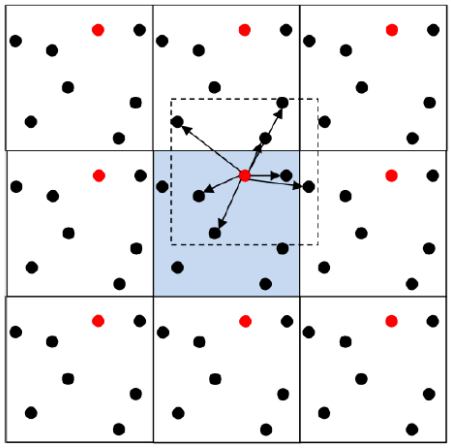

***Figure* 2.1:** Interpretation of PBC in a 2D image. Blue box denotes the central simulation cell. Red sphere shows replicas of each atom. Dashed box and arrows denotes the nearest image of the red atom in central cell[16] (reproduced from ref. 16)

MD simulations are used to predict bulk macroscopic properties. However the simulation box consists of a few nanometers with small number of particles only, which are also present near to box surface. Thus surface defects may also arise. To remove the finite size and surface effects from simulations, periodic boundary conditions are used. In PBC, a central simulation box will be surrounded by its infinite copies mimicking a real bulk system. Minimum image convention is always applied with PBC to calculate short range forces. It means that each atom interacts either with an atom or its image, whoever is nearest[2].

2.1.4 Statistical ensemble

Information regarding statistical ensemble is to be provided as input in MD simulations. Parameters like temperature (T), pressure (P) and number of particles (N) are specified to stipulate the type of ensemble. Three types of ensembles are generally used in MD simulations: microcanonical (NVE); where N, V and energy is fixed, canonical (NVT); where pressure and energy are allowed to fluctuate, isothermal-isobaric (NPT) ensemble, where Pressure, temperature and number of particles are kept fixed. Temperature and pressure in simulations are

controlled using thermostats and barostats respectively. Examples of commonly used thermostats are Berendsen[17], Nose-hoover[18-19] and V-rescale[20] and that of barostats are Berendsen[17] and Parrinello-Rahman[21].

2.2 Grand-canonical monte-carlo (GCMC) simulations

Like MD simulations, monte-carlo (MC) simulations are also used to determine equilibrium molecular properties. The basic system setup is similar in both techniques i.e. both considers atoms as interacting sites, both employ classical force fields and PBC conditions. However they differ in their mode of sampling phase space. In MD, new configurations are generated by integrating newton's equation of motion. While in MC, new configurations are generated by selecting a random molecule and then introducing variations by translating, rotating to create new configurations. Acceptance of these moves is selected on the basis of metropolis criterion and Boltzmann weighted averages are generated to study equilibrium properties. MD determines time-averaged, dynamic properties while MC does not involve time and thus determines ensemble averaged properties[22].

2.2.1 Metropolis monte-carlo algorithm[15]

Steps followed in MC simulations are as follows:

1. First a random configuration, say X is selected and its energy E(X) is computed.

2. A new trial configuration, Y is generated by attempting translational or rotational moves and the energy E(Y) is computed.

3. Acceptance probability of the new configuration is given by:

$$P = \left(1, \exp\left(-\frac{E_p(X) - E_p(Y)}{kT}\right)\right) \qquad \textbf{(2.8)}$$

4. A random number RN, which is uniform in [0,1] is picked. If RN < P, move is accepted, else rejected.

5. Either accepted or rejected, steps 2 and 3 are further repeated to generate new trial configuration.

By this process, a series of configurations is created called as Markov chain of configurations. Markov chain refers to the creation of a memory-less sequence of configurations where moving to a new configuration does not depend on the previous one.

GCMC simulations are widely used monte-carlo simulations to study gas-adsorption phenomenon. In grand canonical (μVT) ensemble: chemical potential, volume and temperature are kept constant while number of particles and energy can be varied. Concept is to run the simulation till chemical potential of the adsorbed gas becomes equal to that of bulk gas and the final amount of adsorbed gas will denote its solubility in the adsorbent. In GCMC simulation, a markov chain is created by means of insertion and deletion along with translational and rotational moves. In an N particle system with volume V, acceptance probabilities for different moves are calculated as shown below:

1. Displacement of particle:

$$acc(s \rightarrow s`) = min\left[1, exp\left\{-\beta\left(\mu\left(s`^{N}\right) - \mu(s^{N})\right)\right\}\right] \quad \textbf{(2.9)}$$

2. Insertion of a particle:

$$acc(N \rightarrow N+1) = \min\left[1, \frac{V}{\Lambda^{3}(N+1)}\, exp\left\{\beta(\mu - U(N+1) + U(N))\right\}\right] \quad \textbf{(2.10)}$$

3. Deletion of a particle:

$$acc(N \rightarrow N-1) = \min\left[1, \frac{\Lambda^{3}N}{V}\, exp\left\{-\beta(\mu + U(N-1) - U(N))\right\}\right] \quad \textbf{(2.11)}$$

Here, s and s` denotes scaled coordinates, U is internal energy, μ is chemical potential. Λ is debroglie wavelength.

In case of adsorption of mixed gases, number of gas species and the number of each species also is taken into account. To increase the acceptance probability, a more efficient method called as configurational bias monte-carlo is used. A detailed description of CBMC method and all monte-carlo algorithms is given in textbook of Frenkel & Smit[15].

2.3 Replica exchange molecular dynamics (REMD)[23]

It is an enhanced sampling method compared to molecular dynamics simulation. In this process several copies of an initial system are simulated at different temperatures at the same time. Exchange of these non-interacting configurations occurs between different temperatures according to above discussed metropolis criterion. This exchange of configurations enables availability of higher temperature configurations to lower temperature also and vice-versa as shown in Figure 2.2. Thus both high and low energy configurations can be sampled allowing efficient exploration of conformational space.

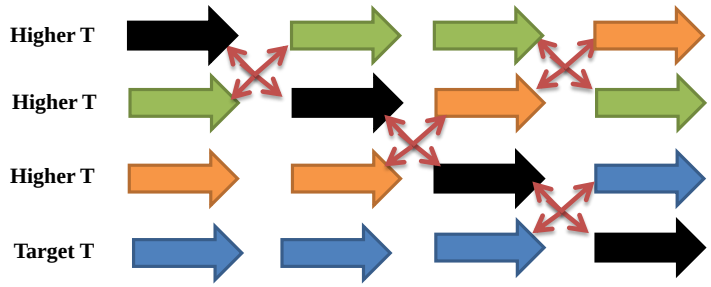

***Figure* 2.2:** Representation of replica exchange molecular dynamics. Large colored arrows denotes replicas propagating at different temperatures in MD

The metropolis criterion[24-25] in monte-carlo simulations accept or reject moves based on energy of the system. At higher temperatures, transition rates and hence probability of exchange are higher. During exchange, a detailed balance condition needs to be satisfied i.e. the forward and reverse update should be equally likely to occur. e.g. if replica 'a' at temp T_c and 'b' at temp T_d are attempting to exchange with transition probability π then,

$$P_c(x_a)P_d(x_b)\pi\left(x_{a,c} \rightarrow x_{b,c}; x_{b,d} \rightarrow x_{a,d}\right) = P_d(x_a)P_c(x_b)\pi\left(x_{a,d} \rightarrow x_{b,d}; x_{b,c} \rightarrow x_{a,c}\right) \quad \textbf{(2.12)}$$

According to metropolis criterion, the probability of exchange will be:

$$\frac{\pi\left(x_{a,c} \rightarrow x_{b,c}; x_{b,d} \rightarrow x_{a,d}\right)}{\pi\left(x_{a,d} \rightarrow x_{b,d}; x_{b,c} \rightarrow x_{a,c}\right)} = e^{-(\Delta E \Delta \beta)} \quad \textbf{(2.13)}$$

Where $\Delta E = E(x_b) - E(x_a)$ *and* $\Delta\beta = \beta_c - \beta_d$

If the exchange is accepted then the temperatures of the replicas are swapped. On completion of simulation, data can be collected at individual temperatures or as ensemble averages. A detailed description of REMD method can be obtained from papers of Sugita and okamoto[23].

In the present thesis, MD simulations and REMD simulations are performed using Gromacs simulation suite[26-27]. Gromacs is one of the fastest MD simulation code with various acceleration and parallelization features. GCMC focused simulations are performed using MCCS-Towhee package[28]. Some analysis reported in this paper are done using Gromacs tools while others are done using self-written codes whose details are given in respective chapters.

2.4 Theoretical background of the studied properties

2.4.1 Glass transition temperature

It is defined as the transition of amorphous materials from a 'brittle' glassy to 'soft' rubbery state on increasing temperature. The range of temperatures at which this transition occurs is called as glass transition temperature. It is characterized by an increase of 17 orders of magnitude in viscosity within a temperature range of 500K[29]. Properties like thermal expansion, heat capacity and shear modulus show sudden change at T_g, a kink or change in slope in the variation of these properties against temperature is used to define T_g. In simulations, T_g is generally calculated from the change in slope of density or specific volume vs. temperature plot[30-31].

2.4.1.1 Theories of glass transition

Although considered as one of the fundamental and oldest problems of condensed matter physics, theories of T_g still holds wide and contrasting views[32]. Some of the basic approaches are free volume, thermodynamic and kinetic theories[33].

2.4.1.1.1 Free volume theory: Proposed by Fox-Ferry and William, Landell, and Ferry. This theory states that glass transition is characterized by an iso-free volume state i.e. at T_g, polymers possess a universal free volume called as fractional free volume (FFV) having value ~ 0.025. On cooling, when FFV reaches this value, it shows that T_g is attained and the polymer becomes glassy. Free volume is related to thermal expansion of material and FFV is calculated using thermal expansion coefficient from equation 2.14.

$$f = f_g + \alpha(T - T_g) \qquad \textbf{(2.14)}$$

Here f_g is the fractional free volume at T_g and α is the coefficient of expansion of free volume. William, Landell and Ferry (WLF) proposed an empirical relationship to correlate relaxation times and temperature[34]. Free volume theory derives WLF equation based on α and FFV as shown in equation 2.15.

$$\ln A_t = \frac{-(\frac{B}{f_0})(T - T_0)}{\frac{f_0}{\alpha} + (T - T_0)} \qquad \textbf{(2.15)}$$

Here f_0 is FFV at temperature T_0, B is a constant and α is thermal expansion coefficient.

2.4.1.1.2 Kinetic theory: It considers glass transition is purely a kinetic/dynamic phenomenon since the position of T_g depends on the rate of cooling and heating in experiments. It uses time dependent properties to explain the transition and propose that glass transition occurs when the time scale of molecular relaxations reaches the time scale of experiment[35].

2.4.1.1.3 Thermodynamic theory: It considers glass transition as a true second order thermodynamic transition which has equilibrium properties; the equilibrium properties however are not observable since it requires infinite time. Gibbs and Demarzio proposed that glass transition occurs due to changes in conformational entropy(S) with temperature. They attempted to explain the Kauzmann paradox[36] which states that as the liquid is cooled, the difference in entropy between liquid and solid state decreases and if the properties like entropy and volume are extrapolated to lower temperatures, there will be a temperature where the difference in entropy will become zero called as glass transition temperature[37]. Adam-Gibbs also gave an expression correlating relaxation time and configurational entropy as shown in equation 2.16.

$$\tau(T) = \tau_\infty \exp(\frac{C}{TS_c}) \qquad \textbf{(2.16)}$$

Here $\tau(T)$ is the relaxation time, S_c is configurational entropy, C is a constant which depends on free energy.

2.4.1.2 Glass transition in polymer blends

A miscible polymer blend exhibits a single glass transition in between those of the individual components. An immiscible blend exhibits two separate and shifted transitions compared to individual components. Equations commonly used to express T_g of miscible blends[38] are:

2.4.1.2.1 Fox equation[39]

$$\frac{1}{T_g} = \frac{w_a}{T_{ga}} + \frac{w_b}{T_{gb}} \qquad \textbf{(2.17)}$$

Where, T_{ga} and T_{gb} are the T_gs of individual components a and b, w_a and w_b are the weight fractions.

2.4.1.2.2 Gordon and Taylor equation[40]

$$T_g = \frac{w_a T_{ga} + k w_b T_{gb}}{w_a + k w_b} \qquad \textbf{(2.18)}$$

Here k is the ratio of thermal expansion coefficients between rubbery and glassy components.

$$k = \frac{\alpha_{lb} - \alpha_{gb}}{\alpha_{la} - \alpha_{ga}} \qquad \textbf{(2.19)}$$

α_l is the thermal expansion coefficient in rubbery state and α_g is the thermal expansion coefficient in glassy state for a and b components

2.4.1.2.3 Kelley-Bueche equation[41]

It is similar to Gordon-Taylor equation, but the volume fraction (φ) is used instead of weight fraction. As $\alpha_l - \alpha_g$ is proposed to be constant for all polymers, so k becomes 1 and the above two equations reduce to their linear form:

$$T_g = w_a T_{ga} + w_b T_{gb} \text{ and } T_g = \varphi_a T_{ga} + \varphi_b T_{gb} \qquad \textbf{(2.20)}$$

Gordon-Taylor and Kelley-Bueche equations are generally used to predict T_g of polymer-plasticizer systems and we have also used these equations for predicting T_g of Polybutadiene rubber-plasticizer mixtures.

2.4.2 Viscosity and its temperature dependence

Viscosity is the measure of resistance towards flow in response to external deformation or stress. Polymer melts are highly viscous owing to their long molecular chain structure which poses strong resistance to flow. Polymers form non-Newtonian fluids i.e. the shear viscosity of polymers depend on the applied shear rate. Another important factor which affects viscosity of polymeric melts is temperature. Viscosity of conventional polymer melts decrease with increasing temperature because of increased thermal mobility of chains[42]. A typical viscosity-temperature plot for an amorphous polymer showing monotonic decrease in viscosity with temperature is depicted in Figure 2.3

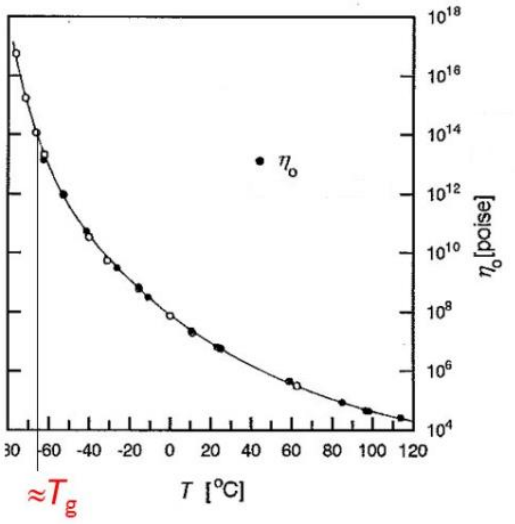

***Figure* 2.3:** Relationship between elastic modulus and temperature[43] (reproduced from ref 43). T is temperature and η is the viscosity, η_0 is zero shear viscosity.

A simple empirical correlation between viscosity and temperature was given by Andrade[44] in 1930 as shown in equation 2.21:

$$\ln \eta = C + \frac{D}{RT} \qquad \textbf{(2.21)}$$

Here η is the viscosity at temperature T, R is the gas constant, C and D are constants, D being the activation enthalpy. While this equation captures the viscosity behavior of fluids, it particularly fails for molten polymers around T_g. In 1951, Doolittle[45] proposed that the temperature dependence of viscosity in polymers can be explained in terms of free volume around glass

transition temperature. Hypothesis was that the increase in temperature would increase free volume in the system reducing inter-chain friction and consequent decrease in flow resistance. Based on this concept, Williams-Landel-Ferry proposed an empirical viscosity relationship now called as the WLF equation. Thus two equations that are widely used to capture temperature dependence of viscosity in amorphous polymers, WLF equation close to T_g and Arrhenius equation at even higher temperatures.

2.4.2.1. Arrhenius equation[46]: At high temperatures, viscosity of polymers is completely a thermally controlled process like Newtonian fluids and shows an exponential decrease as captured by Arrhenius equation.

$$\eta(T) = \eta_0 \exp(\frac{E}{RT}) \qquad \textbf{(2.22)}$$

Here T is temperature, η is the viscosity, η_0 is a coefficient (zero shear viscosity), *E* is the activation energy and *R* is the universal gas constant.

2.4.2.2. Williams lendel ferry (WLF) model[46-47]: Applicable at temperatures from T_g to T_g+100.

$$\eta(T) = \eta_0 \exp(\frac{-C1(T - T_r)}{C2 + T - T_r}) \qquad \textbf{(2.23)}$$

C1, C2, T_r and η_0 are empirical parameters. T_r is generally set to match T_g, ($T_r = T_g + 43$).

While these equations and some others like Vogel-Fulcher-Tammann, VFT equation captures the monotonic decrease in viscosity; there are only a few examples that show inverse or non-monotonic temperature dependence of viscosity.

2.4.3 Solubility and adsorption isotherm

Solubility is the maximum amount of solute that can be dissolved in a solvent at a given temperature and pressure, provided that no phase separation should occur. A measure of solubility is the solubility coefficient, S, which is a thermodynamic factor that depends on the temperature.

2.4.3.1 Gas solubility in polymeric membranes

Since polymeric membranes are usually non-porous, gas absorption in polymeric membranes occurs by solution-diffusion mechanism[48]. Solution-diffusion mechanism depends on three factors: permeability, diffusibility and solubility whose correlation is described as:

$$P = DS \quad \textbf{(2.24)}$$

Where, P is the permeability coefficient which gives a measure of the flux. D is the diffusivity coefficient, which governs the mobility of molecules in the membrane and S is the solubility coefficient which measures the solubility of gases in the membrane[49-50]

Selectivity (α_{ij}) is defined as the ratio between permeability of species i with relation to the species j.

$$\alpha_{ij} = \frac{P_i}{P_j} \quad \textbf{(2.25)}$$

Robeson upper bound: The performance of polymeric membranes is evaluated in terms of Robeson limit. It was discovered by Robeson in 1990 that polymers having high selectivity have low permeability and vice-versa. It is illustrated in the form of Robeson plot as shown in Figure 2.4 in which selectivity is plotted as a function of gas permeation. Efficient gas capture material must aim at touching the Robeson upper bound[51].

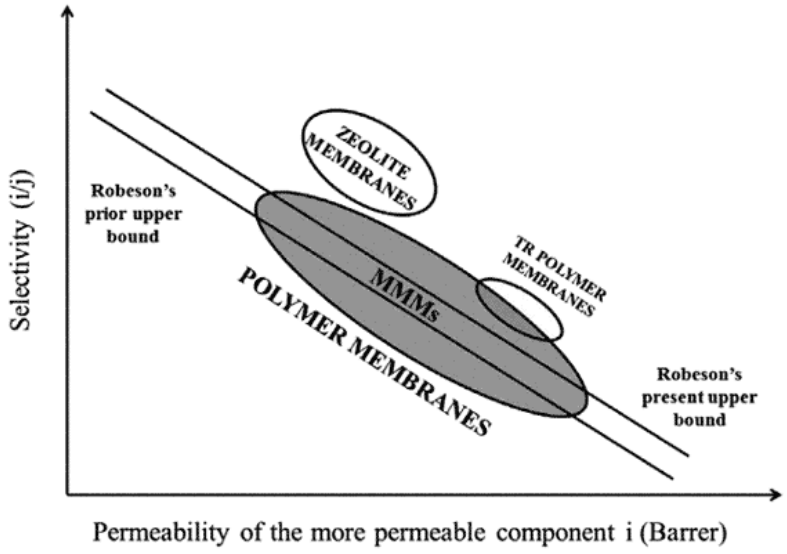

***Figure* 2.4:** Robeson's plot of **selectivity** vs. permeability[51] (reproduced from ref 51)

2.4.3.2 Adsorption isotherms: Effect of pressure on solubility

Ideal systems in terms of solubility would be those where the concentration of a component inside the polymer is proportional to the partial pressure of the component outside the membrane

It can be described using Henry's sorption isotherms where sorption is linear in ideal systems as shown in equation and Figure 2.5.

$$p = k_H c \qquad \textbf{(2.26)}$$

Where '*p'* is the partial pressure of the gas. 'c' is the concentration of solute and 'k_H' is the Henry's law constant.

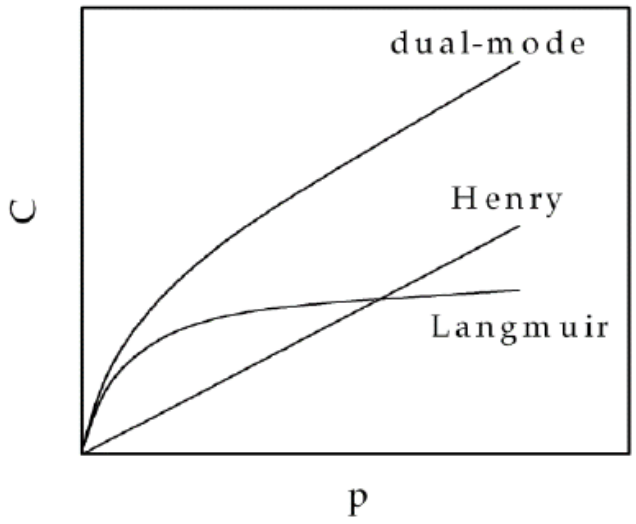

***Figure* 2.5:** Gas sorption from Henry's law, Langmuir adsorption isotherm and dual-mode sorption[52] (reproduced from reference 52)

If the system is not ideal, the sorption will be different from the ideal behavior. The Langmuir sorption describes a dynamic equilibrium between the adsorbed and desorbed molecules using one molecular layer.

2.4.3.2.1 Langmuir adsorption isotherm

Langmuir's theory of adsorption considers a continual rate of evaporation and condensation on the material surface so that there is no accumulation. Three main assumptions of Langmuir's theory are:[49, 53]

(a) Surface is homogenous.

(b) Adsorption is localized which means each interacting molecule has their own adsorption site and they are non-interacting with each other.

(c) Each interacting site can accumulate only one molecule.

The sorption is considered as a chemical reaction of the type:

A (adsorbate) + S(Site) → A_{ad} (adsorbed-complex)

The fraction of absorbate occupied by the sorbent is given by equation 2.27.

$$\theta_A = \frac{v}{v_m} = \frac{k_{eq}^A p_A}{1 + k_{eq}^A p_A} \quad \textbf{(2.27)}$$

where θ gives the fractional occupancy of the sites, p_A is adsorbate partial pressure and K_{eq} is the equilibrium constant. V is the volume of adsorbent and V_m is the volume of the monolayer. Langmuir adsorption isotherm is non-linear as shown in Figure 2.5.

2.4.3.2.1 Dual-sorption model

In glassy polymers, the sorption is highly non-linear and another layer of molecules can be adsorbed on already adsorbed molecules. The Langmuir sorption is then not valid and the sorption is described using the dual mode sorption which is a combination of the sorption of Henrys and Langmuir sorption as per equation 2.28 and shown in Figure 2.5.

$$C_e = C_D + C_H = k_H P + C_H' b_p / (1 + b_p) \quad \textbf{(2.28)}$$

Where C_e is the total concentration of solute, C_D is the concentration due to the Henry's-law contribution, C_H is the concentration in "holes" or the Langmuir contribution, k_H is the Henry's-law constant, *P* is the partial pressure of gas at equilibrium, b is the hole affinity constant of the gas for the Langmuir sites, and C_H' is the hole saturation constant of the polymer for the gas in the Langmuir sorption mode.

Dual sorption model is useful for determining the absorption of gases through glassy polymers while Langmuir sorption model is useful for determining the absorption of gases like CO_2 through rubbery polymers[52].

References

1. Allen, M. P.; Tildesley, D. J., *Computer simulation of liquids*. Oxford university press: 2017.

2. Leach, A. R., *Molecular modelling: principles and applications*. Pearson education: 2001.

3. Jorgensen, W. L.; Maxwell, D. S.; Tirado-Rives, J., Development and testing of the OPLS all-atom force field on conformational energetics and properties of organic liquids. *J. Am. Chem. Soc* **1996,** *118* (45), 11225-11236.

4. Kaminski, G. A.; Friesner, R. A.; Tirado-Rives, J.; Jorgensen, W. L., Evaluation and reparametrization of the OPLS-AA force field for proteins via comparison with accurate quantum chemical calculations on peptides. *The Journal of Physical Chemistry B* **2001,** *105* (28), 6474-6487.

5. Brooks, B. R.; Brooks, C. L.; MacKerell, A. D.; Nilsson, L.; Petrella, R. J.; Roux, B.; Won, Y.; Archontis, G.; Bartels, C.; Boresch, S., CHARMM: the biomolecular simulation program. *Journal of computational chemistry* **2009,** *30* (10), 1545-1614.

6. Brooks, B. R.; Bruccoleri, R. E.; Olafson, B. D.; States, D. J.; Swaminathan, S. a.; Karplus, M., CHARMM: a program for macromolecular energy, minimization, and dynamics calculations. *Journal of computational chemistry* **1983,** *4* (2), 187-217.

7. Duan, Y.; Wu, C.; Chowdhury, S.; Lee, M. C.; Xiong, G.; Zhang, W.; Yang, R.; Cieplak, P.; Luo, R.; Lee, T., A point-charge force field for molecular mechanics simulations of proteins based on condensed-phase quantum mechanical calculations. *Journal of computational chemistry* **2003,** *24* (16), 1999-2012.

8. Oostenbrink, C.; Villa, A.; Mark, A. E.; Van Gunsteren, W. F., A biomolecular force field based on the free enthalpy of hydration and solvation: the GROMOS force-field parameter sets 53A5 and 53A6. *Journal of computational chemistry* **2004,** *25* (13), 1656-1676.

9. Hockney, R.; Goel, S.; Eastwood, J., Quiet high-resolution computer models of a plasma. *Journal of Computational Physics* **1974,** *14* (2), 148-158.

10. Hess, B., P-LINCS: A parallel linear constraint solver for molecular simulation. *Journal of Chemical Theory and Computation* **2008,** *4* (1), 116-122.

11. Hess, B.; Bekker, H.; Berendsen, H. J.; Fraaije, J. G., LINCS: a linear constraint solver for molecular simulations. *Journal of computational chemistry* **1997,** *18* (12), 1463-1472.

12. Ryckaert, J.-P.; Ciccotti, G.; Berendsen, H. J., Numerical integration of the cartesian equations of motion of a system with constraints: molecular dynamics of n-alkanes. *Journal of Computational Physics* **1977,** *23* (3), 327-341.

13. Kirkwood, J. G., Theory of solutions of molecules containing widely separated charges with special application to zwitterions. *The Journal of Chemical Physics* **1934,** *2* (7), 351-361.

14. Onsager, L., Electric moments of molecules in liquids. *Journal of the American Chemical Society* **1936,** *58* (8), 1486-1493.

15. Frenkel, D.; Smit, B., *Understanding molecular simulation: from algorithms to applications*. Academic press: 2001; Vol. 1.

16. Banu, A. M., Molecular simulation studies of metal organic frameworks focusing on hydrogen purification. **2014**.

17. Berendsen, H. J.; Postma, J. v.; van Gunsteren, W. F.; DiNola, A.; Haak, J., Molecular dynamics with coupling to an external bath. *The Journal of chemical physics* **1984,** *81* (8), 3684-3690.

18. Nosé, S., A unified formulation of the constant temperature molecular dynamics methods. *The Journal of chemical physics* **1984,** *81* (1), 511-519.

19. Hoover, W. G., Canonical dynamics: equilibrium phase-space distributions. *Physical review A* **1985,** *31* (3), 1695.

20. Bussi, G.; Donadio, D.; Parrinello, M., Canonical sampling through velocity rescaling. *The Journal of chemical physics* **2007,** *126* (1), 014101.

21. Parrinello, M.; Rahman, A., Polymorphic transitions in single crystals: A new molecular dynamics method. *Journal of Applied physics* **1981,** *52* (12), 7182-7190.

22. Jorgensen, W. L.; Tirado-Rives, J., Monte Carlo vs molecular dynamics for conformational sampling. *The Journal of Physical Chemistry* **1996,** *100* (34), 14508-14513.

23. Sugita, Y.; Okamoto, Y., Replica-exchange molecular dynamics method for protein folding. *Chemical physics letters* **1999,** *314* (1), 141-151.

24. Metropolis, N.; Rosenbluth, A. W.; Rosenbluth, M. N.; Teller, A. H.; Teller, E., Equation of state calculations by fast computing machines. *The journal of chemical physics* **1953,** *21* (6), 1087-1092.

25. Sindhikara, D.; Meng, Y.; Roitberg, A. E., Exchange frequency in replica exchange molecular dynamics. *The Journal of chemical physics* **2008,** *128* (2), 01B609.

26. Hess, B.; Kutzner, C.; Van Der Spoel, D.; Lindahl, E., GROMACS 4: algorithms for highly efficient, load-balanced, and scalable molecular simulation. *Journal of chemical theory and computation* **2008,** *4* (3), 435-447.

27. Van Der Spoel, D.; Lindahl, E.; Hess, B.; Groenhof, G.; Mark, A. E.; Berendsen, H. J., GROMACS: fast, flexible, and free. *Journal of computational chemistry* **2005,** *26* (16), 1701-1718.

28. Martin, M. G., MCCCS Towhee: a tool for Monte Carlo molecular simulation. *Molecular Simulation* **2013,** *39* (14-15), 1212-1222.

29. Blodgett, M.; Egami, T.; Nussinov, Z.; Kelton, K., Unexpected universality in the viscosity of metallic liquids. *arXiv preprint arXiv:1407.7558* **2014**.

30. Fan, H. B.; Yuen, M. M., Material properties of the cross-linked epoxy resin compound predicted by molecular dynamics simulation. *Polymer* **2007,** *48* (7), 2174-2178.

31. Yani, Y.; Lamm, M. H., Molecular dynamics simulation of mixed matrix nanocomposites containing polyimide and polyhedral oligomeric silsesquioxane (POSS). *Polymer* **2009,** *50* (5), 1324-1332.

32. Ngai, K. L., All standard theories and models of glass transition appear to be inadequate: missing some essential physics. In *Soft matter under exogenic impacts*, Springer: 2007; pp 91-111.

33. Ebewele, R. O., *Polymer science and technology*. CRC press: 2000.

34. Gedde, U. W., *Polymer physics*. Springer Science & Business Media: 2013.

35. Rahman, M. S.; Roos, Y. H., *Glass Transition and Phase Transitions in Food and Biological Materials*. John Wiley & Sons: 2017.

36. Kauzmann, W., The nature of the glassy state and the behavior of liquids at low temperatures. *Chemical Reviews* **1948,** *43* (2), 219-256.

37. Gibbs, J. H.; DiMarzio, E. A., Nature of the glass transition and the glassy state. *The Journal of Chemical Physics* **1958,** *28* (3), 373-383.

38. Pinal, R., Entropy of mixing and the glass transition of amorphous mixtures. *Entropy* **2008,** *10* (3), 207-223.

39. Fox, T. G., Influence of diluent and of copolymer composition on the glass temperature of a polymer system. *Bull. Am. Phs. Soc.* **1952,** *1*, 123.

40. Gordon, M.; Taylor, J. S., Ideal copolymers and the second-order transitions of synthetic rubbers. I. Non-crystalline copolymers. *Journal of Chemical Technology and Biotechnology* **1952,** *2* (9), 493-500.

41. Kelley, F. N.; Bueche, F., Viscosity and glass temperature relations for polymer-diluent systems. *Journal of Polymer Science Part A: Polymer Chemistry* **1961,** *50* (154), 549-556.

42. Fox Jr, T. G.; Flory, P. J., Viscosity—molecular weight and viscosity—temperature relationships for polystyrene and polyisobutylene1, 2. *Journal of the American Chemical Society* **1948,** *70* (7), 2384-2395.

43. Strobl, G. R.; Strobl, G. R., *The physics of polymers*. Springer: 1997; Vol. 2.

44. Andrade, E. d. C., XLI. A theory of the viscosity of liquids.—Part I. *The London, Edinburgh, and Dublin Philosophical Magazine and Journal of Science* **1934,** *17* (112), 497-511.

45. Doolittle, A. K., Studies in Newtonian flow. II. The dependence of the viscosity of liquids on free-space. *Journal of Applied Physics* **1951,** *22* (12), 1471-1475.

46. Ferry, J. D., *Viscoelastic properties of polymers*. John Wiley & Sons: 1980.

47. Williams, M. L.; Landel, R. F.; Ferry, J. D., The temperature dependence of relaxation mechanisms in amorphous polymers and other glass-forming liquids. *Journal of the American Chemical society* **1955,** *77* (14), 3701-3707.

48. Kentish, S. E.; Scholes, C. A.; Stevens, G. W., Carbon dioxide separation through polymeric membrane systems for flue gas applications. *Recent Patents on Chemical Engineering* **2008,** *1* (1), 52-66.

49. Paul, D. R.; Yampol'skii, Y. P., *Polymeric gas separation membranes*. CRC press: 1993.

50. Porter, M. C., Handbook of industrial membrane technology. **1989**.

51. Erucar, I.; Keskin, S., Molecular Modeling of MOF-based Mixed Matrix Membranes. *Current Organic Chemistry* **2014,** *18* (18), 2364-2380.

52. Masel, R. I.; Masel, R. I., *Principles of adsorption and reaction on solid surfaces*. John Wiley & Sons: 1996; Vol. 3.

53. Langmuir, I., The adsorption of gases on plane surfaces of glass, mica and platinum. *Journal of the American Chemical society* **1918,** *40* (9), 1361-1403.

PART – A

Rubber, Rubber Composites and Rubber Blends

CHAPTER – 3

Validation of Decade-Old Force Fields of Rubber through Glass Transition Temperature Calculation by Microsecond Atomic-Scale Molecular Dynamics Simulation

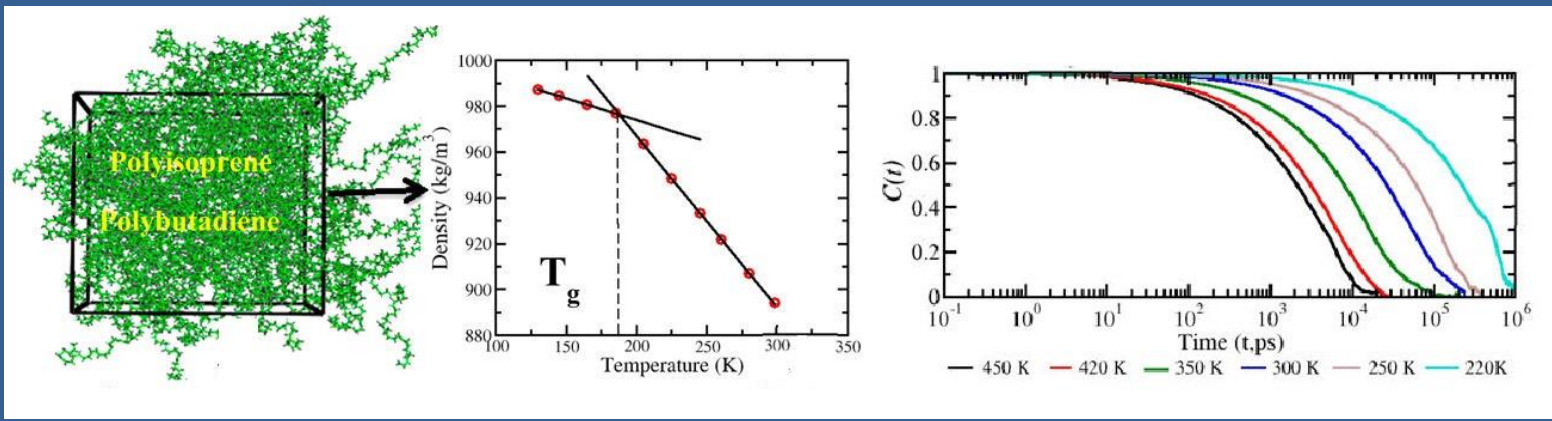

3.1 Introduction

Among elastomeric polymers, rubber holds a preeminent position with its versatile applications in the field of automotive, electronics and rubber goods industries. Rubbers found their optimum use as engineering material only in the form of composites i.e. various ingredients are added to rubber to make it processable. Processability is the ability to efficiently produce desirable functional products from industrial materials using standard industrial equipment. Efficiency here, refers to high quality of products and high productivity[1].

Natural rubber is made of polyisoprene chains and synthetic rubbers are made of polybutadiene, Styrene-butadiene (SBR), acrylonitrile butadiene block copolymer etc. However these polymers cannot be used in their virgin form in rubber/tire industry since they lack the mechanical strength and stiffness required in tire industries. So to overcome this problem, various ingredients are added to the elastomer matrix. The resulting composites (rubber matrix + additives) provide high strength to flexibility ratios, tear strength, abrasion resistance, and aging resistance to the tires[2]. Various additives include fillers, plasticizers, vulcanizing agents, accelerators, retarders, anti-degrading agents etc.

It has been observed that among various macroscopic polymer properties, T_g of the polymers shows a visible change upon addition of even small amount of nanoparticles.[3] And a small variation in T_g can lead to considerable changes in physical properties like hardness, density, viscosity, tensile and sheer elastic moduli[4]. Thus T_g can act as an important tool to modify and improve physical properties of polymers in order to explore novel applications. In fact, some applications in tire industries like wet traction, skid improvement, rolling resistance and wear of a passenger tire have shown to be greatly depend on polymer T_g.[5]

Being motivated by the industrial implications of T_g in rubber industries and its considerable impact on various thermodynamic properties, we have taken up the challenge to calculate T_g from atomistic simulations of 1,4-polyisoprene and 1,4-polybutadiene, the major constituents of natural and synthetic rubber. A clear understanding of glass transition phenomenon requires deep insights of the molecular level interactions[6]. MD simulation has long been a well-established technique in utilizing molecular details to predict macroscopic properties of advanced materials such as polymers and their composites[4,7,8]. Therefore, molecular dynamics simulation technique

has been used in this chapter to calculate T_g of these polymers. The quality of a polymer simulation largely depends on the accuracy of the force fields used. Force field parameters for polymers are mainly obtained from *ab initio* quantum chemical calculations on dimer, trimer or oligomer. Implementing these oligomeric potentials to polymer needs stringent testing and validation against experimental properties. Since the dynamics of polymers in composites is further influenced by the fillers, it becomes even more essential to validate the force fields for pure polymers first, before using them for complex systems like composites. Considering the fact that a properly validated force field is a prerequisite for any simulation, we also aim at validating the existing force fields of rubber so that they can be undoubtedly used in any simulation of rubber or it's composite. Such validation can be achieved by calculating various physical properties of polymers using those force fields and then comparing calculated values with their corresponding experimental counterparts. We have also tuned and refined some force field parameters by performing quantum chemical calculations in order to reproduce accurate density and T_g compared to experiments.

Two decades old force fields of 1,4-polybutadiene (PB) and 1,4-polyisoprene (PI) for both all-atomistic and united-atom models are already available in literature. Mattice et al.[9] in 1991 used modified version of CHARMM 2.1A[10] force field, in which some bond angles and torsions were adapted from the work of De Rosa et al.[11] They simulated single chain of trans-PB[9] and trans-PI[12] confined in crystalline channels and observed coupled conformational transitions in the chain backbone. Li and Mattice characterized local motions of cis-PB as a function of temperature and compared single chain properties with that of the bulk.[13] Moe and Ediger used CFF91 force field to investigate local dynamics of cis-PI in solution[14] and melts[15]. They observed that most of the conformational transitions at smaller length scales in PI chains are cooperative transitions. Colmenero et al.[16] employed Polymer Consortium Force field (PCFF) to understand methyl-group dynamics in PI. They calculated average energy barriers for methyl group reorientations and deduced that these orientations are affected by non-bonded interactions. These force fields were then further employed in many simulation studies mostly focusing on local-structural and conformational transitions in the chains of PB and PI.[17,18,19,20] All these are semi-empirical force fields being designed to represent general liquid-crystalline or polymeric bulk phase properties.

The very first attempt of developing a force field specifically for PB and PI was made by Smith and Paul for PB[21] and Faller et al. for PI[22]. Smith and Paul in 1998 developed united-atom force field for cis-PB using *ab initio* quantum chemical calculations. In the same study, they compared their results with the RIS model predictions of Mark[23], Flory et al.[24] and performed MD simulations to compare calculated properties with experiments. These parameters had been refined by Smith et al.[25] They increased energies of some of the torsional barriers to slow down the rate of conformational transitions. This refined force field had been employed by Harmandaris et al. to united atom model of cis-PI, for understanding the self-diffusion properties of cis-PI oligomer melts.[26] Temperature dependence of densities, diffusion coefficients and chain end free volume was analyzed in this study. Faller et.al in 2001 developed force field for all-atomistic model of trans-PI using *ab initio* quantum calculations and automatic simplex parameterization technique. They calculated end to end vector and bond vector correlation functions to analyze local structural characteristics. In the same study, they mapped their all-atomistic model to a generic bead spring model to get insights of the global dynamics of PI melts. Since their parameterization, these quantum chemically derived force fields[21,22,25] have been unanimously used in many simulation studies[27,28,29] including the recent ones.[30,31,32]

As can be seen, these force fields were parameterized more than a decade ago, as per the computational power available at that time, their complementary simulations either involved oligomers,[22,26] shorter simulation runs of a few nanoseconds,[21,25] or simulations only at higher temperatures[22,25]. Since polymers are macromolecules containing large number of degrees of freedom, a complete exploration of the phase space and consequent equilibration of polymer melts is tardy, particularly at temperatures below T_g. Hence proper equilibration of polymer melts in such shorter times, is likely improbable. Due to these factors, it becomes interesting to check if these force fields can reproduce macroscopic polymer properties at ambient temperature and pressure conditions in properly equilibrated polymer melts.

To pursue this aim, we have performed MD simulations of PB and PI using these force fields and calculated various static and dynamic properties like end to end distance, radius of gyration, density (ρ) along with glass transition temperature and compared them to their corresponding experimental values. Prediction of T_g from volumetric properties obtained from simulations has been employed in many studies. Han et al.[17] calculated T_g for polyisobutylene, cis-1,3-polybutadiene, polypropylene, and polystyrene. T_g had been marked as that temperature where

the slopes of straight line extrapolations of the specific volume−temperature curve change. Similar concept had been employed by Deazle et al.[33] and Fan et al.[34]to determine T_g of polysulfones and polycarbonates. Fried et al. calculated T_g for polyphosphazines[35], Fukuda & Kikuchi for polyisoprene.[36] All of these employed united atom (UA) or anisotropic united atom (AUA) models. Determination of T_g using fully atomistic models have also been reported[37,38,39,40]. But to our surprise, calculation of T_g of PB and PI has never been attempted using these force fields. A probable reason for this is that PB and PI have a simple chemical structure, so these are the very initial polymers studied by MD simulation. And because of this, the force fields are very old. Simulating polymers below T_g at that time was not computationally feasible and equilibrating polymers below T_g is still a computationally expensive process. To fill in this gap, we have calculated T_g of PB and PI using these force fields. We have also tuned some force field parameters by performing quantum chemical calculations to obtain improved density and T_g, hence providing a better and refined force field than the old one. Keeping in mind, the importance of equilibration in polymer simulations as discussed above, we have used a systematic procedure to ensure proper equilibration of the PB and PI melts, which is discussed in section 2. Micro-seconds of simulations have been performed both above and below T_g to ensure complete equilibration of melts. To make sure that equilibration has been achieved through our procedure, we have also calculated end to end distance and vector autocorrelation functions. Both united-atom and all-atom models have been simulated, to compare the results obtained from both the models. This way, further as per application and system size, researchers can chose united-atom or all-atom force field from our work. So here, in one hand we summarize all the force-field parameters available in the literature for PB and PI, tuned them as required and in the other hand microsecond MD simulations have been performed to precisely determine T_g. Besides development of force field of industrially relevant polymers we have used a novel protocol based on simulated annealing (SA) to equilibrate the polymer melts in different temperatures ranging above and below T_g.

3.2 Polymers, models studied and simulation methodology

Rubber is primarily of two types, natural rubber and synthetic rubber. Chemically natural rubber is cis-1,4-polyisoprene or trans-1,4-polyisoprene (*gutta percha*). Cis-1,4-polybutadiene is the main component of synthetic butadiene rubber or styrene butadiene rubber (SBR). However in

all types of rubber, traces of other isomers are always present.[41],[42] Hence a complete force field for rubber must include both cis and trans isomers of PB and PI. A flowchart showing all the polymers and models studied in the paper is given in Figure 3.1

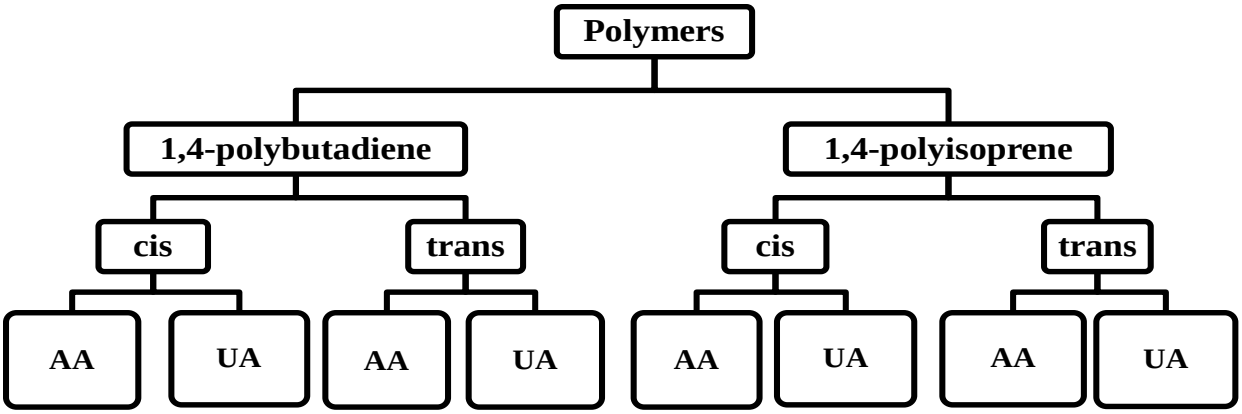

***Figure* 3.1:** Flowchart featuring a total of eight systems, all-atomistic (AA) and united-atom (UA) models of PB and PI studied.

A total of 8 systems have been studied featuring all-atom and united-atom models of cis and trans isomers of PB and PI. For all systems, we chose a chain length of 32-mer, which has been previously optimized for PB to reproduce various thermodynamic and conformational properties.[27] Total number of atoms in all the cases was approximated to 20000. Total potential energy of the systems included the sum of bonded and non-bonded interaction potentials. Bonded interactions include harmonic bond, angle potential, proper dihedral potential of both periodic and Ryckaert−Bellemans[43] forms, improper dihedral potential. Non bonded interactions consisted of Lennard−Jones (LJ) potential and Coulomb electrostatic interactions. All the potential forms were used as implemented in Gromacs-4.6.3 code[44]. For all systems, intramolecular non-bonded interactions have been counted for atoms separated by three and more than three bonds. All 1,4 interactions (LJ and Coulomb) were scaled down by a fudge factor of 0.5. The simulations have been performed using MD code Gromacs-4.6.3. in isobaric-isothermal ensemble (*NpT*) with periodic boundary conditions applied in all three directions. All bonds were constrained using LINCS[45] algorithm so that we can use a time step of 2 fs. The Reaction field method[46] was used for computing electrostatic interactions beyond the cut off (1.2 nm) with a dielectric constant of 3.5 for PB and 4 for PI. Berendsen thermostat with a coupling

constant of 0.1 ps and barostat with a coupling constant of 2 ps were used[47]. All systems have been simulated at 298K and 1 bar pressure to compare obtained densities at room temperature with experimental values.

Glass transition temperature for all eight systems has been evaluated from temperature dependence of the polymer density[39]. All samples were stepwise cooled from 120K above to 100K below experimental T_g. At each temperature, equilibrated density (ρ) was calculated by applying the protocol discussed in Section 3.3. Glass transition temperature was then calculated as the temperature marking discontinuity in the slope of density-temperature (ρ-T) curves.

3.3 Equilibration procedure

As stated in Introduction section, we followed a systematic procedure to achieve proper equilibration of the polymer melts. Conceptually, a good relaxation strategy should be able to bring all the possible initial structures generated, to a reasonable low-energy state[13]. Hence, we employed convergence of potential energy of the system as a criterion to ensure proper relaxation and subsequent equilibration of the melts. To the best of our knowledge, this equilibration protocol has never been used before in polymer melt simulations. To start with, energy minimized chains of 32-mer were randomly packed in a simulation cell. Initial energy minimization of the melt was followed by *NpT* production run, till a constant density is obtained. A drop in potential energy was observed during production run as shown in Figure 3.3. For better sampling of the phase space and to speed up the relaxation of chains, simulated annealing (SA) was done for 200 ns in *NpT* ensemble in which a melt at a particular temperature was stepwise heated and cooled back to the same starting temperature with a temperature step of 20 K and time step of 2 ns yielding a cooling rate of 10.0 Kns^{-1}. We have initially optimized this rate of heating and cooling. As the polymers studied here are based on aliphatic hydrocarbons, there are less number of interaction sites (and no large interactions like hydrogen bonds, electrostatics), therefore the employed rate of heating and cooling are relatively fast. The last snapshot of SA was used as the input for next *NpT* simulation. This production run lasted for several nanoseconds till density again converged. However the drop in potential energy was still observed. So SA step was repeated. These simulated annealing cycles were run in canonical ensemble (NVT) with same annealing parameters. The last snapshot of this SA cycle was then

served as an input for next *NpT* production run. Same cycle (SA followed by *NpT* and then SA) was repeated several times till the convergence criterion for potential energy was achieved. The schematic of the equilibration protocol is shown in Figure 3.2

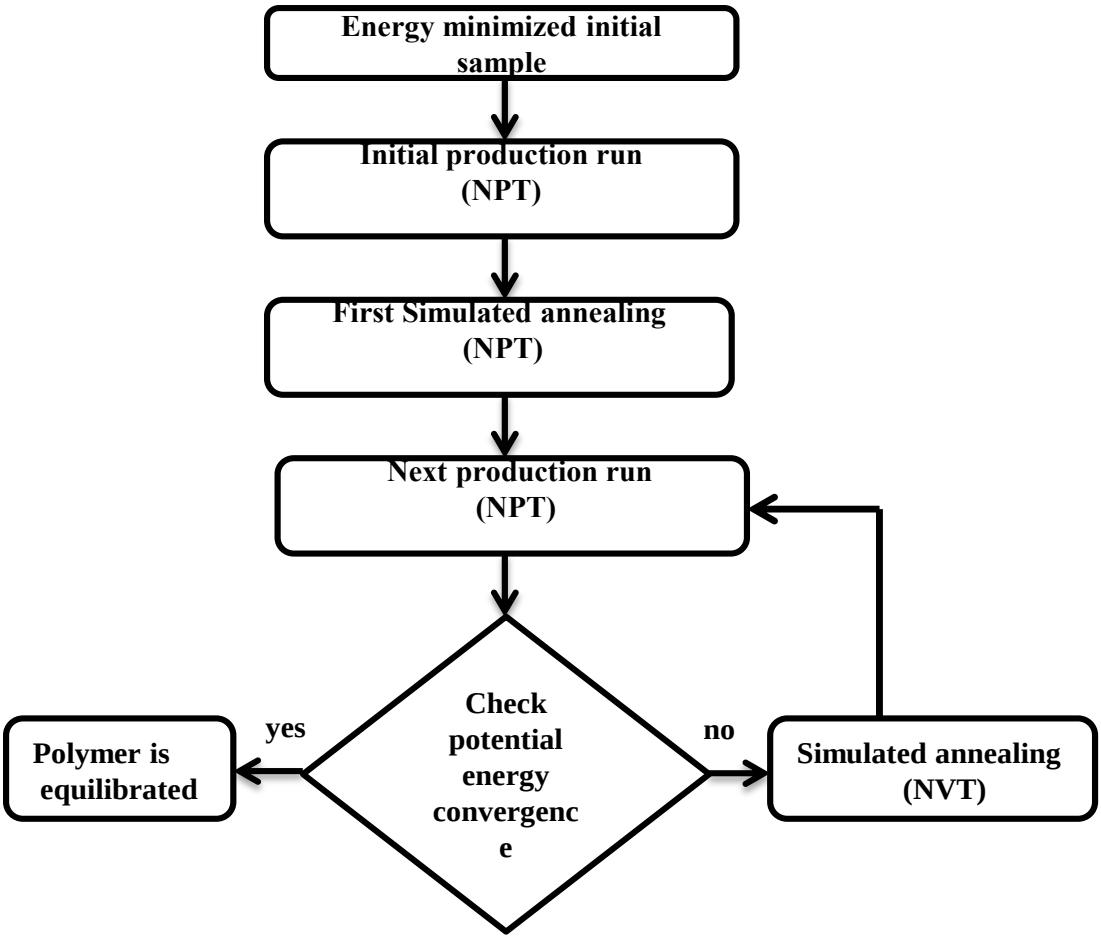

***Figure* 3.2:** Equilibration protocol followed during all simulations.

As expected, these simulations extended to micro seconds, particularly for all atomistic models. The long time trajectories from the last production run have been used for analysis. We present here a demonstrative example of potential energy convergence with time for cis-PB (all-atom) at 205 K and 185 K (inset) in Figure 3.3.

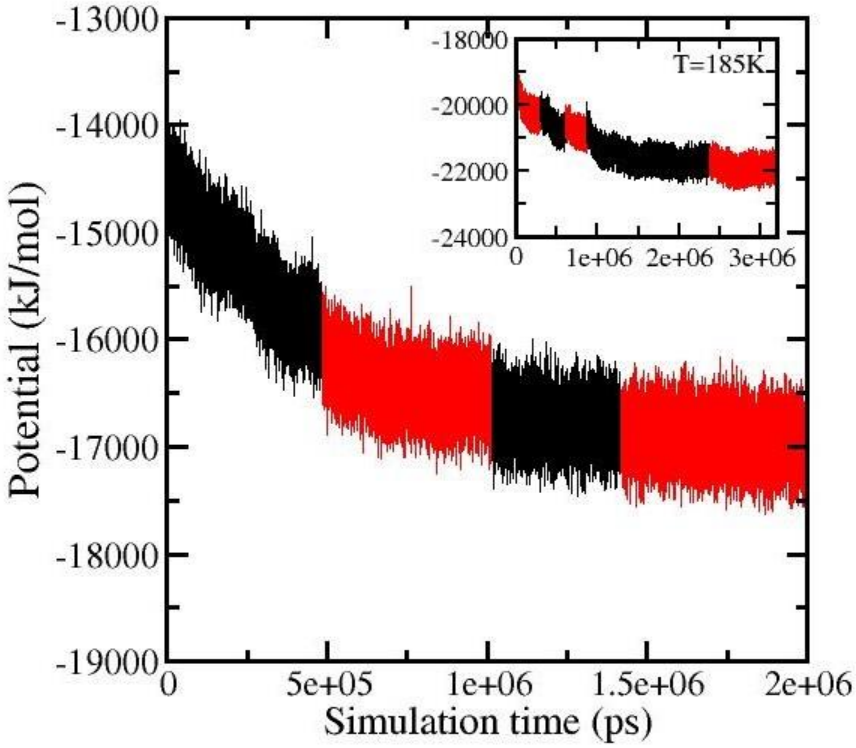

***Figure* 3.3:** Equilibration of polymers: Demonstrative example of potential energy convergence with time. System is cis-1,4-polybutadiene (all-atom) at 205 K and 1 bar. Potential energy convergence at 185 K and 1 bar (temperature below Tg) is shown in the inset. Color change indicates a simulated annealing step in between.

To endorse the fact that complete equilibration has been achieved through our strategy, we determined long length scale orientational characteristics of systems by calculating end to end distance and vector autocorrelations, C(t). The time autocorrelation for end to end vector[48] is given by the following equation,

$$C(t) = \frac{\langle R(\tau)R(\tau+t)\rangle - \langle R\rangle^2}{\langle R^2\rangle - \langle R\rangle^2} \qquad \textbf{(3.1)}$$

For an isotropic collection of chains in a polymer melt, the average end to end vector, $\langle \vec{R} \rangle = 0$, thus equation 3.1 reduced to equation 3.2.

$$C(t) = \frac{\langle R(\tau)R(\tau+t)\rangle}{\langle R^2\rangle} \qquad \textbf{(3.2)}$$

For end to end distance autocorrelation we used magnitude of R ($\sqrt{\vec{R}.\vec{R}}$) instead of $\vec{R}$ in equation 3.1. *C(t)* was computed from the trajectories of the last production run at each temperature. Every snapshot of the trajectory was considered as the time origin (τ). At all temperatures, the autocorrelations approached to zero, demonstrating complete loss of orientation for chains and consequent relaxation of the melts. *C(t)* for cis-PB (all-atom) at different temperatures is shown in Figure 3.4.

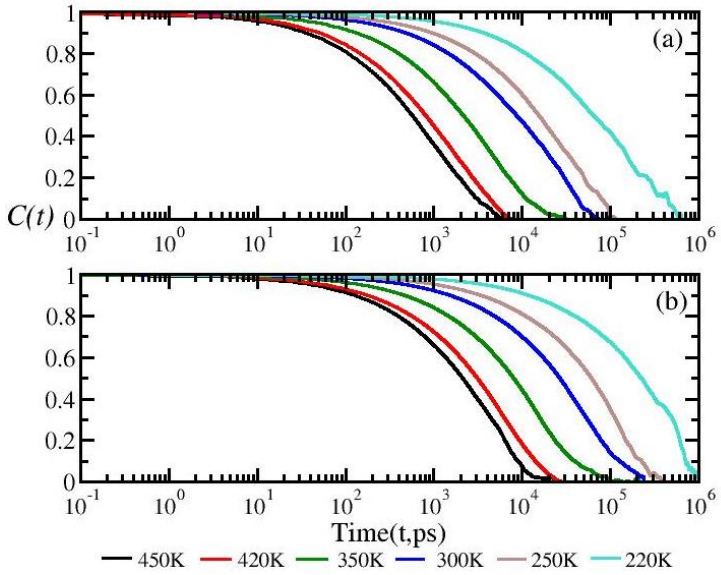

***Figure* 3.4:** Decay of end to end distance autocorrelation (a), given by Equation 3.1 and end to end vector autocorrelation (b), given by Equation 3.2.

It has been observed that end to end distance of chains relaxes faster than end to end vector. We have also observed the evolution of average chain length dimensions i.e. average end to end distance and radius of gyration (R_g) with time in last 1μs of the production run for cis-PB (all-atom at 220 K and deduced that both properties got equilibrated, showing only fluctuations around a constant value as shown in Figure 3.5.

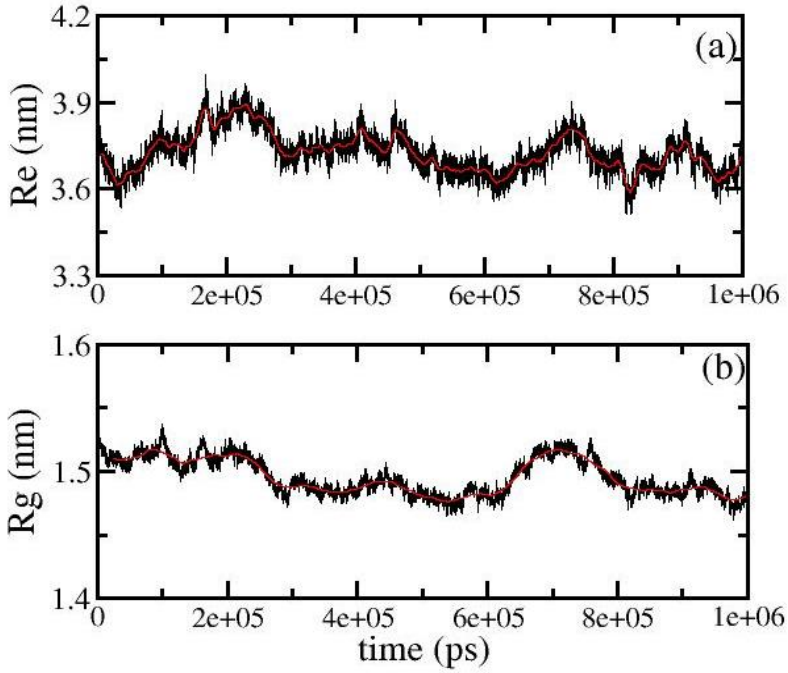

***Figure* 3.5:** (a) End to end distance, Re (b) Radius of gyration, Rg of cis-PB (all-atom) at 220K and 1bar as a function of time (last 1μs of production run)

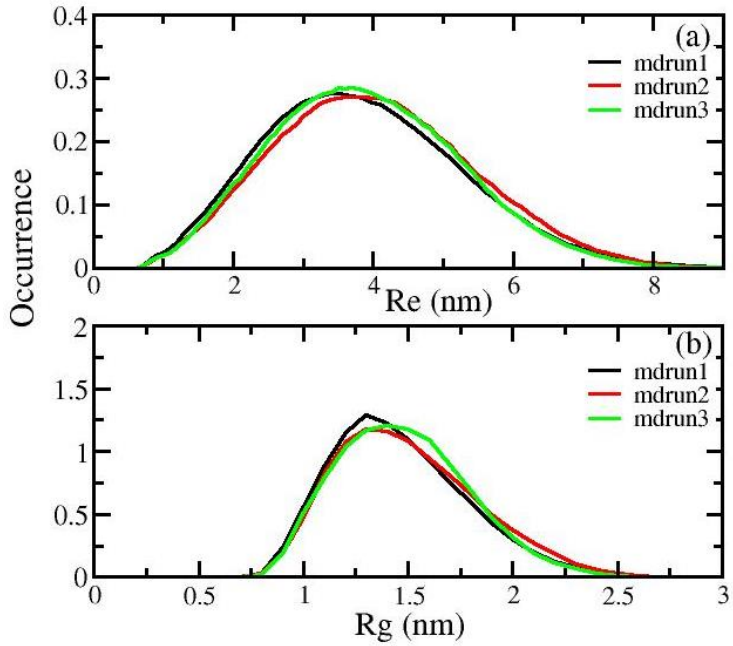

***Figure* 3.6:** Distribution of end to end distance, Re (a) and radius of gyration (b) in last three consecutive production runs of cis-PB (all-atom) at 220K and 1 bar

The overlapping of R_g and R distributions as shown in Figure 3.6 taken from last three consecutive production runs also supports the equilibration of average chain characteristics. As can be seen from Figure 3.4, end to end vector autocorrelation functions at temperatures, even higher than T_g took micro-seconds for complete decay, This strengthens the fact that micro-seconds of simulation are crucial for proper equilibration of PB and PI melts. The other thing that has to be emphasized here is that, mere convergence of density cannot assure that a polymer melt is equilibrated. We have observed that the total energy of the systems continues to drop till micro-seconds of simulation. At temperatures below T_g, polymer remains in glassy state and because of very slow dynamics, complete loss of end to end vector autocorrelation is practically not possible to achieve with in feasible computational times. Therefore at such temperatures, our equilibration criterion of potential energy convergence would be an optimum way to assure equilibration at temperatures below T_g (see inset of Figure 3.3). By following our procedure, we achieved potential energy convergence at about 3 μs for cis PB (all-atom) at 185K, which is a below T_g point as shown in inset of Figure 3.3.

3.4 Results and discussions

3.4.1) Description of the force fields

This section contains a detailed description of the force fields which are validated and in some cases tuned:

Cis and trans 1,4-polybutadiene (united atom model)

The force field validated here is the united atom force field proposed by Smith & Paul21. Since its parameterization, this force field is redundantly used and proved robust enough to reproduce various structural and dynamic properties27,30,49 of cis-PB. The chemical structures of cis-PB and trans-PB are shown in Figure 3.7 and Figure 3.8 respectively.

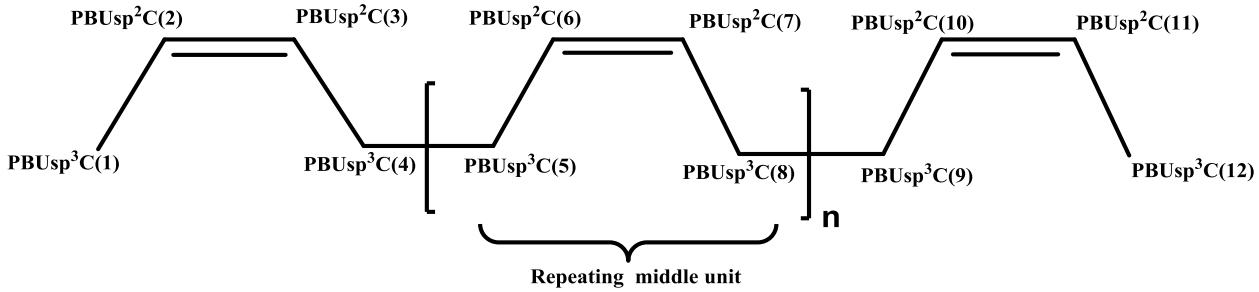

***Figure* 3.7:** Chemical structure of cis-1,4-polybutadiene (united-atom model). Naming of atoms is done in such a way that it represents the type of carbon atom in that polymer. e.g. **PBUsp^{3}C** stands for sp^3 hybridized carbon of polybutadiene(**PB**)-united-atom(**U**).

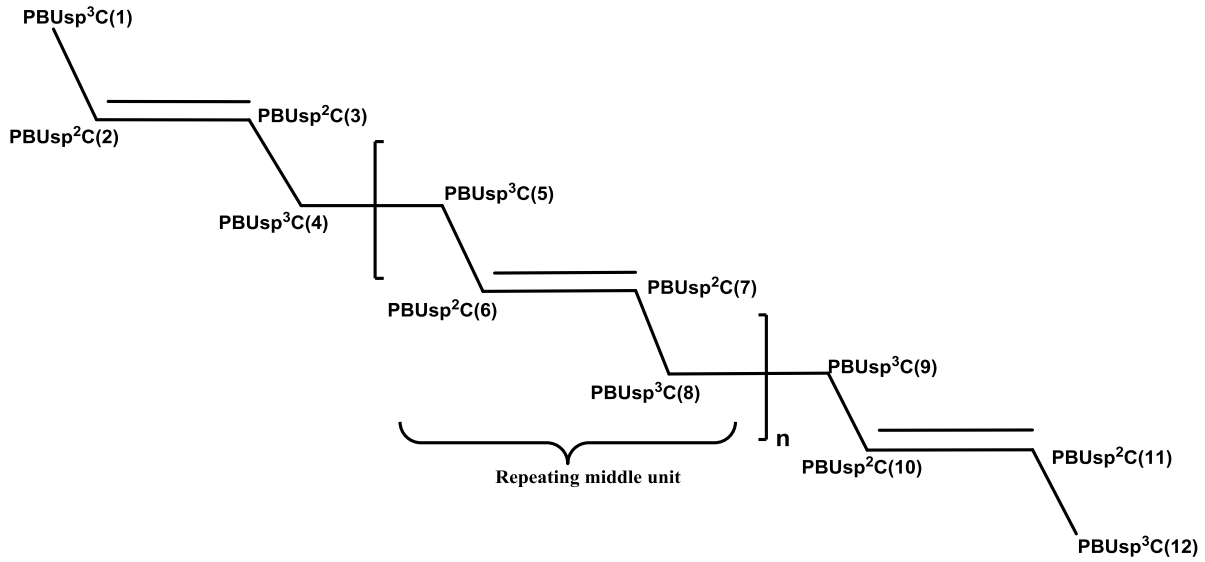

***Figure* 3.8:** Chemical structure of trans-1,4-polybutadiene (united-atom model). Naming pattern**:** **PBUsp^{2}C** stands for sp^2 hybridized carbon of polybutadiene(**PB**)-united-atom(**U**).

We used the same bonded and non-bonded potentials for cis and trans isomers except that a connecting dihedral is different as is given in the reference. A detailed description of force field parameters is given in Table 3.1. Potential functions corresponding to all bonded and non-bonded interactions are given in the force field Table 3.1. No tuning is needed for this force field as it reproduced the experimental density and T_g.

***Table* 3.1:** Force field parameters used for united-atom models of cis-PB and trans-PB. The names of the atoms corresponds to those used in Figure 3.6 and 3.7

Non bonded

Lennard-Jones potential $V_{ij} = 4\varepsilon\left[\left(\frac{\sigma_{ij}}{r_{ij}}\right)^{12} - \left(\frac{\sigma_{ij}}{r_{ij}}\right)^{6}\right]$

i	j	σ_{ij} (nm)	ε_{ij} (kJmol^{-1})
PBUsp^{3}C	PBUsp^{3}C	0.401	0.392
PBUsp^{2}C	PBUsp^{2}C	0.338	0.418
PBUsp^{3}C	PBUsp^{2}C	0.379	0.425

Rigid bonds $V_{ij} = \frac{1}{2}k_{ij}\left(l - l_0\right)^2$

i	j	l_0 (nm)	k_{ij} (kJmol^{-1}nm^{-2})
PBUsp^{3}C	PBUsp^{2}C	0.150	0.0
PBUsp^{2}C	PBUsp^{2}C	0.134	0.0
PBUsp^{3}C	PBUsp^{3}C	0.153	0.0

Angle bending $V_{ijk} = \frac{1}{2}k_{ijk}\left(\theta - \theta_0\right)^2$

i	j	k	θ (deg)	k_{ijk} (kJmol^{-1}rad^{-2})
PBUsp^{3}C	PBUsp^{3}C	PBUsp^{2}C	111.650	481.367
PBUsp^{3}C	PBUsp^{2}C	PBUsp^{2}C	125.890	374.210

Torsions

Ryckaert-Bellemans dihedrals $V_{rb(\phi ijkl)} = \sum_{n=0}^{5} C_n\left(\cos\left(\phi - 180\right)\right)^n$

i	j	k	l	C_0(kJmol^{-1})	C_1(kJmol^{-1})	C_2(kJmol^{-1})	C_3(kJmol^{-1})	C_4 (kJmol^{-1})	C_5(kJmol^{-1})
PBUsp^{3}C	PBUsp^{2}C	PBUsp^{2}C	PBUsp^{3}C	101.253	0.0	-101.253	-4.015	-1.614	0.0

PBUsp^{3}C PBUsp^{3}C PBUsp^{2}C PBUsp^{2}C (cis)	2.411	-2.308	6.387	9.868	-4.415	-11.609
PBUsp^{3}C PBUsp^{3}C PBUsp^{2}C PBUsp^{2}C (trans)	0.655	11.966	4.423	-12.754	-1.368	-3.036
PBUsp^{2}C PBUsp^{3}C PBUsp^{3}C PBUsp^{2}C	-12.974	-18.391	1.473	20.085	1.121	8.300

- Terminal units have same parameters as middle repeating units

Cis and trans-polybutadiene (all-atom model)

All-atomistic models for cis-PB and trans-PB have been shown in Figure 3.9 and Figure 3.10 respectively.

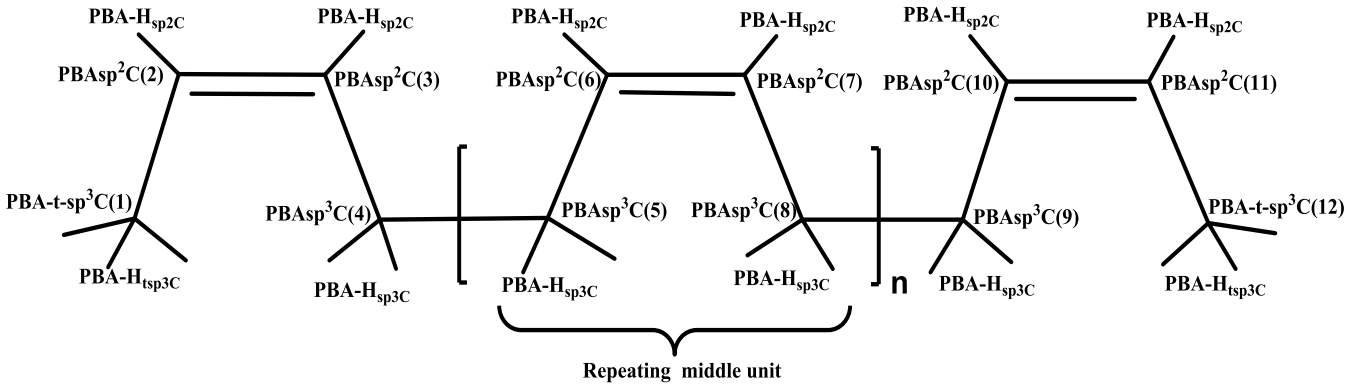

***Figure* 3.9:** Chemical structure of cis-1,4-polybutadiene (all-atomistic model). The start-terminal unit, middle unit and end-terminal unit are shown. Naming pattern: PBA-t-sp3C stands for sp3 hybridized carbon of terminal units of polybutadiene (PB)-all-atom (A).

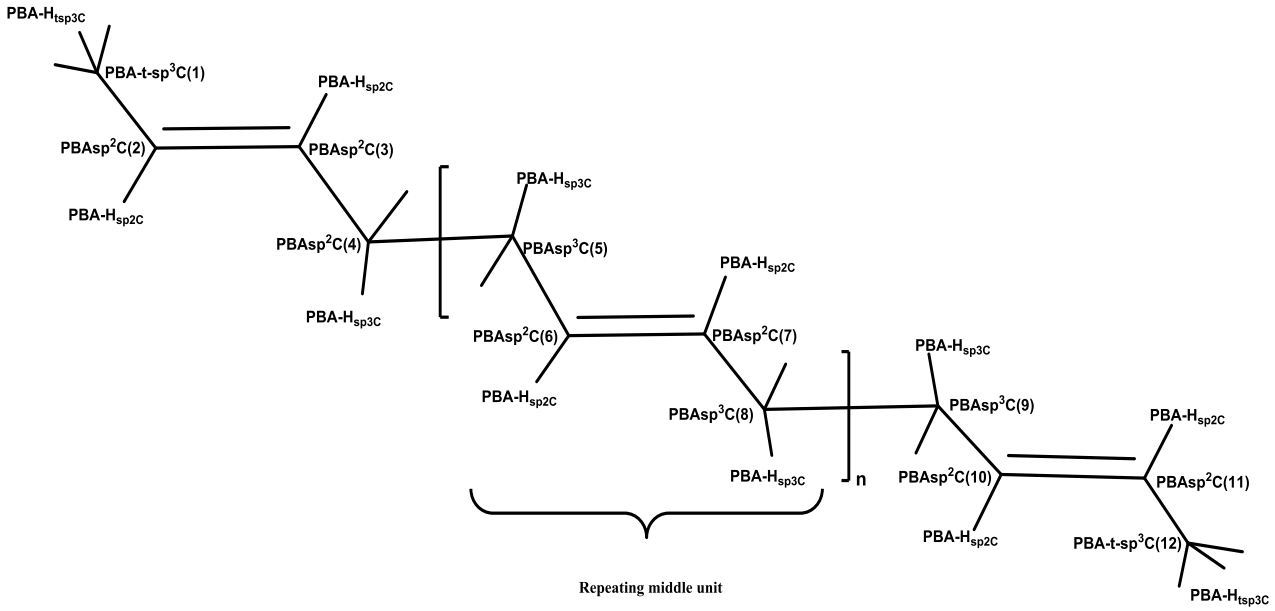

***Figure* 3.10:** Chemical structure of trans-1,4-polybutadiene (all-atom model). Naming pattern**:** **PBA-t-sp^{3}C** stands for sp^3 hybridized carbon of terminal unit of polybutadiene (**PB**)-all-atom (**A**).Charges are shown in Table 3.2

***Table* 3.2:** Charges used for all-atomistic models of cis-PB and trans-PB. The names of the atoms correspond to those used in Figure 3.9 and 3.10

Atom (cis and trans-1,4-polybutadiene)	Charge (q) e
PBAsp^{3}C	-0.120
PBAsp^{2}C	-0.115
PBAsp^3-t-C	-0.180
PBA-H$_{sp3C}$	0.06
PBA-H$_{sp2C}$	0.115
PBA-H$_{sp3tC}$	0.06

Convinced by the satisfactory agreement of T_g obtained from united atom model (UA) with the experiments, we adopted the same bonding parameters for all-atomistic force field as well. Non-bonded parameters (sigma, epsilon) and charges have been taken from OPLS-AA[50,51] force field. Along with UA force field parameters, the remaining hydrogen containing bonds, angles, dihedrals and improper dihedral values have also been taken from OPLS-AA force field. OPLS combination rule which applies geometric mean to the two pairs is used to calculate the non-bonded pair interactions. A detailed description of the force field parameters and potential forms applied is given in Table 3.3.

***Table* 3.3:** Force field parameters used for all-atomistic models of cis-PB and trans-PB. The names of the atoms correspond to those used in Figure 3.9 and 3.10

Non bonded

Lennard-Jones potential $$V_{ij} = 4\varepsilon\left[\left(\frac{\sigma_{ij}}{r_{ij}}\right)^{12} - \left(\frac{\sigma_{ij}}{r_{ij}}\right)^{6}\right]$$

	σ (nm)	ε (kJmol^{-1})
PBAsp^{3}C	0.350	0.276
PBAsp^{2}C	0.355	0.318
PBAsp^3$_t$C	0.350	0.276
PBA-H$_{sp3C}$	0.250	0.126
PBA-H$_{sp2C}$	0.242	0.126
PBA-H$_{sp3tC}$	0.250	0.126

Rigid bonds $$V_{ij} = \frac{1}{2}k_{ij}\left(l - l_0\right)^2$$

i	j	l_0 (nm)	k_{ij} (kJmol^{-1}nm^{-2})
PBAsp^{3}C	PBAsp^{2}C	0.150	0.0
PBAsp^{2}C	PBAsp^{2}C	0.134	0.0

PBAsp^{3}C	PBAsp^{3}C	0.153	0.0
PBAsp^{3}C	PBA-H$_{sp3C}$	0.109	0.0
PBAsp^{2}C	PBA-H$_{sp2C}$	0.108	0.0

Angle bending

$$V_{ijk} = \frac{1}{2} k_{ijk} (\theta - \theta_0)^2$$

i	j	k	θ (deg)	k_{ijk} (kJmol^{-1}rad^{-2})
PBAsp^{3}C	PBAsp^{2}C	PBAsp^{2}C	125.890	374.210
PBAsp^{3}C	PBAsp^{3}C	PBAsp^{2}C	111.650	481.367
PBA-H$_{sp3C}$	PBAsp^{3}C	PBAsp^{2}C	111.650	481.367
PBAsp^{3}C	PBAsp^{2}C	PBA-H$_{sp2C}$	117.000	292.880
PBAsp^{2}C	PBAsp^{2}C	PBA-H$_{sp2C}$	120.00	292.880
PBA-H	PBA-C	PBA-H	109.500	292.880

Torsions

Ryckaert-bellemans dihedrals

$$V_{rb(\phi ijkl)} = \sum_{n=0}^{5} C_n (\cos(\phi - 180))^n$$

i	j	k	l	C_0 (kJmol^{-1})	C_1 (kJmol^{-1})	C_2 (kJmol^{-1})	C_3 (kJmol^{-1})	C_4 (kJmol^{-1})	C_5 (kJmol^{-1})
PBAsp^{3}C	PBAsp^{2}C	PBAsp^{2}C	PBAsp^{3}C	101.253	0.0	-101.253	-4.015	-1.614	0.0
PBAsp^{3}C (cis)	PBAsp^{3}C	PBAsp^{2}C	PBAsp^{2}C	2.411	-2.308	6.387	9.868	-4.415	-11.609
PBAsp^{3}C (trans)	PBAsp^{3}C	PBAsp^{2}C	PBAsp^{2}C	0.655	11.966	4.423	-12.754	-1.368	-3.036
PBAsp^{2}C	PBAsp^{3}C	PBAsp^{3}C	PBAsp^{2}C	-12.974	-18.391	1.473	20.085	1.121	8.300
PBA-H$_{sp3C}$	PBAsp^{3}C	PBAsp^{2}C	PBA-H$_{sp2C}$	0.665	1.996	0.0	-2.661	0.0	0.0

PBA-H_{sp3C}	PBAsp^{3}C	PBAsp^{2}C	PBAsp^{2}C	-0.778	-2.335	0.0	3.113	0.0	0.0
PBA-H_{sp3C}	PBAsp^{3}C	PBAsp^{3}C	PBAsp^{2}C	0.766	2.297	0.0	-3.063	0.0	0.0
PBA-H_{sp3C}	PBAsp^{3}C	PBAsp^{3}C	PBA-H_{sp3C}	0.628	1.883	0.0	-2.510	0.0	0.0

Improper dihedrals $V_{id(\phi ijkl)} = \frac{1}{2} k_{ijkl} (\phi - \phi_0)^2$

i	j	k	l	ϕ (deg)	k_{ijkl} (kJmol^{-1}rad^{-2})
PBA-H_{sp2C} (cis)	PBAsp^{2}C	PBAsp^{2}C	PBA-H_{sp2C}	0	62.760
PBA-H_{sp2C} (trans)	PBAsp^{2}C	PBAsp^{2}C	PBA-H_{sp2C}	180	62.760

- Terminal units have same bonded parameters as middle repeating units

Cis and trans 1,4-polyisoprene (united atom model)

This force field is adapted from the work of Harmandris et al.[26] It has also been used previously to understand the local dynamics[28] and behavior of thin PI films between silica surfaces[52]. Chemical structures of united atom models of cis-PI and trans-PI have been shown in Figure 3.11 and Figure 3.12.

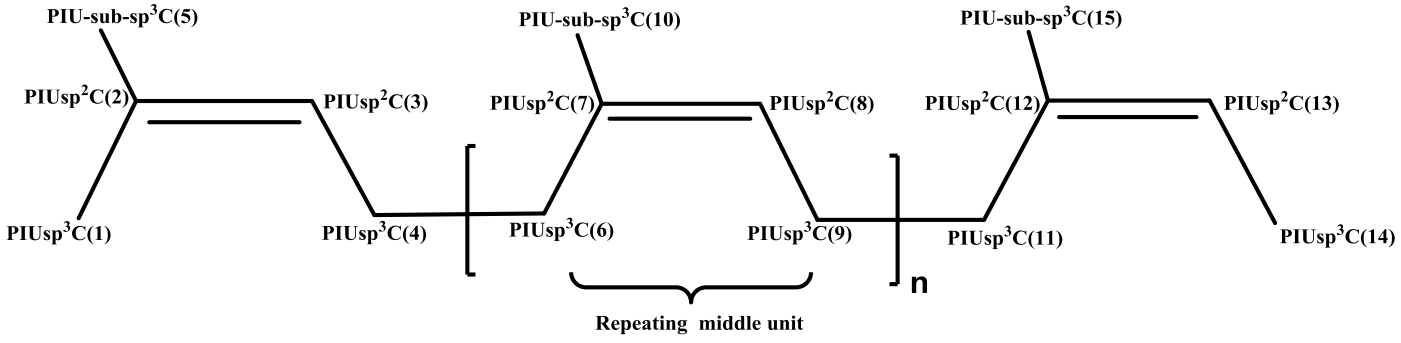

***Figure* 3.11:** Chemical structure of cis-1,4-polyisoprene(united-atom model). Naming pattern: PIUsp3C stands for sp3 hybridized carbon of polyisoprene (PI)-united-atom(U).

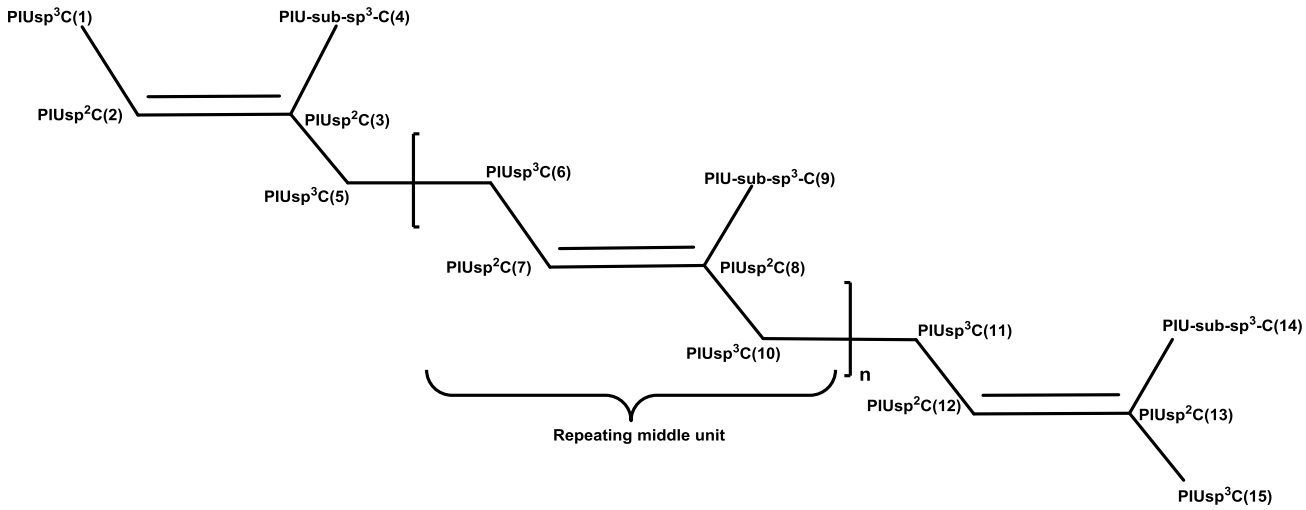

***Figure* 3.12:** Chemical structure of trans-1,4-polyisoprene(united-atom model). Naming pattern: PIUsp2C stands for sp_2 hybridized carbon of polyisoprene (PI)-united-atom (U).

Same force field has been used for both cis and trans models except a connecting dihedral, as is given in smith's paper[25]. Detailed description of the force field parameters is given in Table 3.4. This force field too does not require any tuning and the calculated density and T_g values matched well with the experiments.

***Table* 3.4:** Force field parameters used for united-atom models of cis-PI and trans-PI. The names of the atoms corresponds to those used in Figure 3.11 and 3.12

Non bonded			
Lennard-Jones potential		$V_{ij} = 4\varepsilon\left[\left(\frac{\sigma_{ij}}{r_{ij}}\right)^{12} - \left(\frac{\sigma_{ij}}{r_{ij}}\right)^{6}\right]$	
i	j	σ_{ij} (nm)	ε_{ij} (kJmol^{-1})
PIUsp^{2}C	PIUsp^{2}C	0.338	0.418
PIUsp^{2}C	PIUsp^{3}C	0.379	0.425
PIUsp^{2}C	PIU-sub-sp^{3}C	0.379	0.630
PIUsp^{3}C	PIUsp^{3}C	0.401	0.392
PIUsp^{3}C	PIU-sub-sp^{3}C	0.401	0.610
PIU-sub-sp^{3}C	PIU-sub-sp^{3}C	0.401	0.948
PIUsp^{3}tC(4)	PIU-sub-sp^{3}C(10)	0.401	0.0304

Rigid bonds $V_{ij} = \frac{1}{2} k_{ij} (l - l_0)^2$

i	j	l_0 (nm)	k_{ij} (kJmol^{-1}nm^{-2})
PIUsp^{3}C	PIUsp^{2}C	0.150	0.0
PIUsp^{2}C	PIUsp^{2}C	0.134	0.0
PIUsp^{3}C	PIUsp^{3}C	0.153	0.0
PIU-sub-sp^{3}C	PIUsp^{2}C	0.150	0.0

Angle bending $V_{ijk} = \frac{1}{2} k_{ijk} (\theta - \theta_0)^2$

i	j	k	θ_0 (deg)	k_{ijk} (kJmol^{-1}rad^{-2})
PIUsp^{3}C	PIUsp^{2}C	PIUsp^{2}C	125.890	374.210
PIUsp^{3}C	PIUsp^{3}C	PIUsp^{2}C	111.650	481.367
PIU-sub-sp^{3}C	PIUsp^{2}C	PIUsp^{2}C	125.890	374.210

Torsions

Ryckaert-bellemans dihedrals $V_{rb(\phi ijkl)} = \sum_{n=0}^{5} C_n (\cos(\phi - 180))^n$

i	j	k	l	C_0(kJmol^{-1})	C_1(kJmol^{-1})	C_2(kJmol^{-1})	C_3(kJmol^{-1})	C_4(kJmol^{-1})	C_5(kJmol^{-1})
PIUsp^{3}C (cis)	PIUsp^{3}C	PIUsp^{2}C	PIUsp^{2}C	4.603	1.509	2.835	6.174	-2.666	-12.70
PIUsp^{3}C (trans)	PIUsp^{3}C	PIUsp^{2}C	PIUsp^{2}C	1.491	14.554	4.406	-16.221	-1.339	-3.014
PIUsp^{2}C	PIUsp^{3}C	PIUsp^{3}C	PIUsp^{2}C	-14.036	-20.662	1.410	23.314	1.188	8.400

Improper dihedrals $V_{id(\phi ijkl)} = \frac{1}{2} k_{ijkl} (\phi - \phi_0)^2$

i	j	k	l	ϕ_0 (deg)	k_{ijkl} (kJmol^{-1}rad^{-2})
PIUsp^{3}C	PIUsp^{2}C	PIUsp^{2}C	PIUsp^{3}C	0	160

(cis)					
PIUsp^{3}C (trans)	PIUsp^{2}C	PIUsp^{2}C	PIUsp^{3}C	180	160

- Terminal units have same bonded parameters as middle repeating units

Cis and trans 1,4-polyisoprene (all-atom model)

Faller et al. in 2001 developed all-atomistic force field for trans-1,4-polyisoprene. This force field has also been employed for both cis-PI[31] and trans-PI[29] simulations. They derived bonds, angles and torsional potentials using *ab initio* calculations while non-bonded parameters were derived from cyclohexene force field[53] using automatic simplex parameterization method. Since no charges were assigned to the atoms, the force field parameters are refined in this work to include the effect of the partial charges on the atoms. Chemical structures of cis and trans-PI are shown in Figure 3.13 and Figure 3.14.

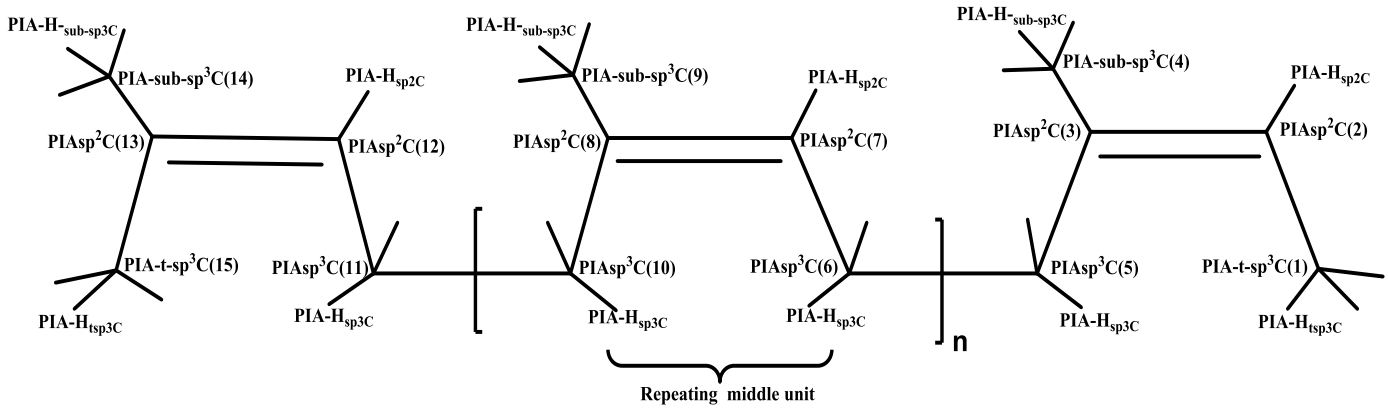

***Figure* 3.13:** Chemical structure of cis-1,4-polyisoprene(all-atom model). Naming pattern: **PIA-sub-sp^{3}C** stands for sp^3 hybridized carbon of methyl substituent of polyisoprene(**PI**)-all-atom(**A**).

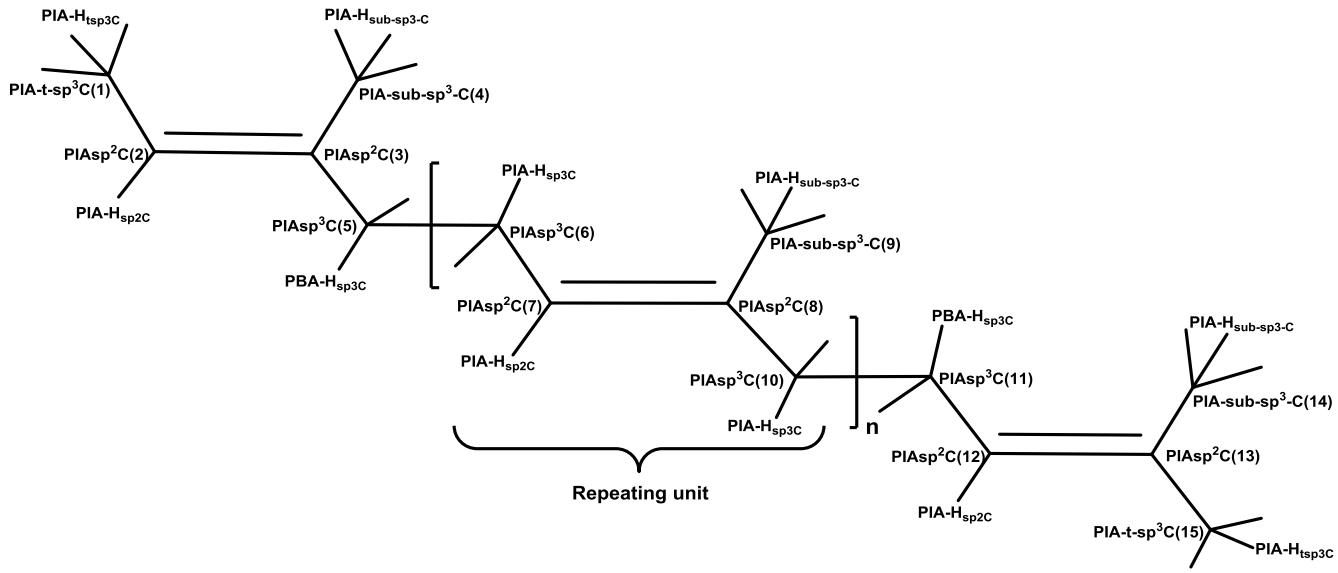

***Figure* 3.14:** Chemical structure of trans-1,4-polyisoprene(all-atom model). Naming pattern: **PIA-H$_{sp2C}$** stands for hydrogen attached to sp^2 hybridized carbon of polyisoprene(**PI**)-all-atom(**A**).

To start with, first of all partial charges on individual atoms were calculated using quantum chemical calculations with Gaussian 09 code[54]. For this, geometry optimization of PI-trimer with B3LYP functional and 6-311g basis set was done followed by charge calculations using CHELPG[55] method. Lorentz-Berthelot rules were used to calculate non-bonded pair interactions. After implementing complete force field along with charges, the proposed equilibration strategy was followed to obtain equilibrated density. But we observed that the resultant density so obtained was considerably (more than 4%) higher than the experimental value[56] of 910 kg/m^3 for cis-PI. Hence some parameters need to be tuned to obtain desired density. It was reported in Faller's paper that the non-bonded parameters were adapted from cyclohexene force field and the sigma value of hydrogen's was slightly reduced from 0.25 nm to 0.24 nm to obtain the experimental density. Thus to match our obtained density with the experimental value, we took the actual value by increasing the sigma of hydrogen's to 0.25 nm which is also the value in OPLS-AA force field for the hydrogen atoms. To optimize this sigma value, first of all we performed simulations of isoprene monomeric melt and calculated enthalpy of vaporization (ΔH_{vap}) to compare with the experimental value, and then we used this sigma value for the polymer. ΔH_{vap}[57] was calculated by Equation 3.3

$$\nabla H_{vap} = \left(\frac{-(V_{nb})}{n}\right) + RT \qquad \textbf{(3.3)}$$

Where Vnb is the sum of total non-bonded potential i.e. LJ and columbic, n is the total number of monomers taken, R is the gas constant and T is the temperature.

The calculated ΔHvap for isoprene melt at 298 K and 1 bar was 30.6 ± 0.5 kJ/mol and the corresponding experimental value[58] reported was 28.3 kJ/mol, thus showing satisfactory agreement with the experimental value. Hence we used this sigma value for hydrogen and calculated charges with other force field parameters (by Faller et al.) to simulate glass transition of cis and trans-PI. Reproducibility of correct Tg for both isomers ratifies the tuning done for the force field. All force field parameters are given in Table 3.5. Calculated charges for cis-PI and trans-PI are shown in Tables 3.6 and 3.7 respectively.

***Table* 3.5:** Force field parameters used for all-atomistic models of cis-PI and trans-PI. The names and numbering of the atoms corresponds to those used in Figure 3.13 and 3.14.

Non bonded		
Lennard-Jones potential	$V_{ij} = 4\varepsilon\left[\left(\frac{\sigma_{ij}}{r_{ij}}\right)^{12} - \left(\frac{\sigma_{ij}}{r_{ij}}\right)^{6}\right]$	
	σ (nm)	ε (kJmol^{-1})
PIAsp^{3}C	0.311	0.313
PIAsp^{2}C	0.321	0.313
PIA-sub-sp^{3}C	0.311	0.313
PIA-t-sp^{3}C	0.311	0.313
PIA-H	0.250	0.2189
Rigid bonds	$V_{ij} = \frac{1}{2}k_{ij}(l - l_0)^2$	

i	j	l_0 (nm)	k_{ij} (kJmol^{-1}nm^{-2})
PIAsp^{3}C (6)	PIAsp^{2}C (7)	0.150	0.0
PIAsp^{2}C (7)	PIAsp^{2}C (8)	0.1338	0.0
PIAsp^{2}C (8)	PIA-sub-sp^{3}C (9)	0.151	0.0
PIAsp^{2}C (8)	PIAsp^{3}C (10)	0.1515	0.0
PIAsp^{3}C (10)	PIAsp^{3}C (11)	0.155	0.0
PIA-C	PIA-H	0.109	0.0

Angle bending $V_{ijk} = \frac{1}{2} k_{ijk} (\theta - \theta_0)^2$

i	j	k	θ_0 (deg)	k_{ijk} (kJmol^{-1}rad^{-2})
PIAsp^{3}C (6)	PIAsp^{2}C(7)	PIAsp^{2}C(8)	128.7	250
PIAsp^{2}C(7)	PIAsp^{2}C(8)	PIA-sub-sp^{3}C(9)	124.4	250
PIAsp^{3}C(7)	PIAsp^{2}C(8)	PIAsp^{3}C(10)	120.2	250
PIA-sub-sp^{3}C(9)	PIAsp^{2}C(8)	PIAsp^{3}C(10)	115.40	250
PIAsp^{2}C (8)	PIAsp^{3}C (10)	PIAsp^{3}C(11)	114.5	250
PIAsp^{3}C(10)	PIAsp^{3}C(11)	PIAsp^{2}C(12)	112.7	250
PIA-C	PIAsp^{3}C	PIA-H_{sp3C}	109.5	250
PIA-C	PIAsp^{2}C	PIA-H_{sp2C}	114.5	250
H	C	H	109.5	250

Torsions $V_{tor} = \sum_{i=1}^{3} k_{ijkl}\left[1-\cos\left(i\left(\tau-\tau_0\right)\right)\right]$

i	j	k	l	τ_0 (deg)	k_{ijkl} (kJmol^{-1})	Periodicity (i)
PIAsp^{2}C (7)	PIAsp^{2}C (8)	PIAsp^{3}C (10)	PIAsp^{3}C (11)	0	2.6	1
PIAsp^{2}C (7)	PIAsp^{2}C (8)	PIAsp^{3}C (10)	PIAsp^{3}C (11)	0	-3.7	2
PIAsp^{2}C (7)	PIAsp^{2}C (8)	PIAsp^{3}C (10)	PIAsp^{3}C (11)	0	5.0	3
PIAsp^{2}C (8)	PIAsp^{3}C (10)	PIAsp^{3}C (11)	PIAsp^{2}C (12)	180	4.85	1
PIAsp^{2}C (8)	PIAsp^{3}C (10)	PIAsp^{3}C (11)	PIAsp^{2}C (12)	180	7.05	3
PIAsp$_3$C (10)	PIAsp$_3$C (11)	PIAsp$_2$C (12)	PIAsp$_2$C (13)	0	-10.55	1
PIAsp$_3$C (10)	PIAsp$_3$C (11)	PIAsp$_2$C (12)	PIAsp$_2$C (13)	0	-6.15	2
PIAsp$_3$C (10)	PIAsp$_3$C (11)	PIAsp$_2$C (12)	PIAsp$_2$C (13)	0	0.25	3

Improper dihedrals $V_{id(\phi ijkl)} = \frac{1}{2} k_{ijkl}\left(\phi-\phi_0\right)^2$

i	j	k	l	ϕ (deg)	k_{ijkl} (kJmol^{-1}rad^{-2})

$PIAsp^3C$ $PIAsp^2C$ $PIAsp^2C$ $PIAsp^3C$ (cis)	0	160
$PIAsp^3C$ $PIAsp^2C$ $PIAsp^2C$ $PIAsp^3C$ (trans)	180	160
$PIAsp^3C$ $PIAsp^2C$ $PIAsp^2C$ PIA-sub-sp^3C (cis)	180	160
$PIAsp^3C$ $PIAsp^2C$ $PIAsp^2C$ PIA-sub-sp^3C (trans)	0	160
PIA-Hsp_{2C} $PIAsp^2C$ $PIAsp^2C$ PIA-sub-sp^3C (cis)	0	160
PIA-Hsp_{2C} $PIAsp^2C$ $PIAsp^2C$ PIA-sub-sp^3C (trans)	180	160

- Terminal units have same bonded parameters as middle repeating units

***Table* 3.6:** Charges used for all-atomistic model of cis-PI

Atom (cis-1,4-polyisoprene)	Charge (q) e
$PIAsp^3$-t-C (15)	-0.02
$PIAsp^3C$ (10)	0.06
$PIAsp^2C$ (8)	0.071
$PIAsp^2C$ (7)	-0.355
PIA-sub-sp^3C (19)	-0.184
PIA-H_{sp3C}	0.01
PIA-H_{sp2C}	0.158

PIA-$H_{sub\text{-}sp3C}$	0.05
PIA-H_{tsp3C}	0.08

***Table* 3.7:** Charges used for all-atomistic model of trans-PI

Atom (trans-1,4-polyisoprene)	**Charge (q) e**
PIAsp^3-t-C (15)	**-0.04**
PIAsp^3C (10)	**0.253**
PIAsp^2C (8)	**0.044**
PIAsp^2C (7)	**-0.345**
PIA-sub-sp^3C (19)	**-0.11**
PIA-$H_{sub\text{-}sp3C}$	**0.06**
PIA-H_{sp2C}	**0.165**
PIA-H_{sp3C}	**-0.11**
PIA-H_{tsp3C}	**0.293**

3.3.2) Validation of the force fields

After a complete description of all the force fields, we present here a comparison of the calculated and the experimental properties.

3.3.2.1) Density: In almost all the cases, these force fields satisfactorily reproduced experimental density of polymers. Table 3.8 contains calculated and experimental densities at 298K and 1 bar pressure for all all-atomistic systems. The density values at different temperatures for united-atom models are shown in Table 3.9. All calculated densities displayed less than 2% deviation (and most of the cases less than 1% deviation) with respect to experimental values[42,56]. This shows that the sigma and epsilon values for the constituent atoms are capable of capturing the packing of the polymer in amorphous phase.

***Table* 3.8:** Calculated polymers melt densities for all-atomistic systems at 298 K and 1 bar

Systems	Density (kg/m^3) (calculated)	**Density (kg/m^3) (experimental)** [42]	Error in density w.r.t experimental value (%)
Cis-PB	894.008 ± 0.030	**900.00**	0.670
Trans-PB	879.387 ± 0.860	**890.00***	1.192
Cis-PI	907.544 ± 0.876	**910.00**[56]	0.260
Trans-PI	880.576 ± 1.860	**890.00***[22]	1.060
* Density approximated from a polymer blend containing mixture of cis and trans isomers			

***Table* 3.9:** Polymer melts densities for united-atom models at 298 K and 1 bar

Systems	Density (kg/m^3) (calculated)	**Density (kg/m^3) (experimental)**[42]	Error in density w.r.t experimental value (%)
Cis-PB	889.706 ± 0.098	**900.00**	1.14
Trans-PB	878.846± 0.150	**890.00***	1.25
Cis-PI	885.103±0.180	**910.00**[56]	2.74
Trans-PI	883.233±0.087	**890.00***[22]	0.76
* Density approximated from polymer blend containing mixture of cis and trans isomers			

3.3.2.2) R_g and R: We have also calculated local structural characteristics of polymer chains in melt by calculating end to end distance (R) and radius of gyration (R_g). R and R_g for all-atomistic models are shown in Table 3.10 while R and R_g for united atom models are shown in Table 3.11. For all polymers, the ratio of $\langle R_e{}^2\rangle/\langle R_g^2\rangle \sim 6$ which shows that all the studied polymer systems are random coils. The all atom and united atom model both represent the structural properties quite accurately.

***Table* 3.10:** Mean square end to end distance, $\langle R^2\rangle$(nm^2) and mean square radius of gyration, $\langle R_g{}^2\rangle$(nm^2) for all-atomistic systems at 298 K and 1bar

Systems	$\langle R^2\rangle$	$\langle R_g{}^2\rangle$	$\langle R^2\rangle/\langle R_g{}^2\rangle$
Cis-PB	14.09 ± .40	**2.36 ± .11**	5.97
Trans-PB	15.35 ± .20	**2.51 ± .14**	6.12
Cis-PI	11.10 ± .78	**2.04 ± .38**	5.44
Trans-PI	17.56 ± .95	**3.21 ± .65**	5.47

***Table* 3.11:** Mean square end to end distance, $\langle R^2\rangle$ (nm^2) and mean square radius of gyration, $\langle R_g{}^2\rangle$(nm^2), for united-atom models at 298 K and 1 bar

Systems	$\langle R^2\rangle$	$\langle R_g{}^2\rangle$	$\langle R^2\rangle/\langle R_g{}^2\rangle$
Cis-PB	12.85 ± 0.50	**2.18 ± 0.30**	5.89
Trans-PB	15.26 ± 1.00	**2.57 ± 0.20**	5.94

Cis-PI	14.10 ± 0.20	**2.28 ± 0.5**	6.18
Trans-PI	17.66 ± 0.15	**2.80 ± 0.10**	6.30

3.3.2.3) Glass transition temperature: T_g is calculated from the change in slope of ρ-T curves. Equilibrated density values at different temperatures for all the eight systems are calculated. Using these densities, ρ-T curves have been plotted and T_g values were calculated. T_g curves for all all-atomistic polymers are shown in Figure 3.15 and are compared to their experimental counterparts in Table 3.12.

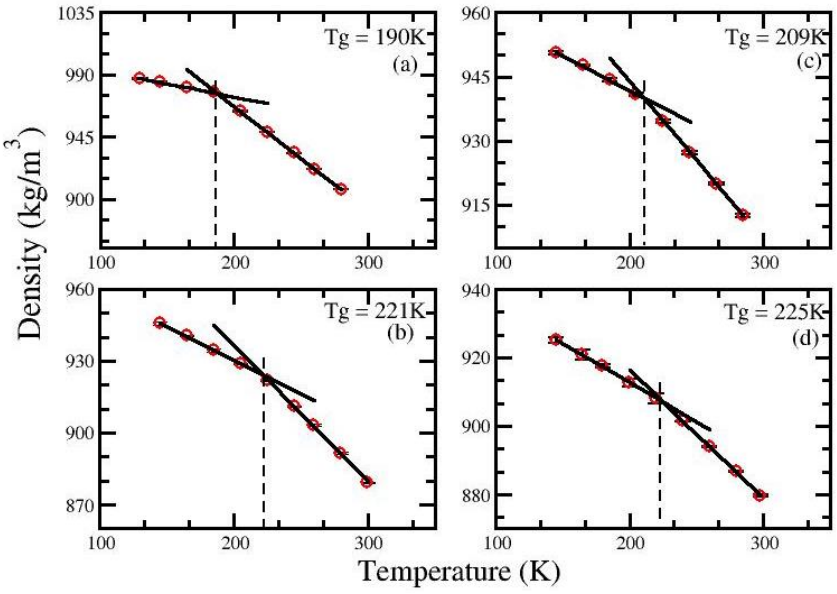

***Figure* 3.15:** Calculated glass transition temperatures for all-atomistic models (a) cis-PB, (b) trans-PB, (c) cis-PI, (d) trans-PI.

***Table* 3.12:** Glass transition temperature (T_g) of all-atomistic systems.

Systems	T_g (K) (calculated)	T_g (K)[59,60] (experimental)	Error in T_g w.r.t experimental (K)
Cis-PB	190	170-178[61]	12
Trans-PB	221	215	6
Cis-PI	209	200	9
Trans-PI	225	215	10

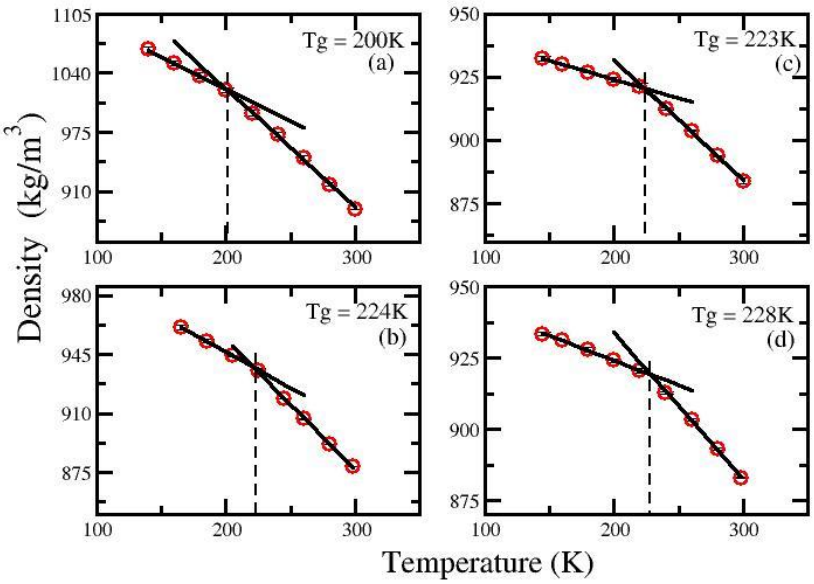

***Figure* 3.16:** Calculated glass transition temperature for united-atom models

(a) cis-PB (b) trans-PB (c) cis-PI (d) trans-PI

***Table* 3.13:** Glass transition temperature (T_g) of united-atom models

Systems	T_g (K) (calculated)	**T_g (K)[59,60] (experimental)**	Error in T_g w.r.t experimental (K)
Cis-1,4-PB	200	**170-178[61]**	22
Trans-1,4-PB	224	**215**	9
Cis-1,4-PI	223	**200**	23
Trans-1,4-PI	228	**215**	13

T_g plots for united atom models are shown in Figure 3.16 and the values are reported in Table 3.13. We found that all the calculated T_g showed excellent agreement with the experiments[59,60]. However probably due to simulation cooling rates (compared to the experiments), T_g for all the polymers are slightly higher (within 5% for all-atom and 10% for united-atom models) as compared to experiments. Glass transition temperatures obtained from all-atomistic force fields are more close to the experimental values than united-atom force fields. This is well known that T_g gets over estimated in united-atom or coarse-grained force field models because of less number of degrees of freedom. In Table 3.14 we have compiled all the information related to simulated polymers and calculated properties.

***Table* 3.14:** Summary of all polymer systems studied, calculated density, T_g and corresponding experimental values.

Polymer	Model	Number of chains	Number of monomers per chain	Density Sim. (kg/m^3) (T=298K, P=1 bar)	Density exp. (kg/m^3) (T=298K, P=1 bar)	**T_g Sim. (K)**	T_g exp. (K)
cis-PB	UA	151	32	889.706	900.00	**200**	178
	All-atom	60	32	894.008		**190**	
trans-PB	UA	153	32	878.846	890.00	**224**	215
	All-atom	63	32	879.387		**221**	
cis-PI	UA	123	32	885.103	910.00	**223**	200
	All-atom	47	32	907.544		**209**	
trans-PI	UA	121	32	883.233	890.00	**228**	215
	All-atom	48	32	880.576		**225**	

3.5 Conclusions

This simulation study aims at providing a force field for rubber which is properly validated and readily implementable in any MD simulation. Among already existing force fields of rubber, we validated some quantum chemically derived force fields of cis and trans isomers of 1,4-polyisoprene and 1,4-polybutadiene. These polymers are the major constituents of natural and synthetic rubber respectively. For validation purpose, we employed MD simulation technique to calculate properties like R_g, R, density and glass transition temperature for each polymer melt

and compared them to their corresponding experimental values. Both united-atom and all-atomistic force fields are validated. Tuning and refinement has also been done for the all-atom force field of PI, using quantum chemical calculations. This refined force field gave much better agreement of density and T_g from the previously reported one, compared to experiments. Prior to the calculation of properties, we ensured complete equilibration of all the polymer melts. A systematic procedure involving convergence of potential energy as criterion of equilibration has been implemented. In order to confirm that our protocol leads to proper equilibration of melts, we calculated end to end distance and end to end vector autocorrelation functions at various temperatures. Complete loss of orientation at all temperatures has been achieved thus verifying our strategy. We observed that extensive microsecond simulations are required for proper equilibration of polymer melts particularly for all-atom models. It has also been observed that even after convergence of density, potential energy still changes and takes more time to converge. Thus convergence of density alone cannot be used as a proof of polymer equilibration. Potential energy convergence is a much better criterion for equilibration. All calculated properties showed excellent agreement (density within 2% and T_g within 5-10%) with the experimental values thereby validating the force fields. In all the cases, calculated T_g are higher than experimental values due to cooling rate in simulations. All-atom models showed better agreement with experimental values compared to united atom models. Thus this study also reveals the efficiency of all atomistic simulations in predicting macroscopic properties of the polymers. As a final remark, we conclude that these validated force fields can now be undoubtedly used for any simulation of rubber and rubber composites.

Future work will address the effect of segmental dynamics on glass transition of these polymers. Effect on T_g by blending these polymers with amorphous and crystalline dopants and in the vicinity of nano-fillers will also be addressed.

A version of this chapter has been published[62].

Sharma, P.; Roy, S.; Varzaneh, H., Validation of Force Fields of Rubber through Glass-Transition Temperature calculation by Microsecond Atomic-Scale Molecular Dynamics Simulation. *JPC B* 2016, 120 (7), 1367-1379

References

1. Kalinchev, E., Controlling the processability of polymeric materials. *International Polymer Science and Technology* **2002,** *29* (5), T/55-T/62.

2. Thomas, S.; Stephen, R., *Rubber nanocomposites: preparation, properties and applications*. John Wiley & Sons: 2010.

3. Chen, F.; Clough, A.; Reinhard, B.; Grinstaff, M.; Jiang, N.; Koga, T.; Tsui, O., Glass Transition Temperature of Polymer–Nanoparticle Composites: Effect of Polymer–Particle Interfacial Energy. *Macromolecules* **2013,** *46* (11), 4663-4669.

4. Porter, D., *Group interaction modelling of polymer properties*. CRC Press: 1995.

5. Kent, J. A., *Handbook of Industrial Chemistry and Biotechnology: Volume 1 and 2*. Springer Science & Business Media: 2013.

6. Kunal, K.; Robertson, C. G.; Pawlus, S.; Hahn, S. F.; Sokolov, A. P., Role of chemical structure in fragility of polymers: a qualitative picture. *Macromolecules* **2008,** *41* (19), 7232-7238.

7. Kremer, K.; Grest, G. S., Dynamics of entangled linear polymer melts: A molecular-dynamics simulation. *The Journal of Chemical Physics* **1990,** *92* (8), 5057-5086.

8. Smith, J. S.; Bedrov, D.; Smith, G. D., A molecular dynamics simulation study of nanoparticle interactions in a model polymer-nanoparticle composite. *Composites science and technology* **2003,** *63* (11), 1599-1605.

9. Dodge, R.; Mattice, W. L., Simulation by molecular dynamics of poly (1, 4-trans-butadiene) as an inclusion complex in the channel of crystalline perhydrotriphenylene. *Macromolecules* **1991,** *24* (10), 2709-2714.

10. Karplus, M., CHARMM: A program for macromolecular energy, minimization, and dynamics calculations. *J Comput Chem* **1983,** *4*, 187217.

11. De Rosa, C.; Napolitano, R.; Pirozzi, B., Conformational and packing energy calculations on the two crystalline modifications of poly (trans-1, 4-butadiene). *Polymer* **1985,** *26* (13), 2039-2042.

12. Zhan, Y.; Mattice, W. L., Simulation of the molecular dynamics of poly (1, 4-trans-isoprene) and isoprene as inclusion complexes in crystalline perhydrotriphenylene. *Macromolecules* **1992,** *25* (13), 3439-3442.

13. Li, Y.; Mattice, W. L., Atom-based modeling of amorphous 1, 4-cis-polybutadiene. *Macromolecules* **1992,** *25* (19), 4942-4947.

14. Moe, N. E.; Ediger, M., Molecular dynamics computer simulation of polyisoprene local dynamics in dilute toluene solution. *Macromolecules* **1995,** *28* (7), 2329-2338.

15. Moe, N. E.; Ediger, M., Computer simulations of polyisoprene local dynamics in vacuum, solution, and the melt: Are conformational transitions always important? *Macromolecules* **1996,** *29* (16), 5484-5492.

16. Alvarez, F.; Alegria, A.; Colmenero, J.; Nicholson, T.; Davies, G., Origin of the distribution of potential barriers for methyl group dynamics in glassy polymers: A molecular dynamics simulation in polyisoprene. *Macromolecules* **2000,** *33* (21), 8077-8084.

17. Han, J.; Gee, R. H.; Boyd, R. H., Glass transition temperatures of polymers from molecular dynamics simulations. *Macromolecules* **1994,** *27* (26), 7781-7784.

18. Gee, R. H.; Boyd, R. H., Small penetrant diffusion in polybutadiene: a molecular dynamics simulation study. *Polymer* **1995,** *36* (7), 1435-1440.

19. Gee, R. H.; Boyd, R. H., Conformational dynamics and relaxation in bulk polybutadienes: A molecular dynamics simulation study. *The Journal of chemical physics* **1994,** *101* (9), 8028-8038.

20. Perico, A.; Moe, N. E.; Ediger, M., Polyisoprene local dynamics in solution: Comparison between molecular dynamics simulations and optimized Rouse–Zimm local dynamics. *The Journal of chemical physics* **1998,** *108* (3), 1245-1252.

21. Smith, G. D.; Paul, W., United atom force field for molecular dynamics simulations of 1, 4-polybutadiene based on quantum chemistry calculations on model molecules. *The Journal of Physical Chemistry A* **1998,** *102* (7), 1200-1208.

22. Faller, R.; Müller-Plathe, F.; Doxastakis, M.; Theodorou, D., Local structure and dynamics of trans-polyisoprene oligomers. *Macromolecules* **2001,** *34* (5), 1436-1448.

23. Mark, J. E., Interpretation of random-coil configurations of trans-1, 4-polybutadiene and trans-1, 4-polyisoprene. *Journal of the American Chemical Society* **1967,** *89* (26), 6829-6835.

24. Abe, Y.; Flory, P., Configurational statistics of 1, 4-polybutadiene chains. *Macromolecules* **1971,** *4* (2), 219-229.

25. Smith, G.; Paul, W.; Monkenbusch, M.; Willner, L.; Richter, D.; Qiu, X.; Ediger, M., Molecular dynamics of a 1, 4-polybutadiene melt. Comparison of experiment and simulation. *Macromolecules* **1999,** *32* (26), 8857-8865.

26. Harmandaris, V.; Doxastakis, M.; Mavrantzas, V.; Theodorou, D., Detailed molecular dynamics simulation of the self-diffusion of n-alkane and cis-1, 4 polyisoprene oligomer melts. *The Journal of chemical physics* **2002,** *116* (1), 436-446.

27. Tsolou, G.; Harmandaris, V. A.; Mavrantzas, V. G., Temperature and Pressure Effects on Local Structure and Chain Packing in cis-1, 4-Polybutadiene from Detailed Molecular Dynamics Simulations. *Macromolecular theory and simulations* **2006,** *15* (5), 381-393.

28. Doxastakis, M.; Theodorou, D.; Fytas, G.; Kremer, F.; Faller, R.; Müller-Plathe, F.; Hadjichristidis, N., Chain and local dynamics of polyisoprene as probed by experiments and computer simulations. *The Journal of chemical physics* **2003,** *119* (13), 6883-6894.

29. Faller, R.; Reith, D., Properties of poly (isoprene): model building in the melt and in solution. *Macromolecules* **2003,** *36* (14), 5406-5414.

30. Kar, S.; Greenfield, M. L., Sizes and shapes of simulated amorphous cis-and trans-1, 4-polybutadiene. *Polymer* **2015,** *62*, 129-138.

31. Harmandaris, V.; Doxastakis, M., Molecular dynamics of polyisoprene/polystyrene oligomer blends: The role of self-concentration and fluctuations on blend dynamics. *The Journal of chemical physics* **2013,** *139* (3), 034904.

32. Pandey, Y. N.; Brayton, A.; Burkhart, C.; Papakonstantopoulos, G. J.; Doxastakis, M., Multiscale modeling of polyisoprene on graphite. *The Journal of chemical physics* **2014,** *140* (5), 054908.

33. Deazle, A.; Hamerton, I.; Heald, C.; Howlin, B., Molecular modelling of high performance polymers. *Polymer international* **1996,** *41* (2), 151-157.

34. Fan, C. F.; Çagin, T.; Shi, W.; Smith, K. A., Local chain dynamics of a model polycarbonate near glass transition temperature: a molecular dynamics simulation. *Macromolecular theory and simulations* **1997,** *6* (1), 83-102.

35. Fried, J.; Ren, P., Molecular simulation of the glass transition of polyphosphazenes. *Computational and Theoretical Polymer Science* **1999,** *9* (2), 111-116.

36. Fukuda, M.; Kikuchi, H., Chain dynamics and conformational transition in cis-polyisoprene: Comparison between melt and subglass state by molecular dynamics simulations. *The Journal of Chemical Physics* **2000,** *113* (10), 4433-4443.

37. Okada, O.; Furuya, H., Molecular dynamics simulation of cis-1, 4-polybutadiene. 1. Comparison with experimental data for static and dynamic properties. *Polymer* **2002,** *43* (3), 971-976.

38. Metatla, N.; Soldera, A., Computation of densities, bulk moduli and glass transition temperatures of vinylic polymers from atomistic simulation. *Molecular Simulation* **2006,** *32* (14), 1187-1193.

39. Yu, K.-q.; Li, Z.-s.; Sun, J., Polymer structures and glass transition: A molecular dynamics simulation study. *Macromolecular theory and simulations* **2001,** *10* (6), 624-633.

40. Chakraborty, S.; Roy, S., Structural, dynamical, and thermodynamical properties of carbon nanotube polycarbonate composites: A molecular dynamics study. *The Journal of Physical Chemistry B* **2012,** *116* (10), 3083-3091.

41. Zorn, R.; Arbe, A.; Colmenero, J.; Frick, B.; Richter, D.; Buchenau, U., Neutron scattering study of the picosecond dynamics of polybutadiene and polyisoprene. *Physical Review E* **1995,** *52* (1), 781.

42. Fetters, L.; Lohse, D.; Richter, D.; Witten, T.; Zirkel, A., Connection between polymer molecular weight, density, chain dimensions, and melt viscoelastic properties. *Macromolecules* **1994,** *27* (17), 4639-4647.

43. Kestemont, E.; Van Craen, J., On the computation of correlation functions in molecular dynamics experiments. *Journal of Computational Physics* **1976,** *22* (4), 451-458.

44. Hess, B.; Kutzner, C.; Van Der Spoel, D.; Lindahl, E., GROMACS 4: algorithms for highly efficient, load-balanced, and scalable molecular simulation. *Journal of chemical theory and computation* **2008,** *4* (3), 435-447.

45. Hess, B., P-LINCS: A parallel linear constraint solver for molecular simulation. *Journal of Chemical Theory and Computation* **2008,** *4* (1), 116-122.

46. Onsager, L., Electric moments of molecules in liquids. *Journal of the American Chemical Society* **1936,** *58* (8), 1486-1493.

47. Berendsen, H. J.; Postma, J. P. M.; van Gunsteren, W. F.; DiNola, A.; Haak, J., Molecular dynamics with coupling to an external bath. *The Journal of chemical physics* **1984,** *81* (8), 3684-3690.

48. Rubinstein, M., RHC Polymer Physics. Oxford University Press: 2003.

49. Solar, M.; Paul, W., Dielectric α-relaxation of 1, 4-polybutadiene confined between graphite walls. *The European Physical Journal E* **2015,** *38* (5), 1-12.

50. Jorgensen, W. L.; Madura, J. D.; Swenson, C. J., Optimized intermolecular potential functions for liquid hydrocarbons. *Journal of the American Chemical Society* **1984,** *106* (22), 6638-6646.

51. Jorgensen, W. L.; Maxwell, D. S.; Tirado-Rives, J., Development and testing of the OPLS all-atom force field on conformational energetics and properties of organic liquids. *Journal of the American Chemical Society* **1996,** *118* (45), 11225-11236.

52. Guseva, D.; Komarov, P.; Lyulin, A. V., Molecular-dynamics simulations of thin polyisoprene films confined between amorphous silica substrates. *The Journal of chemical physics* **2014,** *140* (11), 114903.

53. Faller, R.; Schmitz, H.; Biermann, O.; Müller-Plathe, F., Automatic parameterization of force fields for liquids by simplex optimization. *arXiv preprint physics/9902056* **1999**.

54. Frisch, M. J.; Trucks, G. W.; Schlegel, H. B.; Scuseria, G. E.; Robb, M. A.; Cheeseman, J. R.; Scalmani, G.; Barone, V.; Mennucci, B.; Petersson, G. A.; Nakatsuji, H.; Caricato, M.; Li, X.; Hratchian, H. P.; Izmaylov, A. F.; Bloino, J.; Zheng, G.; Sonnenberg, J. L.; Hada, M.; Ehara, M.; Toyota, K.; Fukuda, R.; Hasegawa, J.; Ishida, M.; Nakajima, T.; Honda, Y.; Kitao, O.; Nakai, H.; Vreven, T.; Montgomery Jr., J. A.; Peralta, J. E.; Ogliaro, F.; Bearpark, M. J.; Heyd, J.; Brothers, E. N.; Kudin, K. N.; Staroverov, V. N.; Kobayashi, R.; Normand, J.; Raghavachari, K.; Rendell, A. P.; Burant, J. C.; Iyengar, S. S.; Tomasi, J.; Cossi, M.; Rega, N.; Millam, N. J.; Klene, M.; Knox, J. E.; Cross, J. B.; Bakken, V.; Adamo, C.; Jaramillo, J.; Gomperts, R.; Stratmann, R. E.; Yazyev, O.; Austin, A. J.; Cammi, R.; Pomelli, C.; Ochterski, J. W.; Martin, R. L.; Morokuma, K.; Zakrzewski, V. G.; Voth, G. A.; Salvador, P.; Dannenberg, J. J.; Dapprich, S.; Daniels, A. D.; Farkas, Ö.; Foresman, J. B.; Ortiz, J. V.; Cioslowski, J.; Fox, D. J. *Gaussian 09*, Gaussian, Inc.: Wallingford, CT, USA, 2009.

55. Breneman, C. M.; Wiberg, K. B., Determining atom-centered monopoles from molecular electrostatic potentials. The need for high sampling density in formamide conformational analysis. *Journal of Computational Chemistry* **1990,** *11* (3), 361-373.

56. Fetters, L. J.; Lohse, D. J.; Graessley, W. W., Chain dimensions and entanglement spacings in dense macromolecular systems. *Journal of Polymer Science Part B: Polymer Physics* **1999,** *37* (10), 1023-1033.

57. Wang, J.; Hou, T., Application of molecular dynamics simulations in molecular property prediction. 1. density and heat of vaporization. *Journal of chemical theory and computation* **2011,** *7* (7), 2151-2165.

58. Stephenson, R. M., *Handbook of the thermodynamics of organic compounds*. Springer Science & Business Media: 2012.

59. Handbook, P., J. Brandrup and EH Immergut. *International Science, Wiley, New York* **1989**.

60. Lu, X.; Jiang, B., Glass transition temperature and molecular parameters of polymer. *Polymer* **1991,** *32* (3), 471-478.

61. Schönhals, A.; Kremer, F., Analysis of Dielectric Spectra. In *Broadband Dielectric Spectroscopy*, Kremer, F.; Schönhals, A., Eds. Springer Berlin Heidelberg: 2003; pp 59-98.

62. Sharma, P.; Roy, S.; Karimi-Varzaneh, H. A., Validation of Force Fields of Rubber through Glass-Transition Temperature Calculation by Microsecond Atomic-Scale Molecular Dynamics Simulation. *The Journal of Physical Chemistry B* **2016,** *120* (7), 1367-1379.

CHAPTER – 4

Understanding Plasticizer Action from Molecular Perspective: A Case Study of Polybutadiene Rubber-Plasticizer Blend

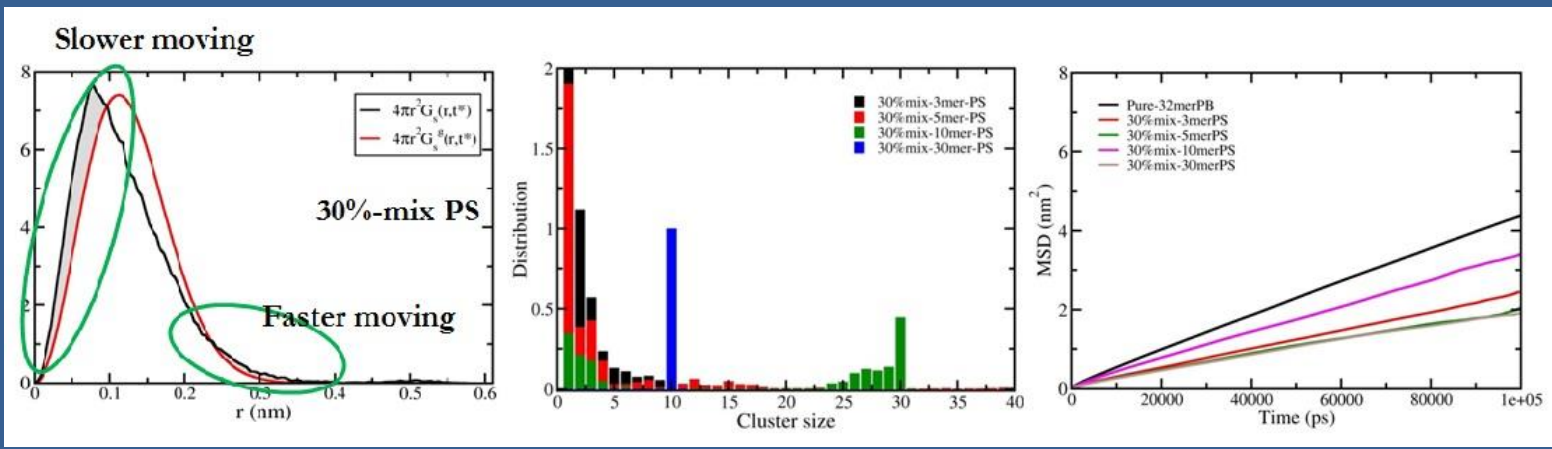

4.1 Introduction

Melt blending of polymers is an efficient and cost-effective method to modify polymeric properties for specific applications. It offers enhanced physico-chemical properties and easier processability characteristics. A popular example wherein polymer blending is crucial for processing and also imparts noticeable changes in mechanical properties exists in rubber industry. Blending of plasticizers in rubber matrix increases flexibility and reduce the stiffness imparted by fillers to permit easier processing[1-3].

For elastomeric materials like rubbers, plasticizers are used to reduce the stiffness to permit easier processing and also to increase low temperature applications. Rubber compounding in tire industry starts with the addition of fillers. After adding fillers in a matrix, viscosity of the rubber compound increases to a level that it becomes difficult to process the compound anymore. To solve this problem, if less filler is added to the polymer, less reinforcement is obtained as well as the composite becomes very expensive. Since, in most cases, fillers (carbon black or silica) are cheaper than those of the pure elastomers, therefore it is always preferred to add a maximum of filler, and subsequent processability-loss is accounted by adding the desired amounts of plasticizers.

4.1.1 Properties of Plasticizers

The most important property a plasticizer should possess is miscibility or solubility in polymer matrix. Plasticization cannot happen if it is immiscible with polymer matrix. Apart from solubility, size, shape and polarity of plasticizers are also influential factors for plasticizer efficiency.

In general, it is proposed that polar plasticizers are compatible with polar rubbers like Nitrile butadiene rubber (NBR), Chloroprene rubber (CR) while non-polar plasticizers are compatible with apolar rubbers like polybutadiene, polyisoprene, styrene butadiene rubber (SBR). Desirable properties of plasticizers include solubility in matrix, compatibility with polymer matrix, i.e. tendency to be in the matrix and diffusion in the matrix.

Plasticizers in rubber industry are of two types:

(a) Mineral oil: Obtained directly from crude-oil. These are apolar, low boiling hydrocarbons.

(b) Synthetic plasticizers: Mineral oil being apolar, is not compatible with polar rubbers like NBR, CR, so plasticizers with desired properties are synthesized. These include phthalates, adipates, phosphoric acid esters etc.

The effect of mixing of elastomers or plasticizers on mechanical properties of rubbers is clearly detectible at macroscopic level. Addition of plasticizer increases the percentage elongation, decrease elastic modulus and tensile strength of rubbers. Changes in mechanical properties are strongly coupled to the glass transition temperature, T_g and accordingly a decrease in T_g is also observed in many studies[5-8]. However fundamental understanding of the key molecular processes accountable for the depression in T_g is still incoherent.

Since plasticizers work for their specific compatible pair of polymer only, the use and behavior of plasticizers, therefore also, cannot be generalized. Yet several studies; particularly on PVC (polyvinylchloride)-plasticizer systems were conducted to understand the reasons for increase in flexibility and theories of plasticizer action have been proposed[9,10].

4.1.2 Theories of plasticization

Several mechanisms and theories have been proposed to explain the effect of plasticizers on polymers.

4.1.2.1 Lubricity theory: This theory was proposed by Kilpatrick[38] Clark, and Houwink[39] ,and it considers the role of plasticizer to reduce inter-molecular friction in polymers. It states that at higher temperatures, plasticizer molecules slides in the inter-chain spaces and when cooled, it acts as a lubricant in between polymer molecules. And that the polymer chains glide back and forth with the plasticizer thus improving flexibility.

4.1.2.2 Gel theory: The gel theory of plasticization assumes polymer model in a three dimensional honey-comb like structure interconnected at varied intervals by polymer-polymer interactions. Plasticizer separates several gel sites by plasticizer-polymer interaction allowing chains to move freely. It was proposed by Aiken[40].

4.1.2.3 Free volume theory: It states that addition of a plasticizer to a polymer matrix increases the free volume of the system. This theory gives clarification for the lowering of the glass transition temperature of a compound by addition of plasticizer. Increased free volume increases polymer mobility and in turn decreases T_g of the compound[41,42].

4.1.2.4 Mechanistic theory: It considers a dynamic association between plasticizer-polymer and plasticizer-plasticizer which is transient and ever-changing. Associations form, they disappear, then reform depending on the concentration and temperature[41].

Of all the above stated theories, free volume theory has gained maximum attention and supported by many experimental[43-46] and simulation studies[47,48]. Many empirical and theoretical equations like Gordon & Taylor[16], Flory-Fox[49,50], Gibbs & Dimarzio[13] have also been proposed to describe the depression in T_g due to plasticization.

The most acknowledged theory in various experiments[11-14] and computational studies[15-17], which also explains the depression in T_g with plasticizer addition is the 'Free volume theory'. It states that plasticizer molecules inserts in between inter-chain spaces, moves them apart, creates more free volume which decreases T_g[18]. But all these theories were proposed from studies on PVC and PVC is a plastic and considering the selectivity of plasticizer-polymer pair, a plasticizer in rubber matrix may lead to different underlying behavior.

While much scientific attention has been focused on selection, properties, working of plasticizer and their impact on bulk polymer properties, a little attention have been paid to the change in structural and dynamic properties of the polymer itself in the presence of plasticizer. And so, questions pertaining behavior of polymer in a particular environment are always open. Thus a detailed analysis of the mechanism of plasticizer action in rubbers becomes essential which is otherwise missing.

To fill this gap, we have performed a comprehensive molecular dynamics simulation study on rubber-plasticizer blends. Synthetic rubber; Polybutadiene (PB) is taken as the matrix and its smaller chain counterpart is selected as plasticizer. Mixture of PB and a high T_g polymer, polystyrene (PS) are also simulated to comprehend any contrasting behavior or anti-plasticization effect, if observed. The ultimate goal is to understand the influence of plasticizer on T_g and molecular mechanisms responsible for the change in T_g with the addition of plasticizers.

Binary mixtures of polybutadiene have been extensively studied to understand the thermodynamic and dynamical mechanical behavior of polymeric blends[19-22]. The dynamic-mechanical response and glass transition of blends apparently are associated with the miscibility and phase behavior at macroscopic level and relaxation mechanisms at molecular level[23-25].

Blends of PB-PS shows dual phase morphology where dispersed phase forms spherical inclusions in continuous matrix[26,27]. Callan et al showed discrete zones of individual phase in electron micrograph of PB-SBR blends confirming that the blends are not homogenous at the molecular level[28]. Marzocca et al. performed dynamic mechanical analysis of PB-SBR mixtures and observed two T_gs indicating phase separation[8]. It is a well-established fact that glass transition arise due to segmental relaxations in polymers[12,29]. Immiscible blends and even thermodynamically miscible blends showing single T_gs, display distinct segmental dynamics for individual components. Theoretical models based on concentration fluctuations and chain connectivity has been proposed to explain the segmental relaxation in blends and its components[21]. The Lodge-McLeish (LM) model[30] suggests that segmental relaxation times of blend components depends only on local concentration in area defined by kuhn length and not on the overall blend composition. At such smaller scales, enhanced local concentrations of a particular segment are observed due to chain connectivity leading to distinct segmental motions[25]. Another class of models[31,32] suggests that enhanced local concentrations arise due to thermal concentration fluctuations along with chain connectivity. The concentration fluctuations occur on larger length scales, in the order of several nanometers, arising from rearrangement of free volume that is associated with glass transition. The relaxation processes in blends have been characterized by non-exponential time dependence using Kohlrausch–Williams–Watts (KWW) functions[33,34] and T_g of miscible blends is calculated from theoretical models like Fox[35], Gordon and Taylor[36] and Kelley-Bueche[37] equations. A significant amount of research focusing on the testing of these theories and models and understanding segmental relaxation mechanisms have been conducted for polybutadiene blends also[20,21,26,38,39]. Paradoxically, these studies primarily focused on correlating segmental dynamics and T_g prediction in blends with effective local concentrations, while the actual reasons behind T_g change, presumably of molecular origin remains lesser explored.

Glass transition and segmental relaxation in polymers is strongly correlated to polymer chain rigidity and free volume. Accessibility of more free volume and lesser chain rigidity would ease the chain mobility leading to faster relaxations and consequent lower glass transition temperatures[29,40,41]. Thus calculation of these molecular properties is crucial to deduce the mechanism of T_g change in rubber-plasticizer systems. Some of the prevalent molecular

measures for characterizing chain rigidity are persistence length, end to end distance, radius of gyration and their autocorrelations[41-44], dihedral autocorrelation[45,46], fraction of frozen torsions[47] etc. Computing these properties along with dynamic properties like mean square diffusion would also assist in the interpretation of flexibility or rigidity at a molecular level. MD simulations have long been proven as state of the art technique to investigate the structure and dynamics in polymeric systems. Thus we have performed MD simulation studies of PB-plasticizer blends to decipher the molecular processes responsible for T_g change with plasticizer addition. Different types, chain lengths and amount of plasticizers are taken to further understand the effect of concentration, plasticizer size and temperature on the properties of PB matrix. Spatial distribution of plasticizers in the PB matrix and resultant dynamic heterogeneity is also explored. Calculated T_gs and other properties of the polybutadiene-plasticizer blends were thoroughly compared with the results of pure polybutadiene systems simulated in our previous paper[48].

4.2 Simulation and system details

4.2.1 Selection of plasticizer for PB matrix

To model rubber-plasticizer blends, an all-atomistic model of 32mer polybutadiene is taken as rubber matrix. A complete description of the force fields and its validation by reproducing glass transition temperature is given in our previous paper[48].

Plasticizers are generally low molecular weight, low T_g compounds miscible with the matrix. Thus we decided to take the same polymer polybutadiene, with a smaller chain length as the plasticizer model. It is chemically similar, miscible and lower T_g counterpart of the polymer matrix. There is an additional motive to justify the selection of plasticizer.

Though addition of plasticizers during rubber processing is essential, the similar phenomenon becomes responsible for ageing of rubbers or degradation of tires. Since a polymer melt is most of the times polydisperse, smaller chains in the system therefore acts as plasticizer for the larger chain matrix thereby creating regions of higher fluidity and lower strength. Thus the tire also becomes susceptible to the adsorption of gases which leads to its degradation. Since it is challenging to control and quantify poly-dispersity in polymers using available experimental techniques, MD simulations can play a crucial role to address this problem and so we selected low T_g PB as the plasticizer. Additional to polybutadiene-plasticizer system, blends of PB with

high T_g polymer, polystyrene are also prepared to compare the effect of blending low T_g and high T_g polymer on polybutadine matrix. Polystyrene may acts as anti-plasticizer for PB.

4.2.1.1 Calculation of glass transition temperatures of PB and PS systems of different chain lengths: To select the low T_g plasticizer and also to confirm that 32mer is the sufficient chain length to represent an experimental system, we simulated PB systems consisting of different chain lengths. Chain lengths were varied from 5mer to 100mer for PB and 3mer to 30mer for PS and their corresponding T_gs were calculated as shown in Figure 4.1a and 4.1b and values are reported in Table 4.1.

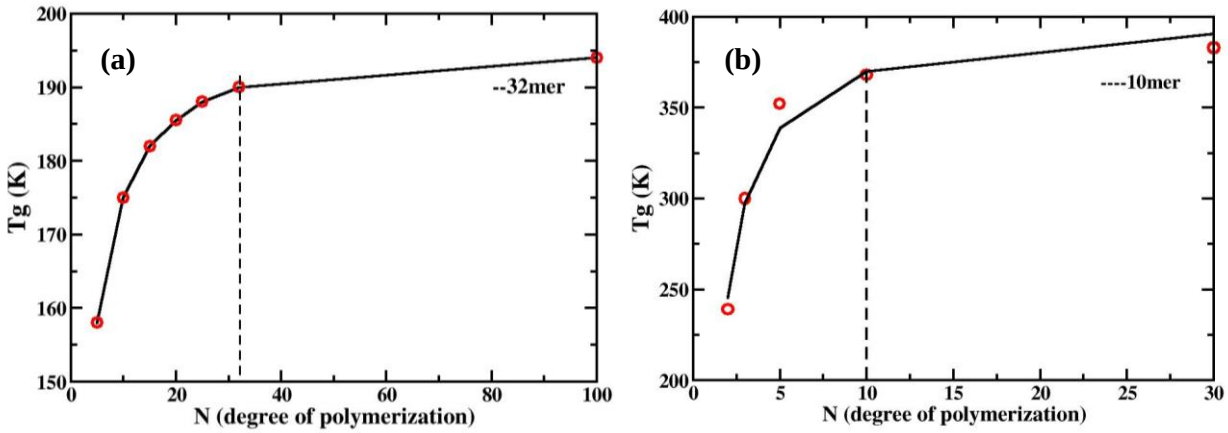

***Figure* 4.1:** T_g vs chain length, N for (a) PB and (b) PS

***Table* 4.1:** T_g of PBs with various chain lengths

Number of monomers in PB chain	T_g (K)	Number of monomers in PS chain	T_g(K)
5	158	2	239
10	174	3	300
15	182	5	359
20	185.5	10	368

25	188	**30**	380
32	190		
100	194		

Dependence of T_g on molecular weight can be can be explained using Fox-flory equation, and our calculated data shows excellent fit with Fox-flory equation[49](4.1) validating the procedure used for T_g calculation as well as T_g values of smaller chain lengths systems.

$$T_g(N) = T_g(\infty) - \frac{K_{ff}}{M_n} \qquad \textbf{(4.1)}$$

Here, $T_g(\infty)$ represents T_g at infinite molecular weight, K_{ff} is a fox-flory constant which depends on free volume in the system, M_n is the number average molecular weight. Calculated T_gs were compared to experimental values and the chain length representing polymeric regime for PB is 32mer (experimental T_g =170-180K[50,51]) and 10mer (experimental T_g=370-380K[52]) for PS. Effect of chain length is more pronounced for PS compared to PB. A variation in change length from 5mer to 100mer showed a difference of ~ 40K while for PS, T_g difference from 3mer to 30mer is ~ 140K.

4.2.1.2 Tg calculation method: Procedure for T_g calculation is adopted from our previous paper[48].

System densities were calculated at temperatures 150K above and 50K below experimental T_g and plotted against temperature. T_g has been marked as the point showing discontinuity in the slope of density-temperature (ρ-T) curves. Each density point is obtained from proper equilibrated systems. Equilibration protocol is also taken from our previous paper where in systems are simulated long enough along with repeated simulated annealing cycles to reach the potential energy convergence.

4.2.2 Preparation of blends

With an objective to understand the influence of low T_g and high T_g polymer on properties of polybutadiene matrix, two types of mixtures were prepared (a) PB matrix with low T_g polymer, plasticizer (b) PB matrix with high T_g polymer, anti-plasticizer. Cis 1,4-PB, 32mer is taken as the

matrix, 5mer PB was taken as model plasticizer because its T_g is 32 K lower than the matrix. We decided to select oligomer with at least 30-40K difference in T_g so that the effect of plasticizer is more pronounced. For second type of blends, all chain lengths of PS, from 3mer to 30mer were taken as anti-plasticizers. For first type of systems, different percentages (5-30%) of 5mer PB were added to PB matrix to understand the effect of plasticizer concentration on T_g of the blend. On the other hand, different chain lengths of PS were added to PB to understand the effect of plasticizer size on T_g in second type of mixtures.

Simulation details

Gromacs package is used for all simulations as well as for the preparation of mixtures. All-atomistic models of PB[48] as well as PS[53,54] were used to prepare pure and mixed polymer blends.

Lorentz-berthelot mixing rules were applied to calculate pair potentials. All potential forms were employed as implemented in Gromacs code[55]. Validation of the models is done by reproducing experimental T_gs for higher chain lengths and fitting to Fox-Flory equation for lower chain lengths as already discussed above.

Number of chains of 32mer PB and both plasticizers, required to achieve a particular blend concentration were added randomly in a simulation box. For initial mixing, all blends were simulated at higher temperatures in NVT ensemble for a few nanoseconds. Mixtures of first type were simulated at 300K since T_g of PB matrix is 190K while that of second type were simulated at 450K because T_g of PS is around 350K. After initial NVT runs, all systems were simulated in NPT ensemble to obtain equilibrated density and converged potential energy for microsecond timescales. Periodic boundary conditions were applied in all directions. For fast computations, bond vibrations were constrained using LINCS[56] algorithm to use a time step of 2 fs. PME method[57] was used for computing electrostatic interactions beyond the cut off (1.2 nm). Berendsen thermostat with a coupling constant of 0.1 ps and barostat with a coupling constant of 2 ps were employed[58]. Mixture composition and their calculated T_gs are given in Table 4.2.

4.3 Results and discussions

4.3.1 Glass transition temperature of polybutadiene-plasticizer blends

Calculated T_gs for both types of mixtures are shown in Table 4.2. T_g of PB decreases with the addition of 5mer PB while increases with the addition of polystyrene as shown in Figure 4.2 and 4.3. All mixtures depict single glass transition temperature; all values are more close to the T_g of parent PB matrix compared to plasticizer. All T_g plots show linear density-temperature correlation above and below T_g.

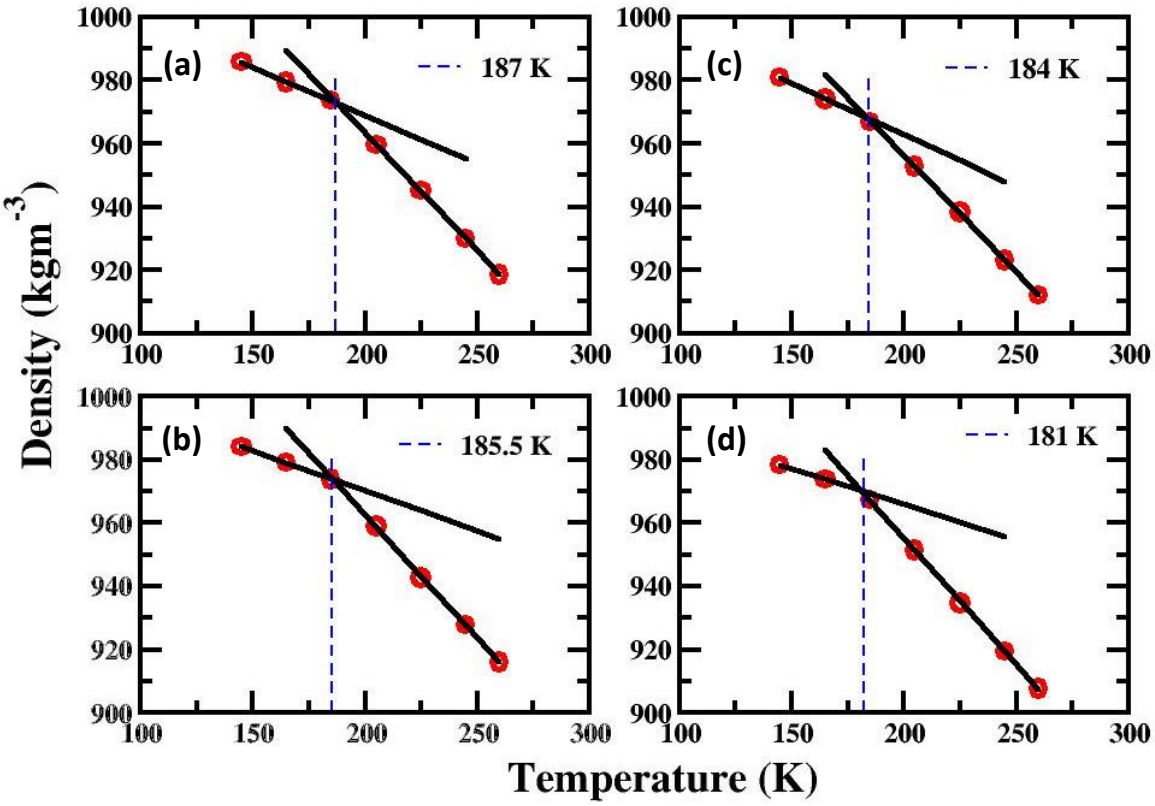

***Figure* 4.2:** Glass transition temperatures of mixtures of first type (a) 5%-5mer-PB+32merPB (b) 10%-5mer-PB+32merPB (c) 20%-5mer-PB+32merPB (d) 30%-5mer-PB+32merPB

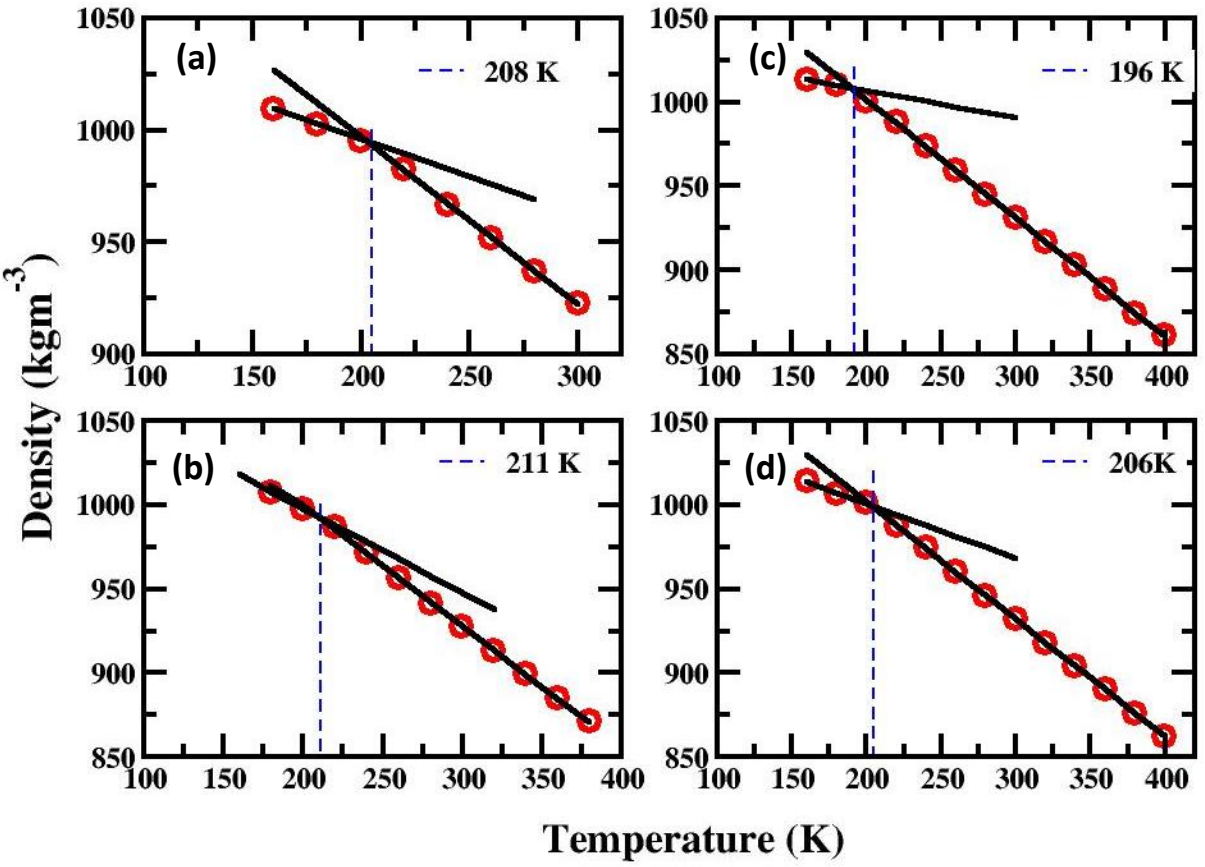

***Figure* 4.3:** Glass transition temperatures of mixtures of second type (a) 30%-3mer-PS+32merPB (b) 30%-5mer-PS+32merPB (c) 30%-10mer-PS+32merPB (d) 30%-30mer-PS+32merPB

Decrease of T_g in the first case (Figure 4.2) proves that 5mer-PB acts as plasticizer for the PB matrix. As the concentration of plasticizer increase, T_g decreases. On the other hand, in the second case, addition of PS increases the T_g of matrix. However there is a non-monotonicity in T_g increment with the chain length of PS. Among 3mer to 30mer, highest increment occur in case of 5mer followed by 3mer, 30mer and then 10mer. This is unusual, since the T_g of PS increases from 3mer to 30mer, but the effect on mixtures does not occur accordingly.

We tested our calculated T_gs with those obtained from empirical mixing rules proposed by Gordon and Taylor[59] as shown in equation 4.2:

$$T_{gm} = \frac{w_1 T_{g1} + k w_2 T_{g2}}{w_1 + k w_2} \qquad \textbf{(4.2)}$$

Here T_{gm} is the T_g of the mixture, w_1, w_2 are the weight fractions of component polymers and T_{g1} and T_{g2} are the glass transition temperatures. *k* is a parameter obtained from specific volume (V_1 and V_2) and T_g (T_{g1} and T_{g2}) of respective polymers using equation:

$$k = \frac{V_2 T_{g1}}{V_1 T_{g2}} \qquad \textbf{(4.3)}$$

T_gs of the mixtures of the first type and those with 3mer and 5mer-PS showed better agreement, ±5K with mixing rules compared to 10mer and 30mer-PS of the second type. Mixture with 10mer-PS particularly showed a difference of 18K compared to mixing rules as shown in Table 2. Since these mixing rules are proposed for miscible mixtures, it may be concluded that mixtures of PB with higher chain length PS are immiscible.

***Table* 4.2:** Calculated T_gs for all systems and its comparison to mixing rules

System	Number of chains of PB matrix	Number of chains of plasticizer	T_g (K) calculated	T_g from mixing rules (K)	% error in T_g (K)
5%mix-5merPB	60	19	187	188.8	0.95
10%mix-5merPB	60	38	185.5	188	1.33
20%mix-5merPB	60	76	184	185	0.54
30%mix-5merPB	60	117	181	183	1.09
30%mix-3merPS	60	100	208	206.7	0.63
30%mix-5merPS	60	60	211	213.5	1.17

30%mix-10merPS	60	30	196	214	8.41
30%mix-30merPS	60	10	206	215	4.19

Mixtures of second type, with 10mer and 30mer-PS showed lesser T_gs compared to mixtures with their lower chain counterparts.

4.3.2 Spatial distribution of plasticizer in mixtures

It has been proposed that plasticizers works best when miscible in the matrix. For 10mer and 30mer-PS mixtures showing lesser activity than 3mer and 5mer, we speculated that, at these higher chain lengths, phase separation may occur. Spatial distribution of PS in the PB matrix is shown in Figure 4.4. It is observed that all 5mer-PB systems and 3mer and 5mer-PS had random distribution of plasticizer in the matrix. While clustering started happening in case of 10mer and 30mer-PS showed the initiation of phase separation as shown in Figure 4.4.

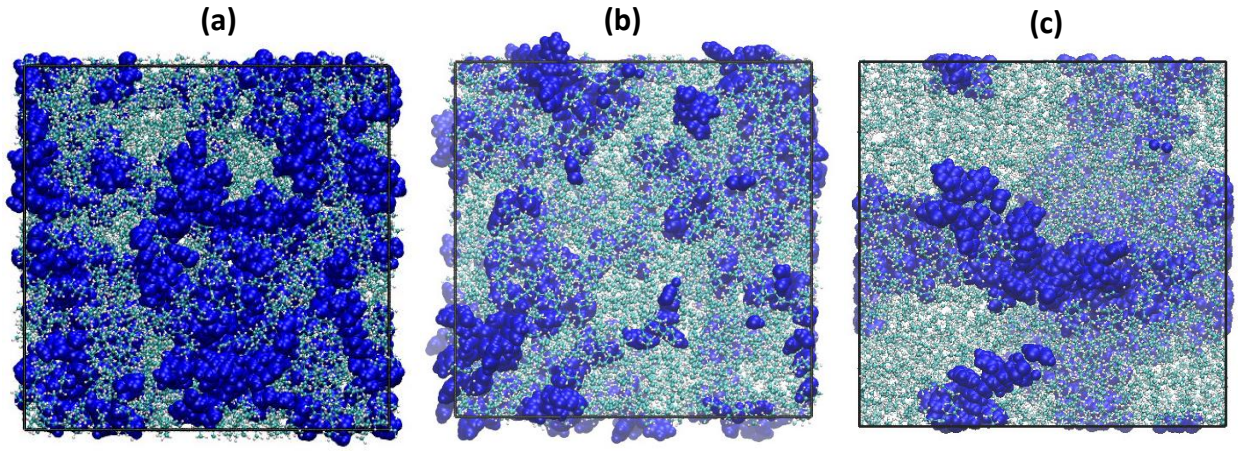

***Figure* 4.4:** Distribution of additive in PB matrix (a) 30%mix-5mer-PB (b) 30%mix-10mer-PB (c) 30%mix-30mer-PB. Blue is 5mer-PB in (a), and PS in (b) and (c), cyan color represents PB matrix.

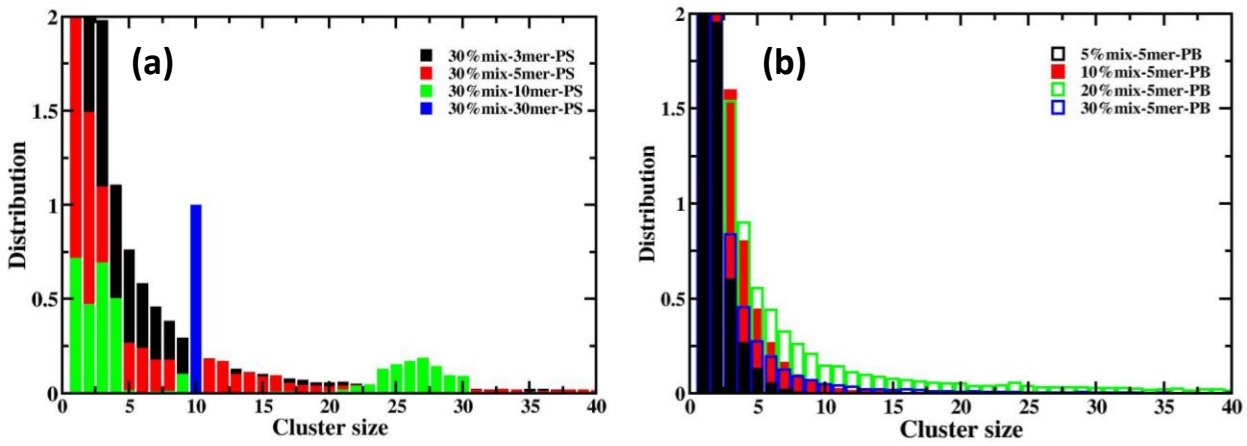

***Figure* 4.5:** Cluster size distribution of (a) mixtures with PS (b) mixtures with 5mer-PB

To further support our observations, we calculated cluster-size distribution of plasticizers in all the mixtures as shown in Figure 4.5. In all systems, monomers scored highest percentage followed by smaller cluster-sizes. However mixtures with 10mer-PS showed existence of higher cluster-sizes also, equal to total number of chains (30 in case of 10mer). 30mer-PS showed only a single cluster-size of 10, which is the total number of chains in system. This shows that all chains were in contact most of time and a percolation network of PS are formed in PB matrix. Presence of higher size clusters for 10mer-PS along with smaller sizes showed the initiation of immiscibility. Because of this reason, these mixtures showed lesser T_g than 3mer and 5mer-PS.

4.3.3 Molecular parameters controlling T_g

Change in glass transition is directly correlated to the changes in free volume and rigidity. Thus we calculated free volume and free volume fraction in pure 32mer-PB matrix and compared it with the mixtures. Free volume is calculated using geometric probe insertion method with gromacs utilities[41,55]. For the mixtures of first type, with low T_g plasticizer, free volume increases with the addition of plasticizers. As the concentration of plasticizer increases, free volume also increase monotonically. These results support the free volume theory that plasticizer molecules adjusts in inter chain spaces, pulls them apart increasing free volume and subsequently decreasing T_g. In mixtures of the second type, free volume decreases with the increase in chain length. Change in free volume with increasing concentration and chain length is not so pronounced so we present results for the extreme cases of T_g change; 30%-mix-5mer-PB and 30%mix-30mer-PS in Table 4.3.

***Table* 4.3:** Density and free volume fraction for the three selected cases

System	Pure-32mer PB	70%-PB + 30%-5merPB (I)	70%-PB + 30%-30merPS (II)
Density (kg/m^3)	894.02±0.06	877.94±0.04	932.23±0.15
Free volume fraction	0.506	0.513	0.490

There are various molecular measures to characterize chain stiffness of polymers. If a chain is flexible, it can sample more conformations and may attain a compact structure compared to the one which is rigid. Size of polymer chain; compact or expanded can be determined from end-to-end distance, R_{end} and R_g. Thus we have compared these local structural features of PB matrix for the systems at 300K and 1bar in Figure 4.6.

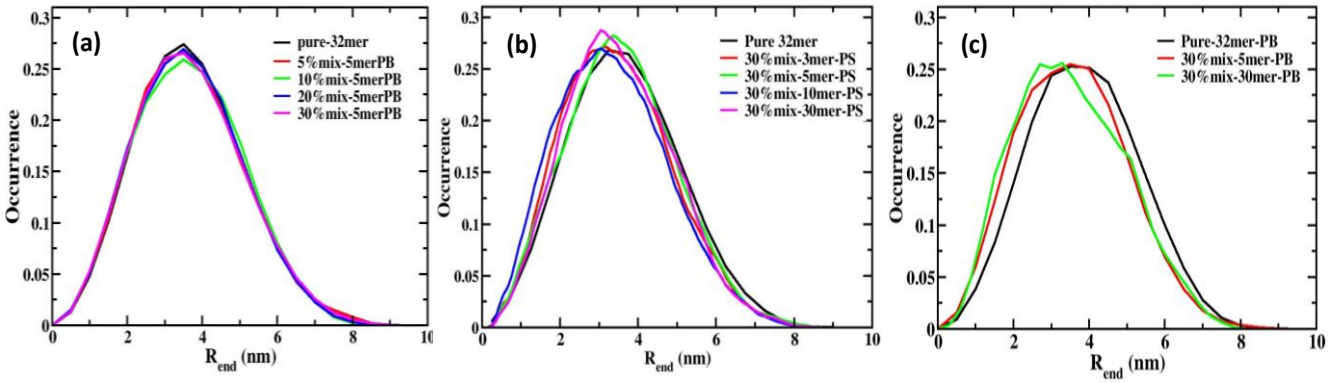

***Figure* 4.6:** End to end distance distribution (a) mixtures with 5mer-PB (b) mixtures with PS (c) comparison between pure-PB, 30%mix-5mer-PB and 30%mix-30mer-PS

Mixtures with PS showed a narrower distribution compared to pure-PB (Figure 4.6c) depicting the presence of a more rigid backbone with limited conformational mobility. Although the change is not so prominent, PS mixture showed peak at a slightly lower value of R_{end}. This may be an expected result because it has been observed experimentally that when PS is put in a PB matrix, they form little globules in the PB matrix[27].

Thus to further characterize the rigidity of the chains, we have calculated torsional autocorrelation function (TACF), C(t) and fraction of frozen torsions for the dihedral joining two butadiene repeating units in PB matrix as shown in Figure 4.7 and Figure 4.8.

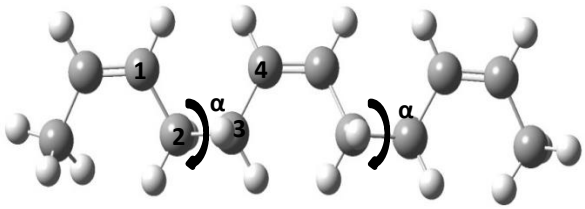

***Figure* 4.7:** Dihedral joining butadiene units in the polymer

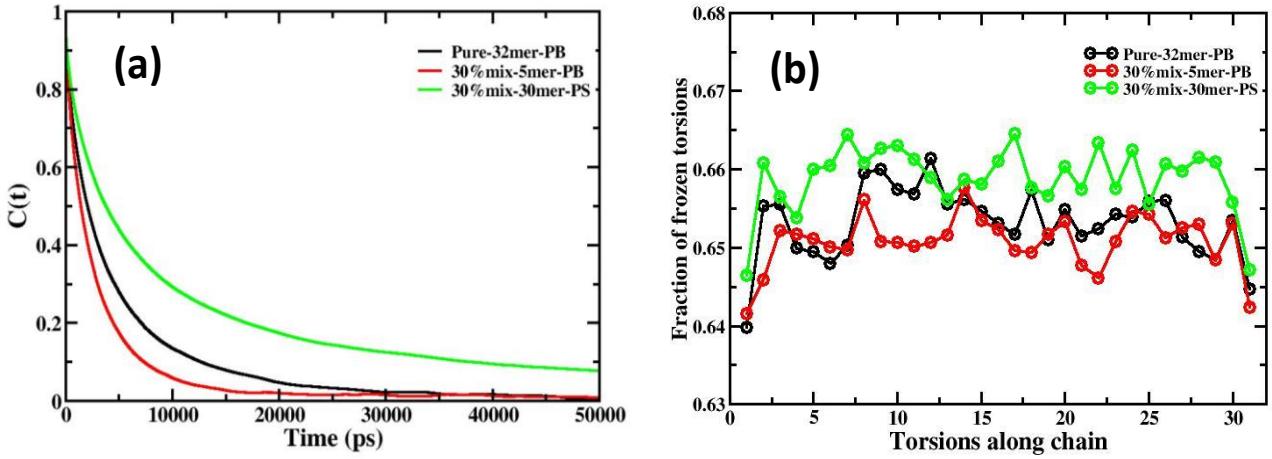

***Figure* 4.8:** (a) Torsional angle distribution (b) Fraction of frozen torsions at 225K, 1bar

TACF is calculated using equation 4.4[60]:

$$C(t) = \frac{1}{N} \langle cos[\alpha(t) - \alpha(t + \Delta t)] \rangle_t \qquad \textbf{(4.4)}$$

here $\alpha(t)$ and $\alpha(t+\Delta t)$ denotes the torsional angle at time t and time $t+\Delta t$ respectively and frozen torsions are calculated using protocol described for polyethylene by Wu et al[47]. If a dihedral showed a change of less than 5K with the increment in time step, it was considered as frozen. Decay of $C(t)$ gives an idea of rigidity of chains. More time $C(t)$ takes to decay, means more rigid the chain is. TACF for PS mixtures clearly takes more time to decay (Figure 4.8a). Similarly PS mixtures show higher fraction of frozen torsions (Figure 4.8b) depicting higher conformational rigidity of PB in PS mixtures. Thus increase in T_g of mixtures with PS originates from higher conformational rigidity of the chains, leading to slower relaxation and consequent higher T_gs.

4.3.4 Dynamic properties: Mean square displacement and dynamic heterogeneity

Lower conformational rigidity and more free volume in plasticizer system may lead to faster dynamics and vice-versa for PS mixtures. The presence of spatial heterogeneity, clustering in case of PS mixtures would definitely lead to dynamic heterogeneity also, since the segments in contact with plasticizer will depict different dynamics than the overall blend. Thus we checked the diffusion as well as the presence of dynamic heterogeneity in the mixtures.

As expected, mean square diffusion of the atoms in PB chains increased in the first type of mixtures and decrease for PS mixtures. Calculated MSD of atoms with time for 32mer-PB at 300K in both types of mixtures is shown in Figure 4.9.

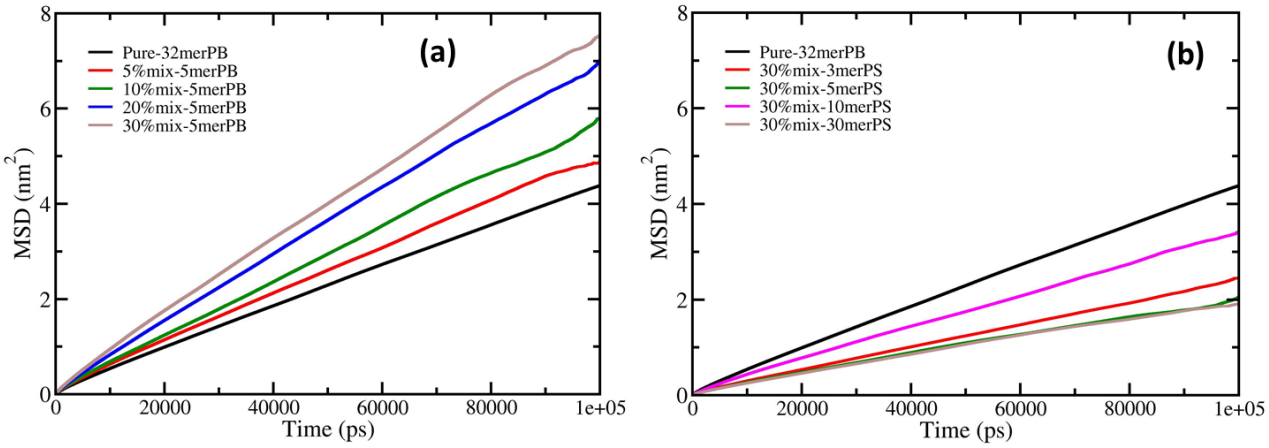

***Figure* 4.9:** MSD of atoms of PB matrix (a) First type, 5mer-PB mixtures (b) second type, PS mixtures

MSD shows a monotonic increase with concentration and decrease with chain length. Thus the structural changes, conformational rigidity of the chains can be correlated to the dynamic properties. As stated, presence of plasticizer may lead to dynamic heterogeneity in mixtures particularly for PS mixtures where clustering of PS chains occurred.

Presence of dynamic heterogeneity can be tested by calculating self-part of van hove correlation function (VHC) as given by equation 4.5[61]:

$$G_s(r,t) = \frac{1}{N}\sum_{i=1}^{N}\langle\delta|r_i(t) - r_i(0)| - r)\rangle \qquad \textbf{(4.5)}$$

VHC gives the displacement of the molecule in a time interval t. $G_s(\mathbf{r}, t)$ characterizes particle motion in terms of their relative mobility. If all molecules follow uniform motion, the distances the molecules travel in definite time intervals lead to Gaussian distribution. We have calculated self-part of the VHC function [$4\pi r2G_s(r, t)$] for center of mass of chains as a function of r for all mixtures. Deviation from the Gaussian form is observed for all mixtures confirming the heterogeneity in the dynamics of PB chains. The deviation from the Gaussian behavior is characterized by the non-Gaussian parameter $\alpha_2(t)$, which is defined as:

$$\alpha_2(t) = \frac{3\langle r^4(t)\rangle}{5\langle r^2(t)\rangle^2} - 1 \qquad \textbf{(4.6)}$$

The value of $\alpha_2(t)$ becomes zero when the dynamics of the system is homogeneous, the value increases with the increase in DH in the system and it becomes maximum when the system touches maximum heterogeneity in dynamics. We have calculated $\alpha_2(t)$ as a function of time and located the time ($t*$) corresponding to the maximum value of α, i.e., maximum heterogeneity in the system. α for pure-32mer and selected mixtures with PB and PS are shown in Figure 4.10.

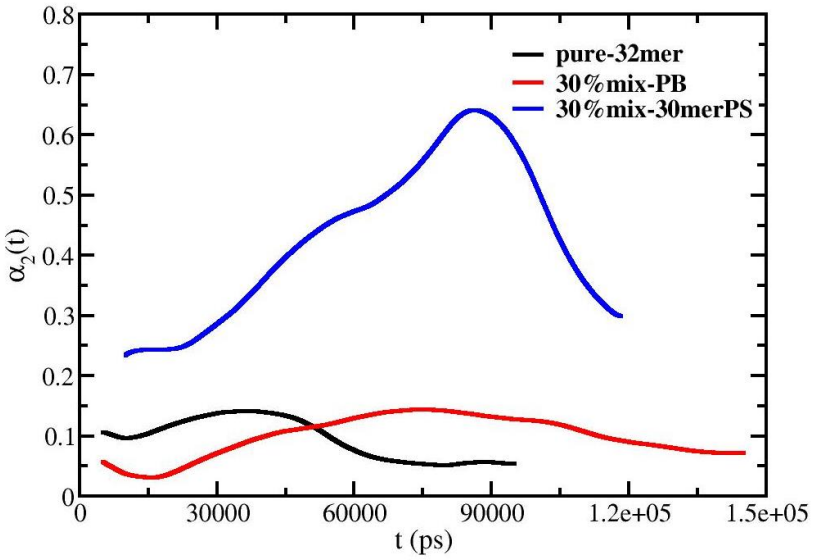

***Figure* 4.10:** Non-Gaussian parameter $\alpha_2(t)$ with time at 225K, 1bar

It is seen that maximum heterogeneity is found in the mixtures with PS. α is calculated for all the mixtures, from that t* is taken and Gs(r,t) is calculated. As shown in Figure 4.10 , t* was highest for PS, similarly here we can see that the % of slow and fast moving molecules are more in case

of mixtures with PS i.e. dynamic heterogeneity is more in case of PS mixtures (c) compared to PB mixtures(b).

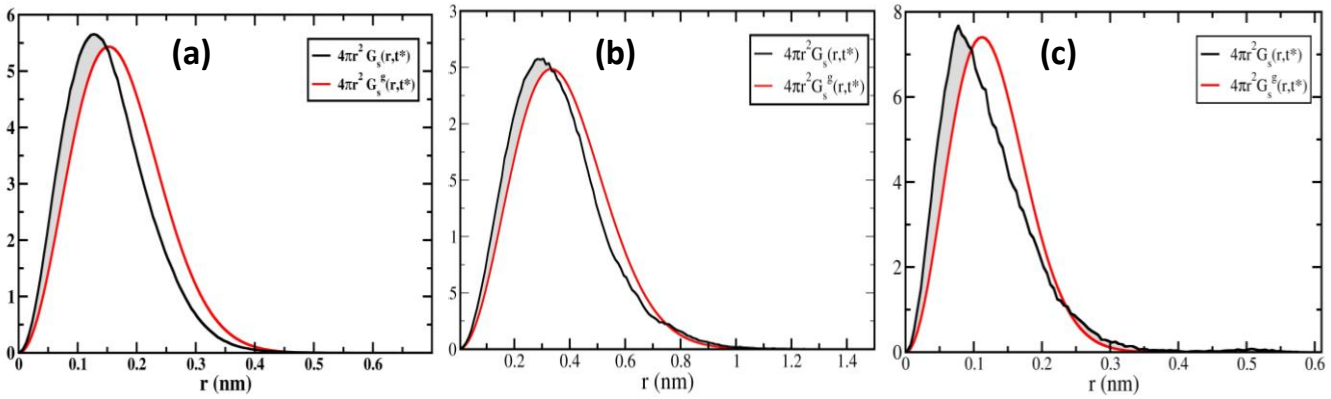

***Figure* 4.11:** Comparison of VHC and its Gaussian form for selected mixtures (a) Pure-PB (b) First type, 5mer-PB mixtures (c) second type, PS mixtures

We have also calculated the VHC function [$4\pi r2Gs(r, t)$] at $t*$, as a function of r for all mixtures as shown in Figure 4.12.

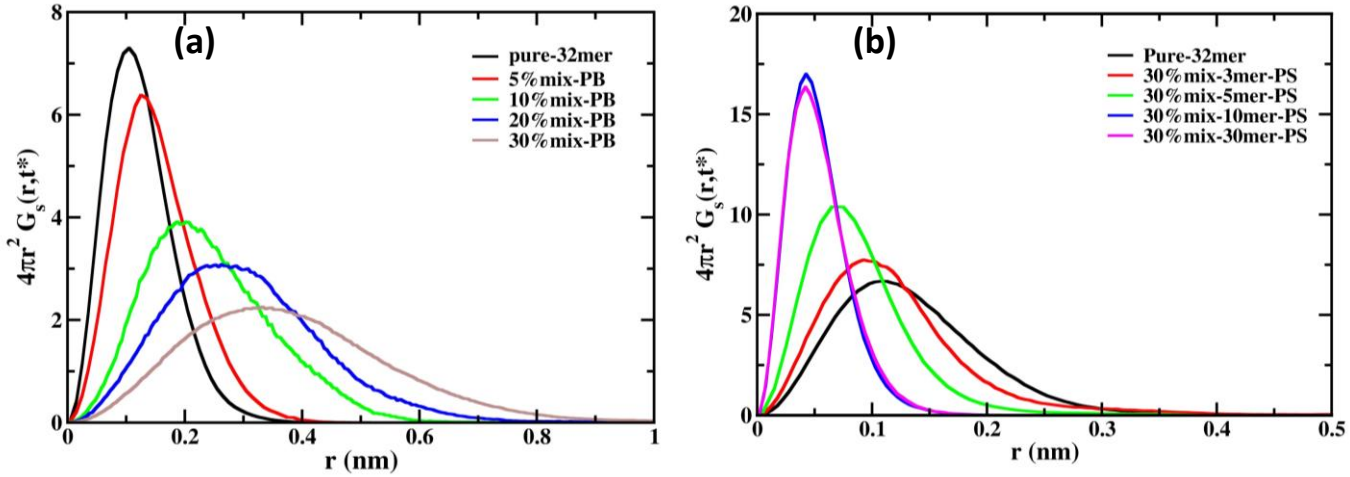

***Figure* 4.12:** Comparison of VHC for all mixtures (a) First type, 5mer-PB mixtures (b) second type, PS mixtures

Self-part of VHC functions probes single particle displacements. Broader distributions in case of mixtures with plasticizers (Figure 4.12a) shows higher displacement probabilities compared to PS mixtures. A similar trend was observed in the MSD plot, where MSD of the PB chains in 30%mix-PB mixtures was higher than rest of the systems. Thus diffusion trends of PB chains can

be correlated with the dynamic heterogeneity in the mixtures. Narrower distributions of VHC and slower diffusion in PS mixtures also corroborates with the structural properties; clustering of PS chains in PB matrix. Thus we can conclude that PS acts as antiplasticizers for PB blends.

4.4 Conclusions

Influence of mixing high and low T_g polymer on structural and dynamic properties of Polybutadiene was analyzed using MD simulations. It is inferred that 5mer-PB acts as plasticizer for 32mer-PB by inducing flexibility in the chains while polystyrene works as antiplasticizer by increasing the rigidity. Plasticizer and anti-plasticizer works by altering glass transition temperature of the polymer matrix. Changes in the glass transition temperatures of the mixtures were successfully captured using fully atomistic simulations. Plasticizers decrease the T_g of blends similar to experimental observations, while antiplasticizers increase the T_g of blends. Molecular weight and miscibility of the additives highly affects the change in T_gs. Higher chain lengths of PS, showing clustering or phase separation in PB matrix showed lesser deviation from the T_g of pure polymers compared to their lower chain length counterparts. Obtained results suggested that polymeric additives affects the overall bulk volume as well as local structural properties of the rubber. Conformational rigidity of the matrix was highly influenced by the addition of plasticizer or antiplasticizers. Our study also delineates the role of plasticizer concentration and size on blend properties. Spatial heterogeneity correlated with dynamic heterogeneity was clearly evident in the mixtures with PS. Increase in the mean square diffusion of particles in the presence of plasticizers also explains the observed flexibility at macroscopic level.

A version of this chapter has been submitted as manuscript.

References

1. Thomas, S.; Stephen, R., *Rubber nanocomposites: preparation, properties and applications*. John Wiley & Sons: 2010.

2. Mark, J. E.; Erman, B.; Roland, M., *The science and technology of rubber*. Academic press: 2013.

3. Thomas, S.; Maria, H. J., *Progress in Rubber Nanocomposites*. Woodhead Publishing: 2016.

4. Wypych, G., *Handbook of plasticizers*. ChemTec Publishing: 2004.

5. Lim, H.; Hoag, S. W., Plasticizer effects on physical–mechanical properties of solvent cast soluplus® films. *Aaps Pharmscitech* **2013,** *14* (3), 903-910.

6. Tang, L.-C.; Wang, X.; Wan, Y.-J.; Wu, L.-B.; Jiang, J.-X.; Lai, G.-Q., Mechanical properties and fracture behaviors of epoxy composites with multi-scale rubber particles. *Materials Chemistry and Physics* **2013,** *141* (1), 333-342.

7. Marzocca, A. J.; Cerveny, S.; Méndez, J. M., Some considerations concerning the dynamic mechanical properties of cured styrene–butadiene rubber/polybutadiene blends. *Polymer international* **2000,** *49* (2), 216-222.

8. Daniels, P. H., A brief overview of theories of PVC plasticization and methods used to evaluate PVC-plasticizer interaction. *Journal of vinyl and additive technology* **2009,** *15* (4), 219-223.

9. Immergut, E. H.; Mark, H. F., Principles of plasticization. ACS Publications: 1965.

10. Kirkpatrick, A., Some relations between molecular structure and plasticizing effect. *Journal of Applied Physics* **1940,** *11* (4), 255-261.

11. Aiken, W.; Alfrey, T.; Janssen, A.; Mark, H., Creep behavior of plasticized vinylite VYNW. *Journal of Polymer Science Part A: Polymer Chemistry* **1947,** *2* (2), 178-198.

12. Machin, D.; Rogers, C., Free volume theories for penetrant diffusion in polymers. *Macromolecular Chemistry and Physics* **1972,** *155* (1), 269-281.

13. Hodge, R.; Bastow, T.; Edward, G.; Simon, G.; Hill, A., Free volume and the mechanism of plasticization in water-swollen poly (vinyl alcohol). *Macromolecules* **1996,** *29* (25), 8137-8143.

14. Zhang, F.; He, G.; Xu, K.; Wu, H.; Guo, S., The molecular dynamics of different relaxation modes in asymmetric chlorinated butyl rubber/petroleum resin blends. *RSC Advances* **2014,** *4* (40), 20620-20625.

15. Anderson, S.; Grulke, E.; DeLassus, P.; Smith, P.; Kocher, C.; Landes, B., A model for antiplasticization in polystyrene. *Macromolecules* **1995,** *28* (8), 2944-2954.

16. Wu, J.; Huang, G.; Wang, X.; He, X.; Xu, B., Changes in the viscoelastic mechanisms of polyisobutylene by plasticization. *Macromolecules* **2012,** *45* (19), 8051-8057.

17. Headquarters, A. C.; Headquarters, A. A., Validation of Polymer-Plasticizer Model Systems for Controlled Drug Release.

18. Gupta, J.; Nunes, C.; Jonnalagadda, S., A molecular dynamics approach for predicting the glass transition temperature and plasticization effect in amorphous pharmaceuticals. *Molecular pharmaceutics* **2013,** *10* (11), 4136-4145.

19. Gordon, M.; Taylor, J. S., Ideal copolymers and the second-order transitions of synthetic rubbers. I. Non-crystalline copolymers. *Journal of Chemical Technology and Biotechnology* **1952,** *2* (9), 493-500.

20. Fox Jr, T. G.; Flory, P. J., Second-order transition temperatures and related properties of polystyrene. I. Influence of molecular weight. *Journal of Applied Physics* **1950,** *21* (6), 581-591.

21. Flory, P. J., *Principles of polymer chemistry*. Cornell University Press: 1953.

22. Gibbs, J. H.; DiMarzio, E. A., Nature of the glass transition and the glassy state. *The Journal of Chemical Physics* **1958,** *28* (3), 373-383.

23. Maeda, Y.; Paul, D. R., Effect of antiplasticization on gas sorption and transport. III. Free volume interpretation. *Journal of Polymer Science Part B: Polymer Physics* **1987,** *25* (5), 1005-1016.

24. Simon, P. P.; Ploehn, H. J., Modeling the effect of plasticizer on the viscoelastic response of crosslinked polymers using the tube-junction model. *Journal of Rheology* **2000,** *44* (2), 169-183.

25. Kim, W. N.; Burns, C. M., Compatibility studies of polystyrene–polybutadiene blends by thermal analysis. *Journal of applied polymer science* **1986,** *32* (1), 2989-3004.

26. Bedrov, D.; Smith, G. D., A molecular dynamics simulation study of relaxation processes in the dynamical fast component of miscible polymer blends. *Macromolecules* **2005,** *38* (24), 10314-10319.

27. Bedrov, D.; Smith, G. D., A molecular dynamics simulation study of segmental relaxation processes in miscible polymer blends. *Macromolecules* **2006,** *39* (24), 8526-8535.

28. Krämer, G.; Griepentrog, M.; Bonaccurso, E.; Cappella, B., Study of morphology and mechanical properties of polystyrene–polybutadiene blends with nanometre resolution using AFM and force–distance curves. *European Polymer Journal* **2014,** *55*, 123-134.

29. Doxastakis, M.; Kitsiou, M.; Fytas, G.; Theodorou, D.; Hadjichristidis, N.; Meier, G.; Frick, B., Component segmental mobilities in an athermal polymer blend: Quasielastic incoherent neutron scattering versus simulation. *The Journal of Chemical Physics* **2000,** *112* (19), 8687-8694.

30. Roland, C.; Casalini, R., The role of density and temperature in the dynamics of polymer blends. *Macromolecules* **2005,** *38* (21), 8729-8733.

31. He, Y.; Lutz, T.; Ediger, M.; Pitsikalis, M.; Hadjichristidis, N.; von Meerwall, E. D., Miscible polyisoprene/polystyrene blends: Distinct segmental dynamics but homogeneous terminal dynamics. *Macromolecules* **2005,** *38* (14), 6216-6226.

32. Joseph, S.; Rutkowska, M.; Jastrzêbska, M.; Janik, H.; Haponiuk, J. T.; Thomas, S., Polystyrene/polybutadiene blends: An analysis of the phase-inversion region and cophase continuity and a comparison with theoretical predictions. *Journal of applied polymer science* **2003,** *89* (4), 1007-1016.

33. Taha, M.; Frerejean, V., Morphology development of LDPE-PS blend compatibilization. *Journal of applied polymer science* **1996,** *61* (6), 969-979.

34. Callan, J.; Hess, W.; Scott, C., Elastomer blends. Compatibility and relative response to fillers. *Rubber Chemistry and Technology* **1971,** *44* (3), 814-837.

35. Arbe, A.; Alvarez, F.; Colmenero, J., Neutron scattering and molecular dynamics simulations: synergetic tools to unravel structure and dynamics in polymers. *Soft Matter* **2012,** *8* (32), 8257-8270.

36. Utracki, L. A.; Wilkie, C. A., *Polymer blends handbook*. Springer: 2002; Vol. 1.

37. Zetsche, A.; Fischer, E. W., Dielectric studies of the α-relaxation in miscible polymer blends and its relation to concentration fluctuations. *Acta polymerica* **1994,** *45* (3), 168-175.

38. Colby, R. H.; Lipson, J. E., Modeling the segmental relaxation time distribution of miscible polymer blends: Polyisoprene/poly (vinylethylene). *Macromolecules* **2005,** *38* (11), 4919-4928.

39. Kohlrausch, R., Theorie des elektrischen Rückstandes in der Leidener Flasche. *Annalen der Physik* **1854,** *167* (2), 179-214.

40. Williams, G.; Watts, D. C., Non-symmetrical dielectric relaxation behaviour arising from a simple empirical decay function. *Transactions of the Faraday society* **1970,** *66*, 80-85.

41. Fox, T. G., Influence of diluent and of copolymer composition on the glass temperature of a polymer system. *Bull. Am. Phs. Soc.* **1952,** *1*, 123.

42. Kelley, F. N.; Bueche, F., Viscosity and glass temperature relations for polymer-diluent systems. *Journal of Polymer Science Part A: Polymer Chemistry* **1961,** *50* (154), 549-556.

43. Lutz, T.; He, Y.; Ediger, M.; Pitsikalis, M.; Hadjichristidis, N., Dilute polymer blends: Are the segmental dynamics of isolated polyisoprene chains slaved to the dynamics of the host polymer? *Macromolecules* **2004,** *37* (17), 6440-6448.

44. Casalini, R.; Ngai, K.; Robertson, C.; Roland, C., α-and β-Relaxations in neat and antiplasticized polybutadiene. *Journal of Polymer Science Part B: Polymer Physics* **2000,** *38* (14), 1841-1847.

45. White, R. P.; Lipson, J. E., Polymer free volume and its connection to the glass transition. *Macromolecules* **2016,** *49* (11), 3987-4007.

46. Kuhire, S. S.; Sharma, P.; Chakrabarty, S.; Wadgaonkar, P. P., Partially bio-based poly (amide imide) s by polycondensation of aromatic diacylhydrazides based on lignin-derived phenolic acids and aromatic dianhydrides: Synthesis, characterization, and computational studies. *Journal of Polymer Science Part A: Polymer Chemistry* **2017,** *55* (21), 3636-3645.

47. Carrillo, J.-M. Y.; Cheng, S.; Kumar, R.; Goswami, M.; Sokolov, A. P.; Sumpter, B. G., Untangling the effects of chain rigidity on the structure and dynamics of strongly adsorbed polymer melts. *Macromolecules* **2015,** *48* (12), 4207-4219.

48. Faller, R. Influence of chain stiffness on structure and dynamics of polymers in the melt. Universitätsbibliothek Mainz, 2000.

49. Zhang, T.; Luo, T., Role of chain morphology and stiffness in thermal conductivity of amorphous polymers. *The Journal of Physical Chemistry B* **2016,** *120* (4), 803-812.

50. Bulacu, M.; van der Giessen, E., Effect of bending and torsion rigidity on self-diffusion in polymer melts: A molecular-dynamics study. *The Journal of chemical physics* **2005,** *123* (11), 114901.

51. Bulacu, M.; van der Giessen, E., Molecular-dynamics simulation study of the glass transition in amorphous polymers with controlled chain stiffness. *Physical Review E* **2007,** *76* (1), 011807.

52. Wu, R.; Qiu, X.; Zhang, T.; Fu, K.; Yang, X., Atomistic molecular insight into the time dependence of polymer glass transition. *The Journal of Physical Chemistry B* **2015,** *119* (30), 9959-9969.

53. Sharma, P.; Roy, S.; Karimi-Varzaneh, H. A., Validation of Force Fields of Rubber through Glass-Transition Temperature Calculation by Microsecond Atomic-Scale Molecular Dynamics Simulation. *The Journal of Physical Chemistry B* **2016,** *120* (7), 1367-1379.

54. Bogoslovov, R.; Hogan, T.; Roland, C., Clarifying the molecular weight dependence of the segmental dynamics of polybutadiene. *Macromolecules* **2010,** *43* (6), 2904-2909.

55. Schönhals, A.; Kremer, F., Analysis of dielectric spectra. In *Broadband dielectric spectroscopy*, Springer: 2003; pp 59-98.

56. Handbook, P., J. Brandrup and EH Immergut. *International Science, Wiley, New York* **1989**.

57. Rieger, J., The glass transition temperature of polystyrene: results of a round robin test. *Journal of Thermal Analysis and Calorimetry* **1996,** *46* (3-4), 965-972.

58. Müller-Plathe, F., Local structure and dynamics in solvent-swollen polymers. *Macromolecules* **1996,** *29* (13), 4782-4791.

59. Qian, H.-J.; Carbone, P.; Chen, X.; Karimi-Varzaneh, H. A.; Liew, C. C.; Müller-Plathe, F., Temperature-transferable coarse-grained potentials for ethylbenzene, polystyrene, and their mixtures. *Macromolecules* **2008,** *41* (24), 9919-9929.

60. Hess, B.; Kutzner, C.; Van Der Spoel, D.; Lindahl, E., GROMACS 4: algorithms for highly efficient, load-balanced, and scalable molecular simulation. *Journal of chemical theory and computation* **2008,** *4* (3), 435-447.

61. Hess, B., P-LINCS: A parallel linear constraint solver for molecular simulation. *Journal of Chemical Theory and Computation* **2008,** *4* (1), 116-122.

62. Frenkel, D.; Smit, B., *Understanding molecular simulation: from algorithms to applications*. Academic press: 2001; Vol. 1.

63. Berendsen, H. J.; Postma, J. P. M.; van Gunsteren, W. F.; DiNola, A.; Haak, J., Molecular dynamics with coupling to an external bath. *The Journal of chemical physics* **1984,** *81* (8), 3684-3690.

64. Pinal, R., Entropy of mixing and the glass transition of amorphous mixtures. *Entropy* **2008,** *10* (3), 207-223.

65. Okada, O.; Furuya, H.; Kanaya, T., Molecular dynamics simulation of cis-1, 4-polybutadiene. 2. Chain motion and origin of the fast process. *Polymer* **2002,** *43* (3), 977-982.

66. Karimi-Varzaneh, H. A.; Müller-Plathe, F.; Balasubramanian, S.; Carbone, P., Studying long-time dynamics of imidazolium-based ionic liquids with a systematically coarse-grained model. *Physical Chemistry Chemical Physics* **2010,** *12* (18), 4714-4724.

CHAPTER – 5

Glass Transition Temperature from Higher Temperature Correlations

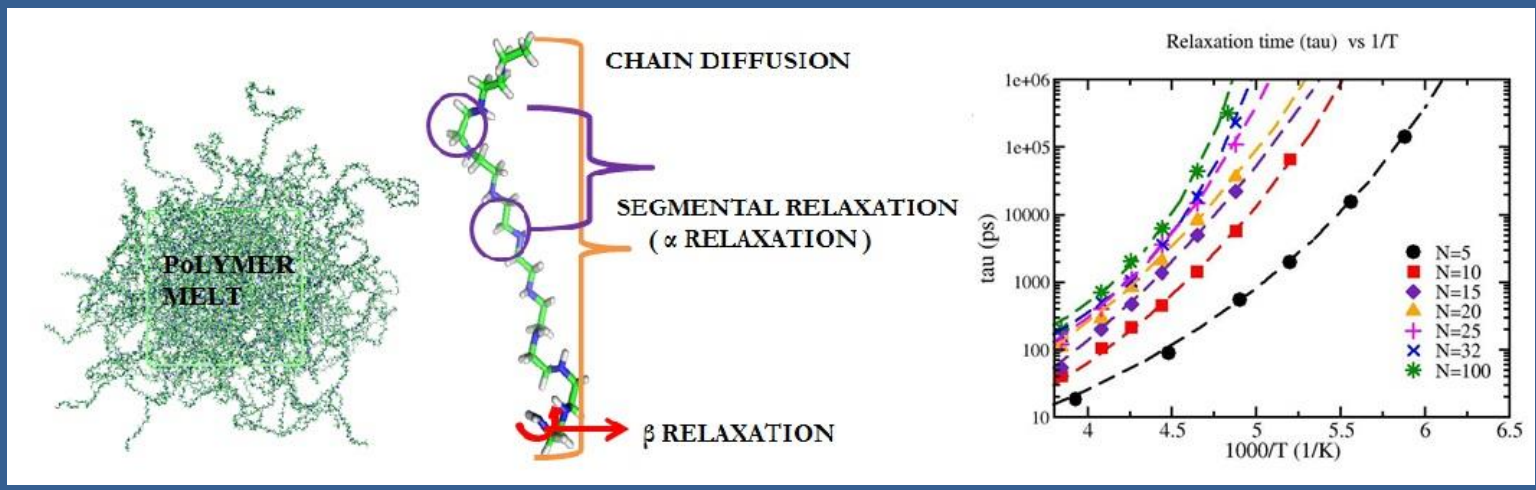

5.1 Introduction

Glass transition temperature is unarguably the most important parameter controlling polymer properties. It denotes the transition of amorphous polymers from molten rubbery state to brittle glassy state. Rapid cooling or quenching of the polymer leads to formation of glassy state in cases where crystallization does not happen. Conversion to glass occurs in a narrow temperature interval called as glass transition range which is marked by an increase of 2-2.5 orders of magnitude in molecular relaxation times. Relaxation time in this range typically reaches 100 sec, the laboratory timescale[1-3].

Relaxation mechanisms in polymers occur at different length and time scales. Typically there are three different type of relaxations; the chain relaxations (γ, normal mode relaxation), segmental relaxations (α relaxations) and side groups relaxation (β relaxations). At a particular temperature, normal mode relaxations of end-to-end vectors are typically slower than segmental relaxations which are further slow compared to β relaxations. Among these the glass transition is highly correlated to α relaxation and it is said that glass transition occurs when the segmental relaxation times reaches 100 sec as shown in Figure 5.1. We have also used the same definition to calculate T_g in this study.

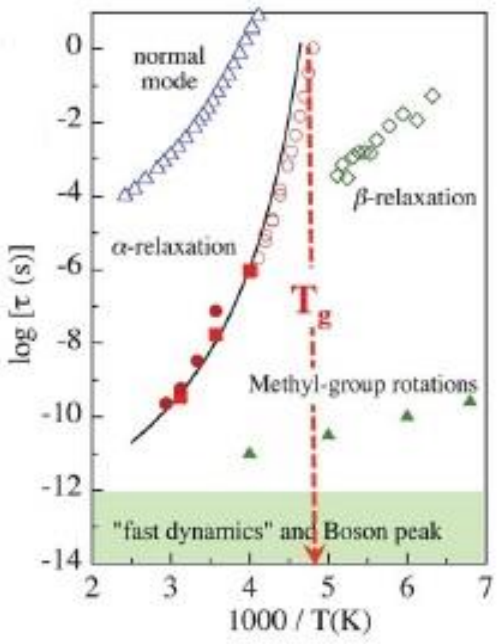

***Figure* 5.1:** Temperature dependence of relaxation times[1] (reproduced from reference 1)

Alpha (α) relaxations are highly temperature dependent. At temperatures above T_g, mobility of the chains increases due to thermal energy and availability of more free volume, leading to faster segmental relaxations and vice-versa at lower temperatures. However, the behavior of structural relaxations in polymer is very complex and shows different types of correlations between different temperature ranges as per T_g[4]. There are various molecular measures to evaluate segmental relaxations e.g. dipole moment autocorrelation functions, torsional autocorrelation functions, intermediate incoherent scattering functions etc.[1,5]

At temperatures higher than $2T_g$, α relaxations show a typical Arrhenius type dependence on temperatures. Below this temperature, deviations from Arrhenius behavior start. From temperature between $2T_g$ to $1.2\text{-}1.3T_g$, α and β relaxations could be easily distinguished and this temperature is called as cross-over temperature, T_c. Below T_c, the temperature dependence of relaxation times, τ is explained by Vogel-Fulcher-Tamman (VFT) Equation[6].

$$\tau_R(T) = \tau_\infty \, exp\left[\frac{C}{T - T_0}\right] \tag{5.1}$$

Here τ_R is the relaxation time, τ_∞ is the infinite temperature relaxation times, C is material specific parameter and T_0 is called as VFT temperature, these are empirical constants[7]. We propose that if all these constants are known, then one can calculate T_g from VFT equation by putting $\tau_R = 100\ sec$.

As discussed in Chapter 3 and 4, T_g calculation from density-temperature plot in MD simulations can be computationally very expensive, since it require density points below T_g also whose equilibration can be time and power consuming. Meanwhile when we analyzed rubbers and rubber-plasticizer systems in the previous chapters and there we calculated T_g for all systems. We found the process computationally very expensive since potential energy convergence at 185K for polybutadiene rubber took around 3-4 microseconds[8]. Motivated by that we decided to device a protocol in which T_g can be calculated from extrapolations at higher temperatures, which will have lesser time and computational cost. Taking basic concepts of segmental relaxation and its temperature dependence, we have proposed a protocol for calculating T_g of a polymer system by simulating at temperatures higher than experimental T_gs. This protocol is

based on the calculation of segmental relaxation times using incoherent intermediate scattering functions and then extrapolating temperature dependence of relaxation times to 100 sec to calculate T_g. Calculation of T_g using incoherent intermediate scattering functions has never reported in literature to the best of our knowledge. The protocol is discussed in section 5.2, followed by testing of protocol for different polymers in Results and discussion section and then conclusions.

5.2 Computational details

Polymers studied in this chapter are Rubbers; polybutadiene and polyisoprene, both united and all-atom model. The protocol is tested on various chain lengths of polybutadiene also. All models, force fields and simulation parameters are same as discussed in chapter 3 and 4. Proposed protocol is shown in the form of a flowchart in Figure 5.2

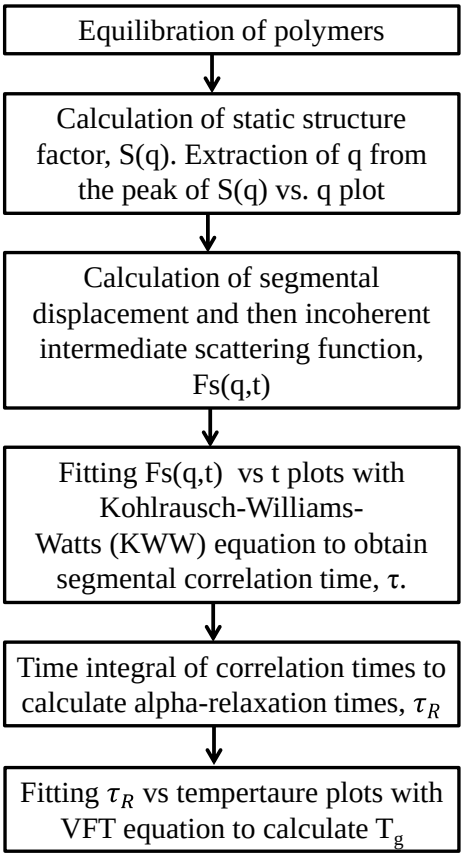

***Figure* 5.2:** Protocol for calculating glass transition temperatures from segmental relaxation times as temperatures higher than experimental T_g

5.3 Results and discussion

Testing of the protocol was firstly done on equilibrated polymer melt of 32mer-PB at 298K and 1 bar. Incoherent intermediate scattering function $F_s(q,t)$[9] were calculated to analyze the alpha relaxation phenomenon.

$$F_s(q,t) = \langle cos\{q.[r(t0+t) - r(t0)]\}\rangle \quad \textbf{(5.2)}$$

Here q is the scattering vector, $r\ (t_0+t)$-$r\ (t_0)$ denotes the displacement of atoms during time t. Brackets, < > denotes ensemble average for all atoms and various time origins t_0. Here, since we are focusing on segmental relaxation, we calculated displacement of the center of mass of the butadiene repeating units as shown in Figure 5.3a. 'q' is taken from the first peak of static structure factor, S(q) which denotes the intermolecular interactions. The second peak corresponds to the intramolecular contribution[10]. Structure factor is calculated by taking Fourier transform of intermolecular pair correlation function g(r) as shown in Figure 5.3b.

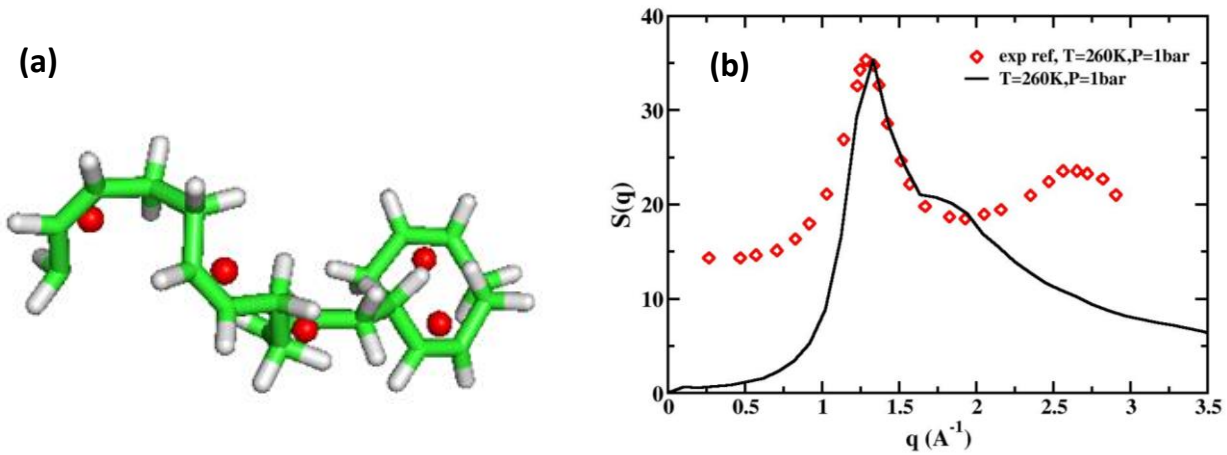

***Figure* 5.3:** (a) Centre of mass of butadiene repeat units in PB (shown in red) (b) Static structure factor of PB, red curve shows experimental results

The calculated structure factor matches well with the experimental results of Richter et al[11], as shown in Figure 5.3b. The second peak is shifted and that is obvious because of the difference in the microstructure of the simulated and experimental systems where vinyl, trans and 1,3 content of PB is also present whereas our system consists of pure cis 1,4PB. Second step involves calculating structure factor at different temperatures to find $F_s(q,t)$ and subsequently τ_R at

different temperatures as shown in Figure 5.4a.With the decrease in temperature the peak position shifted to higher q values. Similar behavior has been observed by Paul et al.[10]

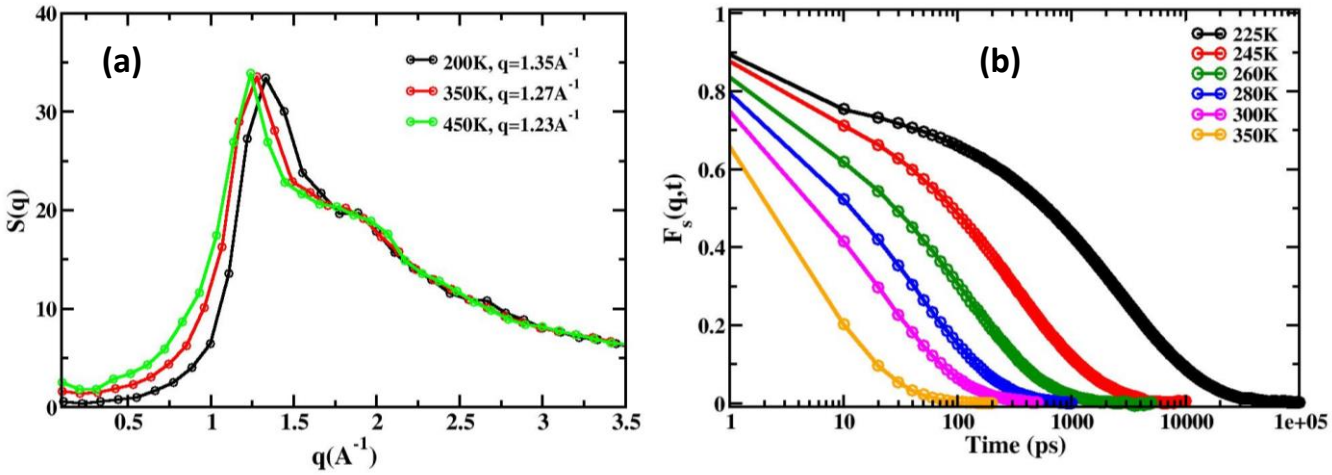

***Figure* 5.4:** (a) Structure factors at different temperatures (b) $F_s(q,t)$ at different temperatures (q in the range: 1.2-1.4 A^{0-1}). Symbols show the calculated values and solid lines shows the fits using KWW equation.

Using these structure factors, we calculated $F_s(q,t)$ at different temperatures. It is observed that these scattering functions show typical temperature dependence and a two-step relaxation at lower temperatures typical of glass formers (Figure 5.4b). Exponential decrease in $F_s(q,t)$ curves is fitted to a stretched exponential function using Kohlrausch-Williams-Watts (KWW) equation as shown in Figure 5.4b.

$$C(t) = \exp\left[-\left(\frac{t}{\tau_{KWW}}\right)^{\beta}\right] \quad \textbf{(5.3)}$$

The correlation times (τ_{KWW}) were calculated from the KWW equation, whose time integral (equation 5.4) were taken to calculate alpha-relaxation time, τ_R.

$$\tau_R = \frac{\tau_{KWW}}{\beta}\Gamma\left(\frac{1}{\beta}\right) \quad \textbf{(5.4)}$$

Similarly τ_R is calculated at different temperatures, above T_g of PB (190K) and in the final step, temperature dependence of relaxation times for amorphous polymers are plotted and fitted using Vogel-Fulcher-Tamman (VFT) equation (5.5).

$$\tau_R(T) = \tau_\infty \, exp\left[\frac{C}{T - T_0}\right] \qquad \textbf{(5.5)}$$

Here τ_R is the relaxation time, τ_∞, C and T_0 are the constants. Figure 5.5 shows τ_R vs. 1/T curves for all the chain lengths studied, and their fit to VFT equation. From that we have obtained fitting parameters τ_∞, C and T_0. Since we have already discussed that at T_g, τ_R has value around 100sec, we used this criterion, put all the fitted parameters in VFT equation (5.5) and calculated temperature (T) at which τ_R =100 sec. That temperature is the glass transition temperature.

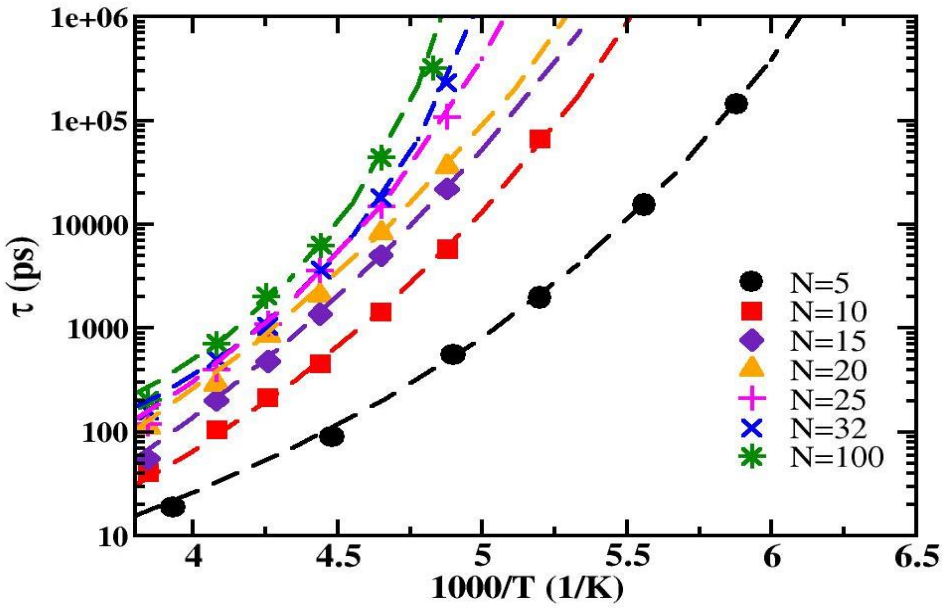

***Figure* 5.5:** Temperature dependence of relaxation times, symbols represents the values and lines represent the fit with VFT equation. N is the chain length of simulated polybutadienes

Calculated T_gs using $F_s(q,t)$ approach for pure polybutadiene systems with different chain lengths is shown in the Table 5.1.

Table 5.1: Calculated T_gs from $F_s(q,t)$ approach and their comparison with those calculated from density-temperature plots taken from Chapter 4.

System	T_g (K) calculated	T_g from Fs(q,t) (K)	Diff. in T_g (K)
5mer	158	155	3
10mer	174	169	5
15mer	182	183.2	1.2
20mer	185.5	180	5.5
25mer	188	183.3	4.7
32mer	190	192	2
100mer	194	198	4
➢ Tau calculation temperature should start from exp. T_g + 50K			

It is interesting to see that T_g values calculated from proposed protocol matches well with those calculated from ρ-T plots. An important point to emphasize here is that the temperature for

$F_s(q,t)$ calculation should be between T_g+50K to T_g+ 100K. We have tried different temperature ranges for calculating τ_R and corresponding T_g from that. This temperature range may depict the range excluding cross-over temperature. We obtained our best results as shown in Table 5.1 by using this temperature range only. Since our approach of T_g calculation from higher temperature correlations proved successful for different chain lengths of polybutadiene, we tested this approach for polyisoprene as well. We found the calculated T_g within ±10K range.

5.4 Conclusions

Calculating glass transition temperatures from density-temperature dependence is computationally expensive. So we proposed a protocol for T_g calculation from higher temperature correlations. Suggested method involves calculation of segmental relaxation times and T_g from its temperature dependence. Testing of the protocol on polybutadiene and polyisoprene rubbers gave satisfactory agreement with those calculated from ρ-T plots. Thus we recommend that our proposed method of T_g calculation is validated and can be used for other elastomers also.

Manuscript in preparation.

References

1. Arbe, A.; Alvarez, F.; Colmenero, J., Neutron scattering and molecular dynamics simulations: synergetic tools to unravel structure and dynamics in polymers. *Soft Matter* **2012,** *8* (32), 8257-8270.

2. Bormuth, A.; Henritzi, P.; Vogel, M., Chain-Length Dependence of the Segmental Relaxation in Polymer Melts: Molecular Dynamics Simulation Studies on Poly (propylene oxide). *Macromolecules* **2010,** *43* (21), 8985-8992.

3. Robertson, C.; Santangelo, P.; Roland, C., Comparison of glass formation kinetics and segmental relaxation in polymers. *Journal of non-crystalline solids* **2000,** *275* (3), 153-159.

4. Williams, M. L.; Landel, R. F.; Ferry, J. D., The temperature dependence of relaxation mechanisms in amorphous polymers and other glass-forming liquids. *Journal of the American Chemical society* **1955,** *77* (14), 3701-3707.

5. Lutz, T.; He, Y.; Ediger, M., Segmental dynamics of dilute polystyrene chains in miscible blends and solutions. *Macromolecules* **2005,** *38* (23), 9826-9835.

6. Garca-Coln, L.; Del Castillo, L.; Goldstein, P., Theoretical basis for the Vogel-Fulcher-Tammann equation. *Physical Review B* **1989,** *40* (10), 7040.

7. Kunal, K. Influence of chemical structure and molecular weight on fragility in polymers. The University of Akron, 2009.

8. Sharma, P.; Roy, S.; Karimi-Varzaneh, H. A., Validation of Force Fields of Rubber through Glass-Transition Temperature Calculation by Microsecond Atomic-Scale Molecular Dynamics Simulation. *The Journal of Physical Chemistry B* **2016,** *120* (7), 1367-1379.

9. Van Zon, A.; De Leeuw, S., Structural relaxations in glass forming poly (butadiene): A molecular dynamics study. *Physical Review E* **1998,** *58* (4), R4100.

10. Bennemann, C.; Baschnagel, J.; Paul, W., Molecular-dynamics simulation of a glassy polymer melt: Incoherent scattering function. *The European Physical Journal B-Condensed Matter and Complex Systems* **1999,** *10* (2), 323-334.

11. Gkourmpis, T.; Mitchell, G. R., Three Dimensional Picture of the Local Structure of 1, 4-Polybutadiene from a Complete Atomistic Model and Neutron Scattering Data. *Macromolecules* **2011,** *44* (8), 3140-3148.

PART – B

Star telechelic poly (D, L lactide)

Viscosity-Temperature Dependence

CHAPTER –6

Understanding Molecular Mechanisms responsible for Anomalous Rheological Properties of Star Telechelic Polylactide Ionomer

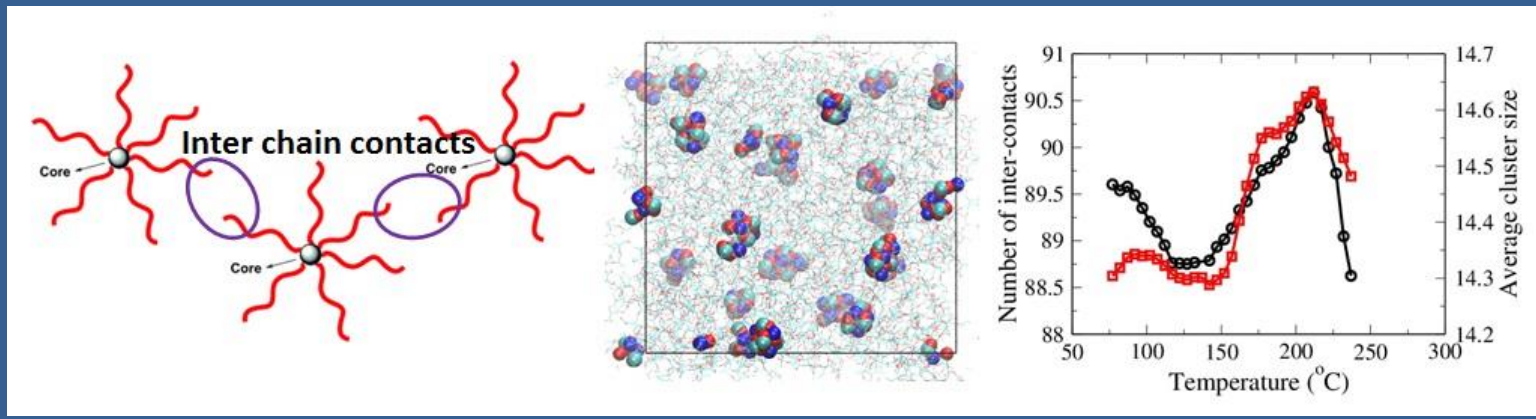

6.1 Introduction

Deployment of polylactide (PLA) in packaging applications is increasing because of its zero carbon footprint and excellent solid-state properties[1]. It is also emerging as a promising material to address the problem of plastic waste because of its biorenewable origin and compostability.[2] However, melt processing of PLA is often limited by its low melt elasticity (due to lower entanglement density) and strong temperature dependence of viscosity (due to high flow activation energy)[3].

Ionization of polymers; introducing ionic groups in a nonpolar polymer matrix is an interesting and potential approach to improve several properties of the base polymer including melt rheology[4-6]. Substituting polar groups on the chain ends of apolar polymers introduces additional polar interactions like hydrogen bonds, ionic bonds apart from classical topological ones, entanglements. Due to which temporary ionic associations or networks are formed, consequently ionomers generally show improved physical properties compared to their non-ionic counter-parts viz. increased glass transition, sol-gel transition and mechanical properties and also melt rheology[7-8]. For polymers containing polar backbones, the ionic groups with their counter ions associate strongly via dipolar interactions to form clusters and multiplets, which phase separate at nanometer length scales from the dielectric polymer matrix. The ionic clusters act as transient cross-link points for the polymer chains and restrict their mobility even at high temperatures in the melt state[9]. In general, the melt viscosity and elasticity of ionomers shows noticeable changes and are significantly higher than those of the base polymers.

Viscosity of conventional polymer melts decrease with increasing temperature because of increased thermal mobility of chains[10]. The two equations that are widely used to capture temperature dependence of viscosity in amorphous polymers, WLF equation close to T_g and Arrhenius equation at even higher temperatures as discussed in Chapter 2.

However increase in viscosity with temperature is a very unusual observation and there are a very few known systems that shows such anomalous behavior. Highly sulphonated polystyrene (SPS) a LCST solution and LCST blend[14] and star telechelic poly (D, L lactide) have depicted such results. For SPS, Weiss et al. suggested that the formation of chain ends mediated ionic clusters restricts the chain motion thus viscosity increased[15-16]. Poly(L-lactide) (PLLA) polymer consists of 6 arms terminating with carboxylic acid groups and it shows a mono-tonic decrease in

viscosity with temperature[3]. However star telechelic ionomer, formed by replacing acid groups with sodium-carboxylate ions displays a non-monotonic viscosity-temperature dependence showing viscosity maximum at a temperature higher than T_g[17]. PDLLA ionomer comparatively shows quite prominent viscosity fluctuations of two orders of magnitude (10^6 to 10^4 Pas) as shown in Figure 6.1a. It also shows an increase in the viscoelastic modulus, G' with temperature (Figure 6.1b).

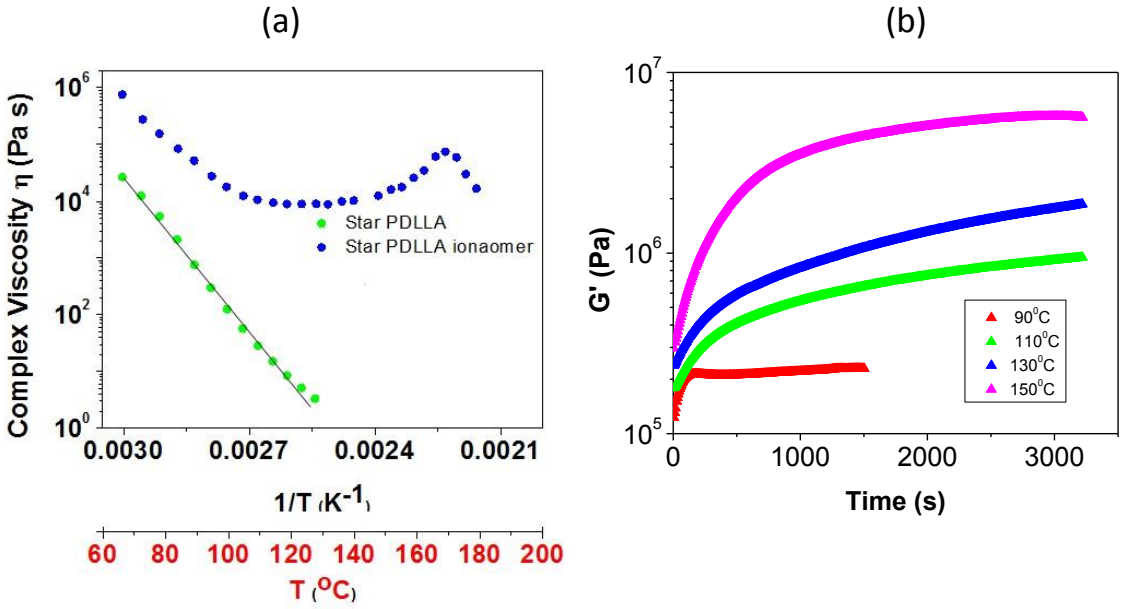

***Figure* 6.1:** (a) Viscosity vs. temperature plot of poly (D, L lactide) ionomer and polymer. Blue symbols: ionomer, green symbols: polymer. (b) Temperature dependence of viscoelastic modulus, G'.

The anomalous non-monotonic temperature dependence alludes to significant structural and dynamical changes in the association pattern of the terminal ionic groups, which is implicated in the formation of a percolated network leading to gel formation. While thermal fluctuations can disrupt such associations, on the other hand increased mobility of the terminal groups is essential for the ion dipoles to find each other and form the clusters. In order to test this hypothesis of two competing molecular processes that might lead to the observed non-monotonic behavior, we performed molecular dynamics simulations to elucidate the molecular interactions that might lead to such anomalous behavior.

6.2 Computational details

We performed atomistic MD simulations of PDLLA ionomer melt consisting of 16 ionomer molecules. Replica Exchange Molecular Dynamics (REMD) technique[18] was used to enhance the sampling of the conformational space. To start with, an all-atomistic model of single star ionomer was constructed using material studio software[19]. Single ionomer was simulated using stochastic dynamics (SD) at temperatures higher than T_g, 327^{o}C to check the equilibrium geometry of the ionomer as shown in Figure 6.2b.

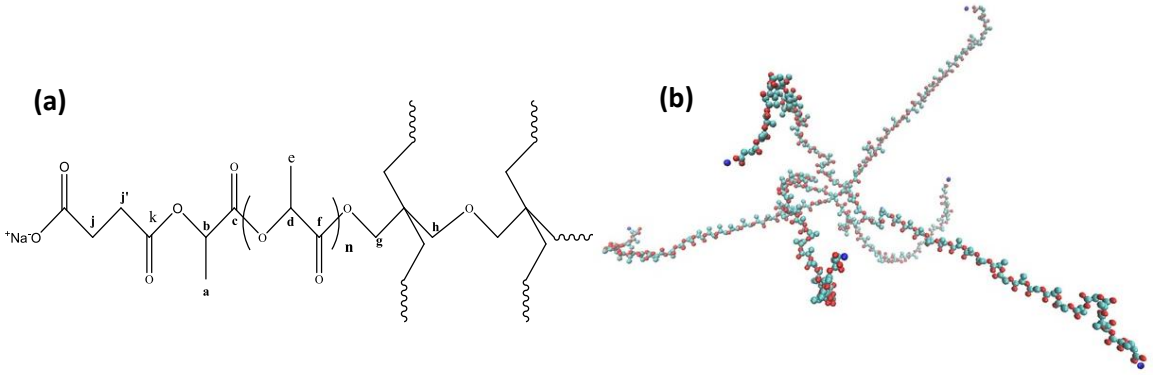

***Figure* 6.2:** (a) chemical structure of PDLLA ionomer (b) Simulated structure of single star PDLLA ionomer

16 ionomers were added randomly in a box to build a melt. The ionomer melt was initially simulated at higher temperature of 327^{o}C for proper equilibration of the system. After that simulated annealing (SA) was done from 77^{o}C to 327^{o}C to extract structures at lower temperatures for simulations. Melts at individual temperatures were obtained from SA and two types of simulations have been performed: (i) Replica exchange molecular dynamics (REMD) simulations, to capture the structure and energetics, where 33 replicas were taken with a temperature difference of 5^{o}C in the range of 77-237^{o}C. (ii) NPT simulations in the range of 77-237^{o}C, were performed to capture the dynamics.

All-atom OPLS force field[20] was used to model the system, only methylene groups were treated as united atoms. All bonds were constrained using LINCS[21] algorithm to reduce the computational cost. V-rescale thermostat[22] and Berendsen[23] barostat were used to maintain the temperature and pressure during simulations. Particle mesh Ewald[24] (PME) was used to calculate long range electrostatics and the cut-off used for short range Coulomb and Lennard Jones

interactions was 1.2 nm. Complete step-wise procedure is depicted in a flowchart shown in Figure 6.3.

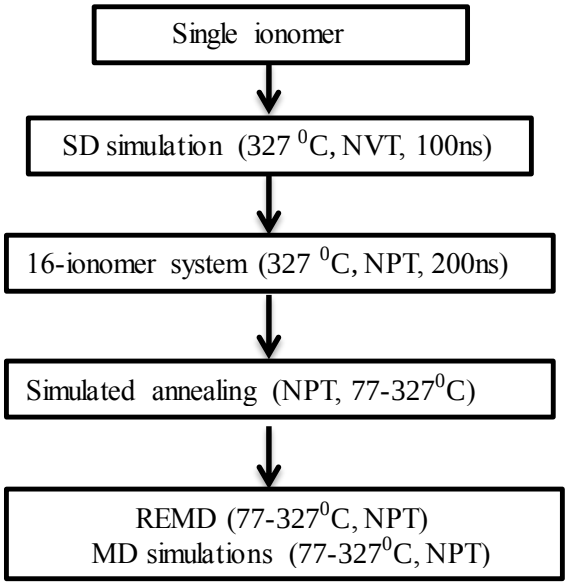

***Figure* 6.3:** Procedure followed during MD simulation

6.3 Results and discussions

6.3.1 Clustering of ionic end groups

Figure 6.4a shows a representative snapshot of the melt where the clusters formed by the ionic end groups of the ionomer arms are highlighted. This clearly shows that the ionic dipoles have a strong tendency to associate and form clusters leading to formation of a percolated network. The viscosity of melt would strongly depend on strength of the interactions and size of the clusters. One of the molecular measures of defining the strength of interactions would be the number of contacts formed between the terminal COO^- groups and the average size of the clusters formed by these tail groups. The temperature dependence of these two quantities is shown in Figure 6.4b. Interestingly, both quantities demonstrate almost identical non-monotonic temperature dependence similar to the experimental measurement of temperature dependence of viscosity.

The position of the peak observed in simulations is shifted by ~30°C, but the qualitative trend is extremely well reproduced.

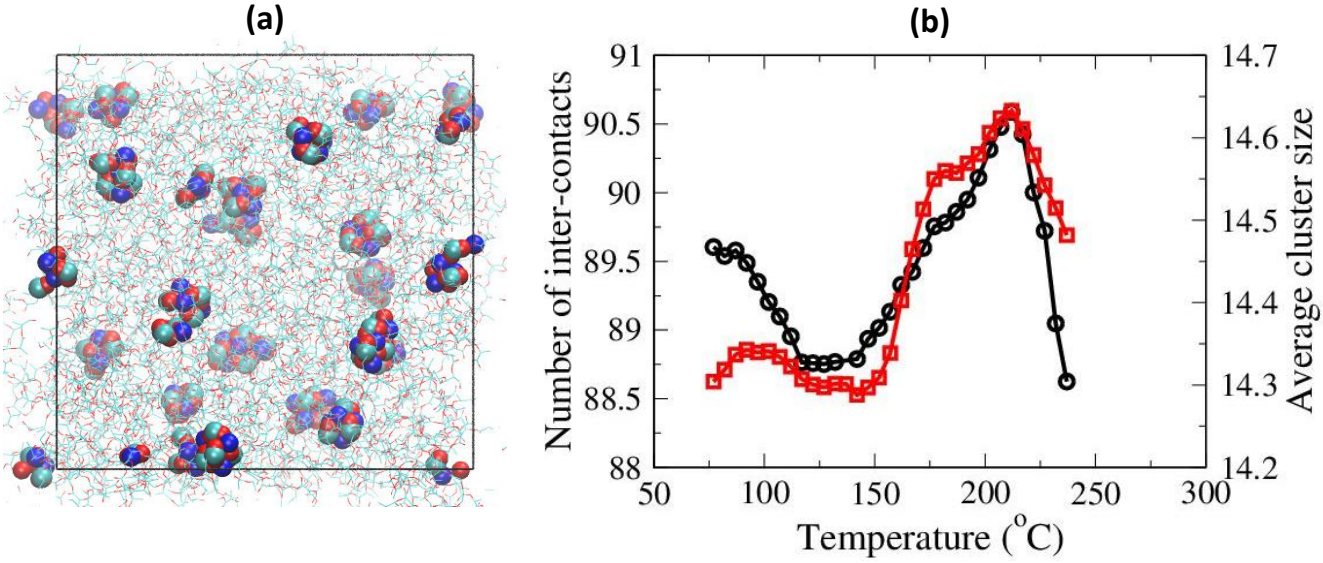

***Figure* 6.4:** (a) A representative snapshot showing the clustering of COO^-Na^+ end groups (cyan: carbon, red: oxygen, blue: sodium ion) (b) Temperature dependence of the average number of inter-COO contacts and average cluster size (black circles: average number of contacts, red squares: average cluster size)

Calculation of inter/intra contacts and cluster size

Contacts were calculated from REMD simulations. For calculating the chain-end contacts, we first calculated the radial distribution function (RDF) of carbons (C9) of COO^- chain ends as shown in the Figure 6.5a.

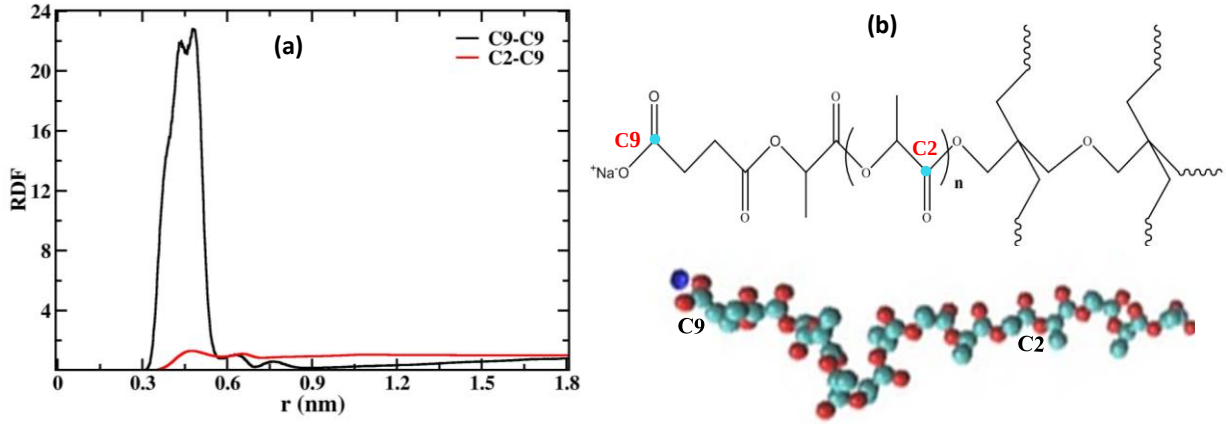

***Figure* 6.5:** (a) RDF of C9-C9 (black), RDF of C2-C9 (Red). (b) Structure representation of C2 and C9 carbons. C9 is the chain-end COO- carbon and C2 is the middle repeat unit (C=O) carbon.

Chain ends clearly showed a prominent peak compared to repeat units. The peak in the RDF shows the most probable distance between C9 and C9. If the distance between two C9-C9 atoms is within the position of peak in RDF, they will be considered to be in contact e.g. here, the C9-C9 RDF peak occurs at ~0.5 nm which is taken as the cut-off and the number of contacts calculated using this cut-off are shown in Figure 6.4b.

This observation clearly suggests a direct connection between the observed viscosity and the clustering of ionic end groups. Cluster size distribution at various temperatures is shown in Figure 6.6. We find that with the increase in temperature, tendency to form larger clusters also increases. Figure 6.4b shows that the average cluster size is largest at 212^{o}C and inter-COO^{-} contacts are also highest at this temperature.

(a)

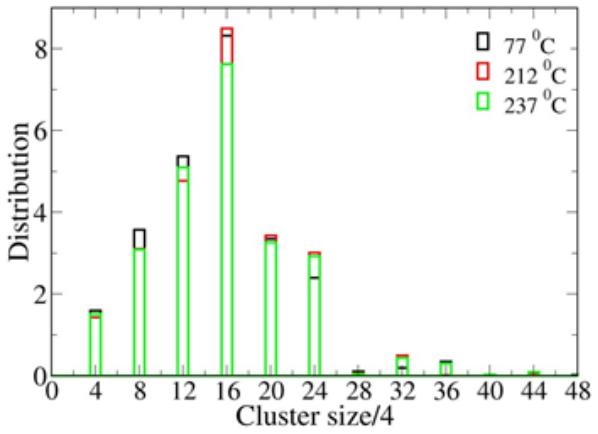

(b)

Cluster Size	Distribution		
	77 °C	212 °C	237 °C
2	3.57	3.11	3.14
3	5.37	4.78	5.1
4	8.32	8.50	7.63
5	3.35	3.43	3.27
6	2.4	3.0	2.93
7	0.11	0.07	0.05
8	0.19	0.50	0.44
9	0.43	0.02	0.31
10	0.01	0.01	0.03
11	0.00	0.04	0.09

***Figure* 6.6:** (a) Cluster size distribution averaged over all frames at three representative temperatures (lowest temperature: 77^{o}C, highest viscosity temperature: 212^{o}C, highest temperature: 237^{o}C) (b) Numerical values for the distribution of cluster size (same as (a)).

We further looked into the composition of various types of clusters formed in the system. There can be two types of contacts forming between the tail ends: intra-molecular contacts, where the arms belong to the same ionomer molecule, and inter-molecular contacts, where the arms belong to two separate molecules. The inter-molecular contacts are primarily responsible for formation

of a percolation network spanning multiple molecules. Snapshots showing composition of these two different types of contacts are shown in Figure 6.7. We have observed that as the cluster size increases, the contribution of inter-molecular contacts in the cluster also increases. For example, a cluster size of four may contain two intra and two inter chains (Figure 6.7a), while a cluster-size six may contain all different chains (Figure 6.7b).

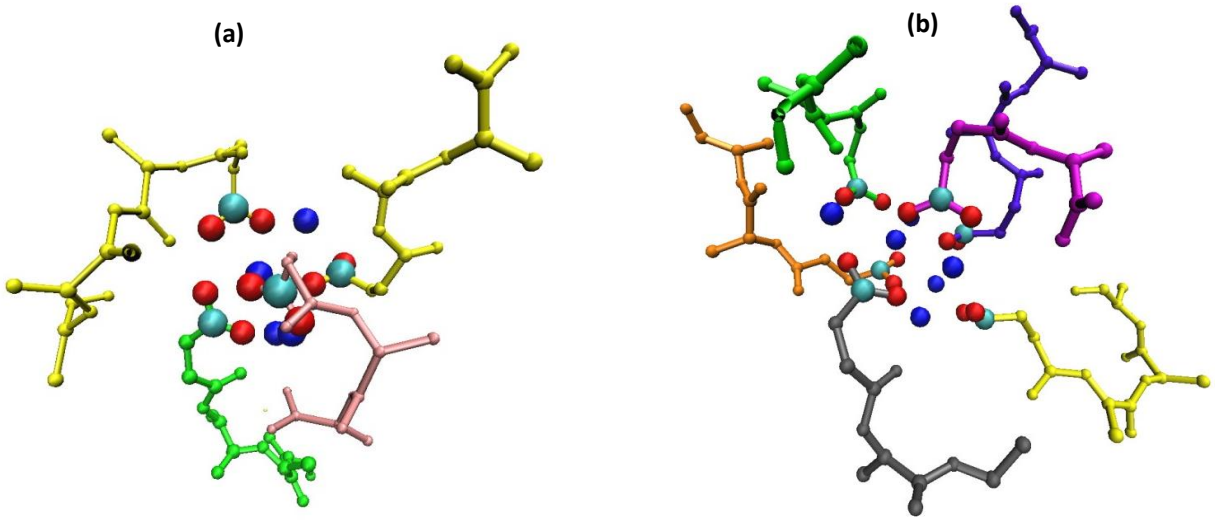

***Figure* 6.7:** (a) cluster with four COO^-Na^+ groups (b) Cluster with six COO^-Na^+ groups (cyan: carbon, red: oxygen, blue: Sodium). Different colors represent arms of different star-ionomers

We analyzed the temperature dependence of the strength of interactions between the ionic tail groups, and Figure 6.8 shows that the most favorable interactions leading to the observed trend of viscosity are the electrostatic interactions between the tail-end COO^-Na^+ groups. A similar non-monotonous temperature dependence of the average interaction energy is observed (Figure 6.8).

6.3.2 Interaction energies (IE)

Interaction energies were calculated from REMD runs. Negative IE represents attraction and positive interaction energy shows repulsion. If the attraction energy increases, the groups come close to each other, associate and the viscosity increases. In Figure 6.8a, a non-monotonic trend, with a dip in the IE is seen around 212 ^oC, depicting strong attraction between ionic end groups, hence higher viscosity. In Figure 6.8b, opposite trend is observed for the IE between tail-end-repeat-units, showing unfavorable interactions. Similar monotonic decrease in negative IE is

observed in Figure 6.8c, which shows IE of the whole system excluding tail-ends. Thus the most prominent interactions leading to the non-monotonic viscosity-temperature trend are the tail-end COO^-Na^+ interactions.

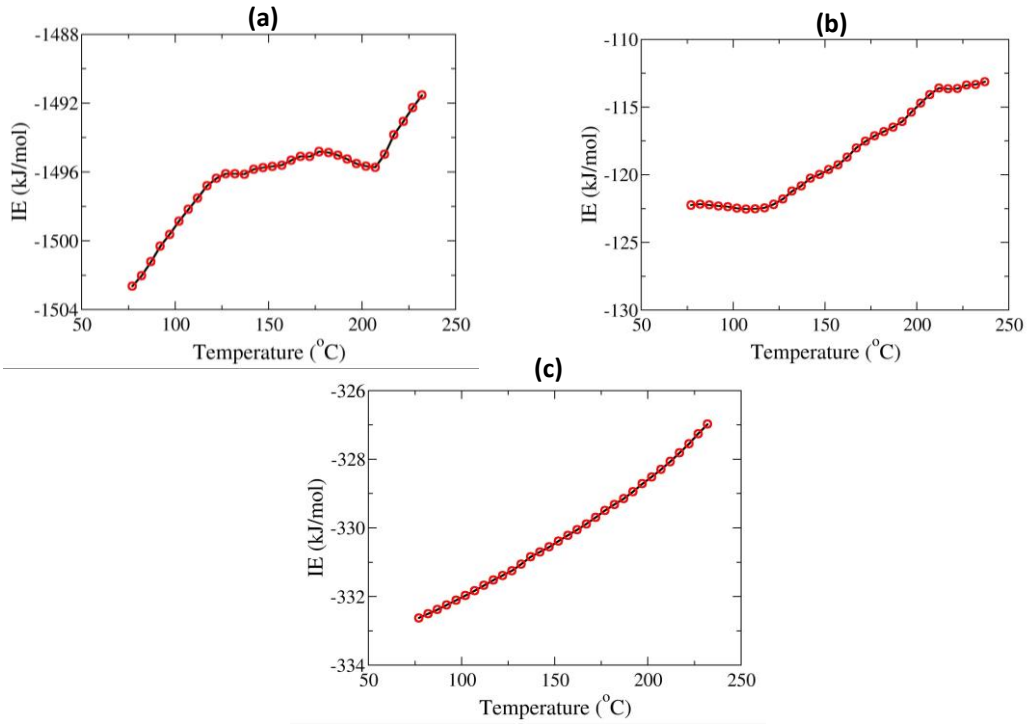

***Figure* 6.8:** (a) Average interaction energy (IE) between tail-end COO^-Na^+ -COO^-Na^+ (b) Average IE between COO^-Na^+ -repeat unit (O-C=O-CH-CH3) (c) Average IE of the system excluding the tail-ends

6.3.3 Comparison of system dynamics

So far we have demonstrated that the time averaged and ensemble averaged properties from equilibrium simulations could provide excellent agreement with experimentally observed non-monotonic temperature dependence of viscosity. Subsequently, we have also performed non-equilibrium MD simulations with sharp changes in temperature in order to understand some of the dynamical features of this system as observed in the experimental time sweep data (Figure 6.1b), where the rate of increase in viscosity is more at higher temperatures. All of these simulations were started from a configuration with very low number of contacts between the tail groups. We have simulated these systems at increasingly higher temperatures in the range of 212 – 302^{o}C. Figure 6.9a shows the time evolution of the number of contacts in these systems. It is

quite evident, that at higher temperatures the system is more mobile leading to faster formation of contacts and clusters. But at lower temperatures the kinetics and diffusion is sluggish and thus formation of clusters is slow as well.

In order to understand how self-diffusion of tail groups might affect the formation of such contacts and vice versa, we show ensemble averaged mean square displacement ($MSD = \langle(r_i(t) - r_i(t_0))^2\rangle$) of chain ends in Figure 6.9b, where $(r_i(t) - r_i(t_0))$ is the displacement of *i*-th particle in time interval Δt ($t-t_0$). A clear correlation between formation of contacts and MSD can be seen. At higher temperatures, MSD is higher due to faster self-diffusion of the terminal groups; consequently the rate of forming contacts is also higher. However once the contacts are formed, a clear suppression of the dynamics can be seen from the saturation of the MSD curves. This behavior is similar to the time sweep observed experimentally. However the selected temperature range here is higher than experiment, since at lower temperatures the dynamics is so sluggish that the changes are not observed in the rather limited timescale of MD simulations. Note that the MSD captures only short time-scale (tens of nanoseconds) of self-diffusion due to the local motions of the terminal groups, and not the global viscous response of the melt due to formation of the percolation network.

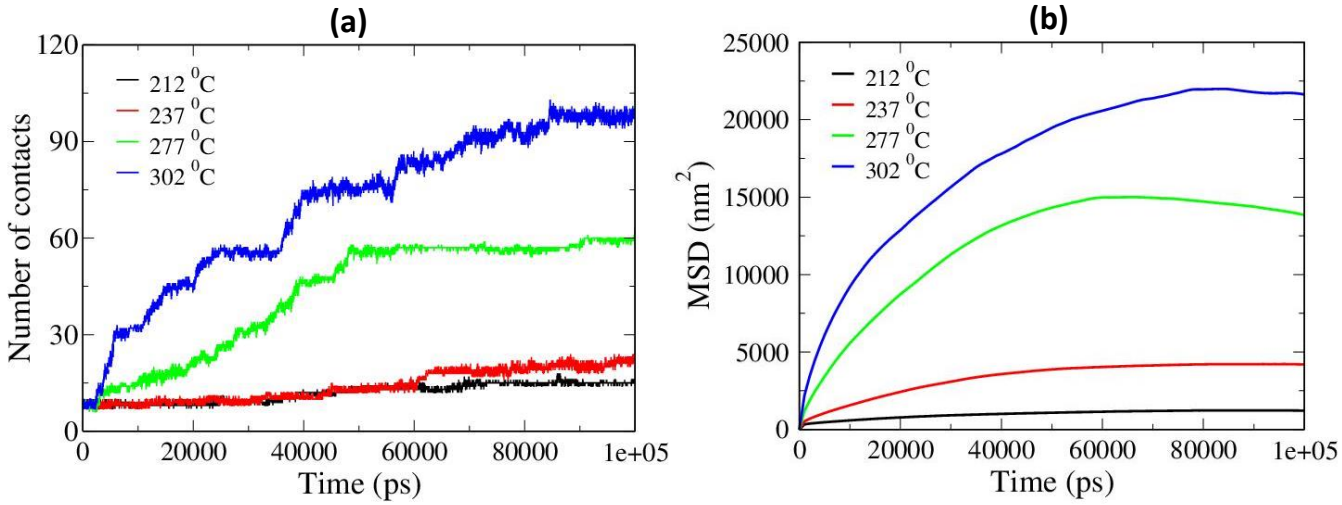

***Figure* 6.9:** (a) Number of contacts with time (b) MSD of chain-end COO^-Na^+ groups with time

6.4 Conclusions

From the above discussions, we can conclude that at the lower temperatures (77-122^{o}C), usual trend of viscosity decrease with the increase in temperature is observed. At intermediate temperatures (125-212^{o}C), due to the supply of thermal energy, diffusive motion of the chains increases and more chain ends can find each other leading to clustering of ionic end groups. In this temperature window, larger clusters form at higher temperatures leading to higher viscosity since more inter-chain contacts are formed leading to stronger and extended percolation network. At even higher temperatures (217-237^{o}C), thermal energy overpowers the association of chains, thus viscosity continues to decrease. Thus, a clear connection between the molecular clustering and temperature dependence of viscosity can be established.

A version of this chapter has been submitted as manuscript.

References

1. Lim, L.-T.; Auras, R.; Rubino, M., Processing technologies for poly (lactic acid). *Progress in polymer science* **2008,** *33* (8), 820-852.

2. Auras, R.; Harte, B.; Selke, S., An overview of polylactides as packaging materials. *Macromolecular bioscience* **2004,** *4* (9), 835-864.

3. Kulkarni, A.; Lele, A.; Sivaram, S.; Rajamohanan, P.; Velankar, S.; Chatterji, A., Star telechelic poly (L-lactide) ionomers. *Macromolecules* **2015,** *48* (18), 6580-6588.

4. Eisenberg, A.; Hird, B.; Moore, R., A new multiplet-cluster model for the morphology of random ionomers. *Macromolecules* **1990,** *23* (18), 4098-4107.

5. Rigdahl, M.; Eisenberg, A., Viscoelastic properties of sulfonated styrene ionomers. *Journal of Polymer Science Part B: Polymer Physics* **1981,** *19* (10), 1641-1654.

6. Greener, J.; Gillmor, J.; Daly, R., Melt rheology of a class of polyester ionomers. *Macromolecules* **1993,** *26* (24), 6416-6424.

7. Bazuin, C.; Eisenberg, A., Ion containing polymers: Ionomers. ACS Publications: 1981.

8. Stadler, F. J.; Pyckhout-Hintzen, W.; Schumers, J.-M.; Fustin, C.-A.; Gohy, J.-F. o.; Bailly, C., Linear viscoelastic rheology of moderately entangled telechelic polybutadiene temporary networks. *Macromolecules* **2009,** *42* (16), 6181-6192.

9. Eisenberg, A., Glass transitions in ionic polymers. *Macromolecules* **1971,** *4* (1), 125-128.

10. Fox Jr, T. G.; Flory, P. J., Viscosity—molecular weight and viscosity—temperature relationships for polystyrene and polyisobutylene1, 2. *Journal of the American Chemical Society* **1948,** *70* (7), 2384-2395.

11. Strobl, G. R.; Strobl, G. R., *The physics of polymers*. Springer: 1997; Vol. 2.

12. Ferry, J. D., *Viscoelastic properties of polymers*. John Wiley & Sons: 1980.

13. Williams, M. L.; Landel, R. F.; Ferry, J. D., The temperature dependence of relaxation mechanisms in amorphous polymers and other glass-forming liquids. *Journal of the American Chemical society* **1955,** *77* (14), 3701-3707.

14. Vlassopoulos, D., Rheology of critical LCST polymer blends: poly (styrene-co-maleic anhydrite)/poly (methyl methacrylate). *Rheologica acta* **1996,** *35* (6), 556-566.

15. Weiss, R.; Fitzgerald, J.; Kim, D., Viscoelastic behavior of lightly sulfonated polystyrene ionomers. *Macromolecules* **1991,** *24* (5), 1071-1076.

16. Weiss, R.; Agarwal, P., Influence of intermolecular interactions on the melt rheology of a propylene–acrylic acid copolymer and its salts. *Journal of Applied Polymer Science* **1981,** *26* (2), 449-462.

17. Kulkarni, A. Thesis in preparation.

18. Sugita, Y.; Okamoto, Y., Replica-exchange molecular dynamics method for protein folding. *Chemical physics letters* **1999,** *314* (1), 141-151.

19. Accelrys Software Inc., M. S. R. N., Release 6.0, Accelrys Software Inc., San Diego.

20. Jorgensen, W. L.; Maxwell, D. S.; Tirado-Rives, J., Development and testing of the OPLS all-atom force field on conformational energetics and properties of organic liquids. *Journal of the American Chemical Society* **1996,** *118* (45), 11225-11236.

21. Hess, B., P-LINCS: A parallel linear constraint solver for molecular simulation. *Journal of Chemical Theory and Computation* **2008,** *4* (1), 116-122.

22. Bussi, G.; Donadio, D.; Parrinello, M., Canonical sampling through velocity rescaling. *The Journal of chemical physics* **2007,** *126* (1), 014101.

23. Berendsen, H. J.; Postma, J. v.; van Gunsteren, W. F.; DiNola, A.; Haak, J., Molecular dynamics with coupling to an external bath. *The Journal of chemical physics* **1984,** *81* (8), 3684-3690.

24. Darden, T.; York, D.; Pedersen, L., Particle mesh Ewald: An N· log (N) method for Ewald sums in large systems. *The Journal of chemical physics* **1993,** *98* (12), 10089-10092.

PART – C

Polyethyleneimine: CO_2 Capture Applications

CHAPTER – 7

CO_2 Capture by Polyethyleneimine: Role of Structural and Dynamical Heterogeneity

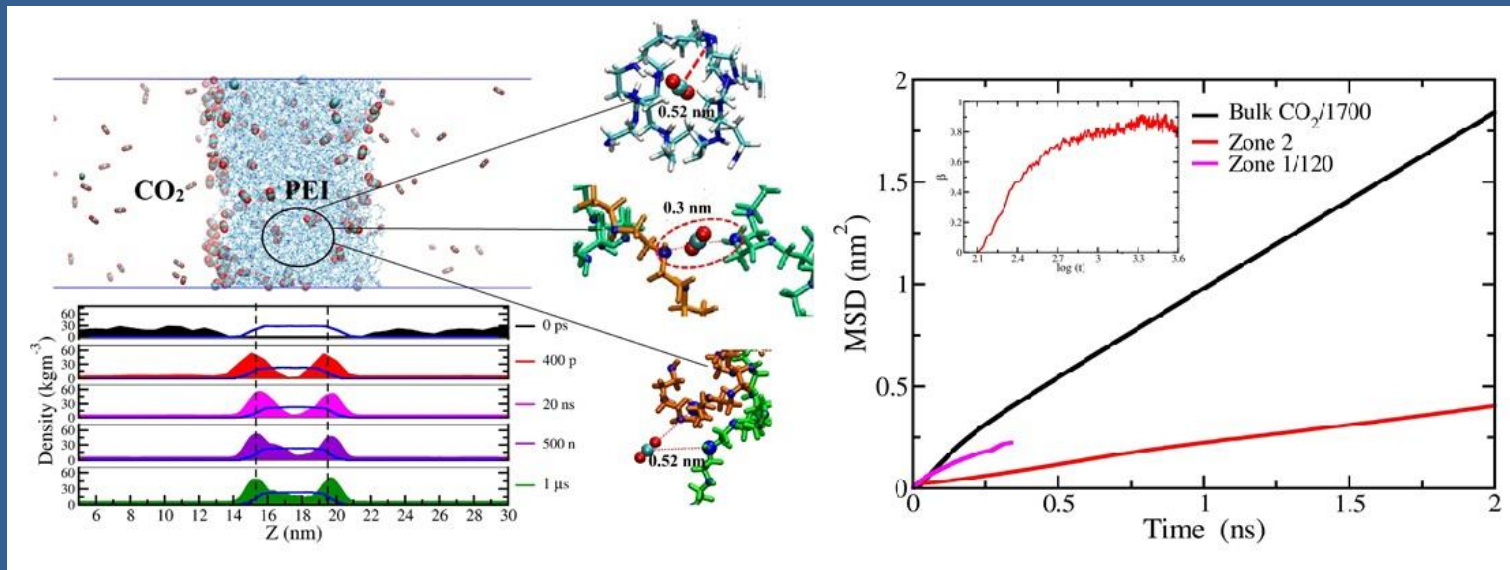

7.1 Introduction

Global warming has become a serious concern worldwide. Increase in the concentration of greenhouse gases, particularly CO_2, in the atmosphere contributes most to it[1]. CO_2 capture and storage (CCS) can be a potential solution to the problem. Among the various established technologies for CO_2 capture, amine scrubbing is the most extensively used one[2-3]. It is based on the selective chemical absorption of the acidic CO_2 gas by basic amine solutions like alkanolamines. Although employed on a large scale, this technology is considered far from being optimal. It suffers from various drawbacks like energy intensive sorbent regeneration, degradation, volatility and corrosion with time[4-5]. Thus alternative options for CO_2 capture have always been sorted.

A brief overview of the existing carbon capture technologies is presented below[6]:

7.1.1 Absorption based: It exploits the chemistry between CO_2 and absorbing material. CO_2 being a Lewis acid, reacts with Lewis bases to form complexes, which then can be removed. Alkanolamines are the most widely used solvent amines for CO_2 capture. CO_2 reacts differently with primary and secondary amines as shown:

Primary or secondary amine $2R_1R_2NH + CO_2 \rightarrow R_1R_2NH^+ + R_1R_2NCOO^-$ *(carbamate)*

Tertiary amine $R_1R_2NH + H_2O + CO_2 \rightarrow R_1R_2NH^+ + HCO_3^-$ *(bicarbonate)*

Primary and secondary amines are more reactive towards CO_2 compared to tertiary amines which requires the presence of water in reaction.

7.1.2 Cryogenic separation: It involves cooling and condensation of flue gas for separation. Based on the difference in boiling points and volatilities, CO_2 is separated from other flue gases.

7.1.3 Adsorption based: CO_2 capture in porous materials involves adsorption. If the interaction of CO_2 with the adsorbent is due to weak Van der Waals and electrostatic forces, physisorption occurs. Chemisorption occurs if there is a formation of covalent bond.

7.1.4 Membrane separations: Membranes act as sieves to separate different gases from a flue gas mixture based on selectivity and permeability.

There are various mechanisms for membrane separation depending on the type of membrane used.

7.1.4.1 Knudsen diffusion: It includes separation of gases through membranes which have pores small enough to avoid bulk diffusion. It is applicable at low pressures only. Separation of gases occurs due to the difference in mean path, which changes due to collision with walls and in turn depends on the molecular weight. Thus heavy gases follow lesser mean path and thus lesser separation. Selectivity is inversely proportional to molecular weight here and thus CO_2/N_2 and CO_2/H_2 selectivity is less than one.

7.1.4.2 Molecular sieving: In this process, gas molecules are separated on the basis of the difference in their diameter or size.

7.1.4.3 Surface diffusion: It involves movement of gas molecules through different adsorption sites along the pore walls or membrane surface. Separation is achieved due to the difference in the interaction of individual gases with adsorption sites.

7.1.4.4 Capillary condensation: It occurs as a result of the difference in vapor pressure of different gases. Gases having lower vapor pressure can undergo condensation in the pores of adsorbents and start diffusing rapidly than other gases.

7.1.4.5 Solution-diffusion: It occurs due the difference in the solubility of gases and their diffusion through the membrane. This is the most common process of gas separation in polymeric membranes.

Of all these processes, absorption using solvent amines suffers from various issues like degradation, volatility and high cost of regeneration. Similarly cryogenic separation is also inefficient in terms of cost and energy since it involves refrigeration, necessary for the process. Solid sorbents and Membranes have emerged as promising alternates to aqueous amine solutions.[4-5, 7] Adsorption always has lower heats of sorption compared to absorption, which reduces the regeneration costs. Membranes are space efficient and are easy to integrate in power plants. Structural variations like casting into thin films or sheets etc. can also be induced in membranes, which make them better processable materials for industries[4, 7-8]. Adsorption based materials are also casted in membranes these days. Various examples of solid adsorbents and membranes for CO_2 capture are activated carbon, porous silica, MOFs (Metal organic frameworks), COFs (covalent organic frameworks), zeolites, inorganic membranes, polymeric membranes etc.

Polar membranes like polysulphones, polycarbonates, polypyrolles, polyamides, polyimides have been widely used for CO_2 capture due to polar interactions with the gas. Among polymeric membranes, polymeric amines form the largest class of materials for CO_2 capture[6]. Glassy polyamines like Polybenzimidazole are generally used at high temperature and pressures[9]. While rubbery polyamines are generally impregnated over porous solid supports and display excellent CO_2 capture capacity in pre-combustion or low temperature and pressure applications[10-11].

Solid-supported polyamines have emerged as promising substitutes to aqueous amine solutions. Tunable porosities, thermal stability with added chemical selectivity from polyamines makes these solid adsorbents efficient candidates for CO_2 capture[7, 12-13]. Among polyamines, Polyethylenemine (PEI) having low volatility and high amine density in the backbone has been extensively used for CO_2 capture[10, 14-16]. Highly efficient CO_2 capture sorbents have been prepared by incorporating PEI with different support materials like porous silica[17], activated carbon[18], carbon nanotubes[19], organic frameworks[20] etc. The most famous examples comprise "molecular baskets" formed by Song and coworkers[17, 21] in which PEI molecules were loaded in the pores of silica (baskets) and PEI adsorption capacity was doubled. It was proposed that PEI loading on high surface area silica sieves exposed more amine sites to surface, thus adsorption capacity increased. Further enhancement in sorption capacity was attained by increasing silica pore size, volume[22-24] and addition of hydrophobic moieties[25] to silica. Higher pore size provided more free volume/spaces for CO_2 diffusion, mobilization of PEI chains and addition of hydrophobic groups exposed hydrophilic amine moieties to the surface leading to increased sorption.

In the same study by Song et al.[17] PEI loading in the silica pores were altered from 0 to 100% to increase the amine interaction sites, however sorption capacity was highest at 50% and then decreased. It was hypothesized that higher PEI loading increased CO_2 binding sites but it also evoked diffusion limitation. Later Li and Ding et al. performed GCMC simulations of single silica-PEI composite[26] (up to 24% loading only) and showed that the increase in adsorption capacity with loading is correlated with the morphological changes in PEI. It was observed that at higher (24%) loading, PEI multilayer is formed so CO_2 can freely diffuse between free spaces of inter-layers leading to increased CO_2 sorption.

Small angle neutron scattering studies on PEI-silica composites[27] also showed that PEI morphology in the pore changes from surface-attached monolayer to plugs/aggregates with

higher loading (>50%). These morphological changes in PEI were also correlated to silica-PEI interactions. It was observed that higher silica-PEI interactions leads to PEI coating on pore-surface and limits the availability of binding amine sites for CO_2 while weak silica-PEI interactions leads to formation of PEI aggregates which hampers CO_2 diffusion.

These studies[17, 22-25, 27] clearly highlights that CO_2 capture in PEI sorbents is a complex interplay of structure, dynamics and interactions between support, polymer and the gas and there is always a trade-off amongst achieving high accessibility of binding amine sites and high accessibility of mass transport/free volume.

While much of the researches focused on balancing this trade-off; enhancing sorption capacity, by changing supports[13, 15, 20, 28], altering support-polymer structure and interactions[22, 25, 29-30], a few attempts were made to modify[27, 31-32] or analyze the polymer properties[33-34] .

Carrillo et al. also deduced a structure-dynamics correlation in PEI-support system using neutron scattering and coarse grained MD simulations[34]. Variable diffusivity of PEI chains was observed depending on the nature of support (attractive to repulsive), solvent (ideal or athermal), and level of pore fillings. This work was recently extended by Jones et al.[33] and PEI dynamics in bulk and silica-PEI composite was compared. Two modes of motion have been detected, a slow (timescale ~ 200ps) motion due to diffusion of center of mass of chains and faster motion (20ps) attributed to locally confined, jump diffusion of PEI side branches. Confinement/support decreased the dynamics of chains but the faster motions were unaffected. It was proposed that faster PEI dynamics is requisite for a better sorbent since it allows easy and fast accessibility of amine binding sites.

These simulation studies definitely provide insights on the structure and dynamics of PEI in sorbents and their effect on the overall sorption property but the detailed molecular mechanism of CO_2 sorption still remains unclear. Moreover none of these simulation studies are conducted in the presence of CO_2 and attractive interactions between PEI and CO_2 would significantly affect these properties.

In a real PEI melt; in the presence or absence of support, chains can pack randomly leading to different local structural conformations. These conformations *viz.* pores, loops, interfaces, aggregates etc. can create spatial heterogeneity in the whole melt affecting the distribution of binding amine sites as well as free volume which will ultimately affect CO_2 sorption in the melt.

Thus questions pertaining detailed molecular mechanism, energetics, adsorption kinetics, sorption heterogeneity at PEI interface and bulk, effect of PEI local conformations on adsorption, CO_2 structure and dynamics in PEI, still remains unanswered. The actual process of CO_2 adsorption in bulk PEI at longer length (50-mer) and timescales (~ μs) has never been explored. Thus to fill this gap, we have done a systematic computational investigation of CO_2 adsorption in bulk PEI using GCMC as well as MD simulation techniques.

7.2 Computational models and methodology

7.2.1 Molecular dynamics simulation

The computational model employed in the present study was created by placing CO_2 on both sides of a well equilibrated box of linear PEI (L-PEI) as shown in Figure 7.1a. The equilibrated box of PEI was initially created and equilibrated in *NpT* ensemble using repeated simulated annealing as discussed by Roy et al[35] and shown in Figure 7.1b.

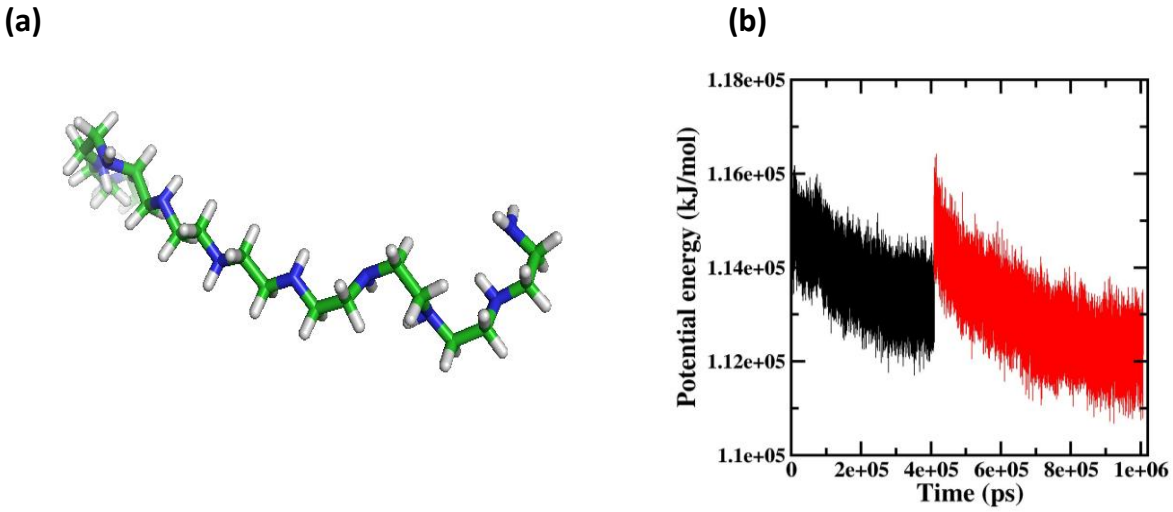

***Figure* 7.1:** (a) Snapshot of a single PEI chain. Green:carbon, white:hydrogen, blue:nitrogen (b) Equilibration of PEI: Potential energy convergence with time. Color changes indicate a simulated annealing step in between

The PEI slab was centered in a box with dimensions 5.8x5.8x32.5 nm (for 10 bar) and sandwiched between two layers of CO_2, containing molecules corresponding to equilibrated CO_2 density at 10 bar. The initial configuration was created such that the slab of CO_2 molecules was separated from PEI layer by a vacuum of 1nm similar to prior literature on CO_2-IL systems[36]. All

simulations were performed using Gromacs-5.0.5 code[37]. Amber forcefield[38] has been employed to simulate all-atomistic model of L-PEI since it has been validated previously in other simulation studies[39-40]. PEI melt consists of 63 chains of linear PEI each having 50 repeat units (structure shown in Figure 7.1a.). Total number of atoms in the resultant PEI melt was ~ 25000. Extensively used TraPPE-flexible force field model[41-43] was employed for CO_2 simulations.

PEI-CO_2 Simulations have been performed in isothermal-isobaric (*NpT*) ensemble. V-rescale thermostat[44] and Berendsen[45] barostat have been used to keep the temperature and pressure fixed during simulations. Particle mesh Ewald[46] (PME) method was used for computing long range electrostatics. A cut-off distance of 1.2 nm is used for short-range columbic and Lennard Jones interactions. Simulations have been conducted at 298K, 1 and 10bar pressures.

7.2.2 Grand canonical Monte Carlo (GCMC) simulations

GCMC simulations were performed using MCCS Towhee software package[47-48]. Input chemical potential of pure CO_2 was calculated using Widom's insertion method[49] in Isothermal-isobaric (*NpT*) ensemble. This method is based on thermodynamic definition of chemical potential. It calculates the change in free energy associated with the insertion of a test particle into an N particle system at a particular temperature and pressure. An equilibrated box of CO_2 containing 512 molecules was taken as the N particle system into which CO_2 molecule was inserted. 1.2 X 10^5 monte-carlo moves of CO_2 insertion have been attempted for appropriate statistical averaging and average chemical potential have been calculated, shown in Figure 7.2a.

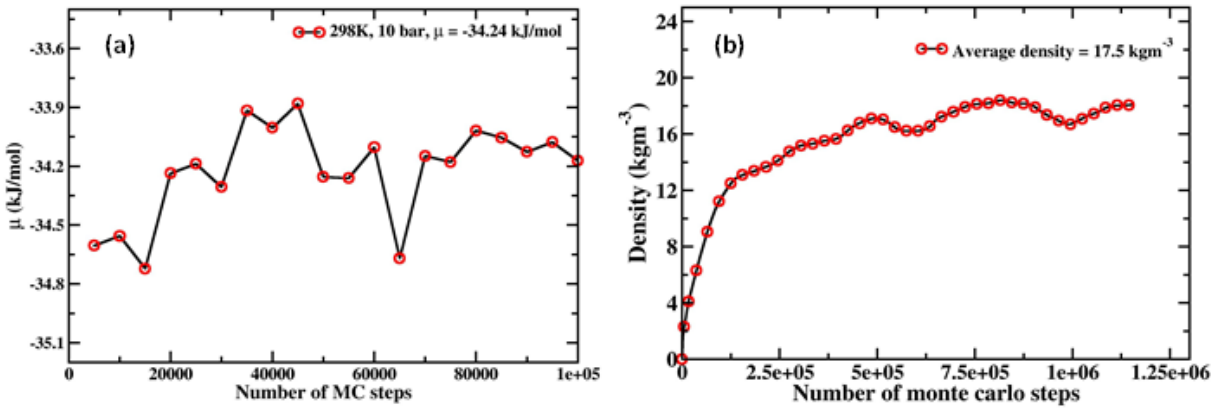

***Figure* 7.2:** (a) Chemical potential with monte carlo steps (b) Covergence of CO_2 density in PEI with Monte Carlo steps at 298K and 10bar

Grand canonical (μVT) ensemble is used to determine the number of CO_2 molecules adsorbed by PEI. Equilibrated box of PEI, prepared as discussed in section 7.2.1 is taken as the adsorbent. Temperature and calculated chemical potential value of CO_2 are given as input. Configurational-bias algorithm was used for insertion/deletion moves as discussed by Martin and Siepmann [48] and Martin and Thompson [50]. GCMC calculations were run for 1.2 million moves till the simulation results converged. Calculations were done at 298K and 1-10bar pressures to obtain adsorption isotherms. Theoretical explanation and detailed description of chemical potential calculations and GCMC calculations can be obtained from Towhee documentation[51].

7.3 Results and Discussions

7.3.1 GCMC simulations-CO_2 adsorption in bulk PEI

CO_2 adsorption behavior in PEI was initially studied using GCMC simulations. Figure 7.3a shows a representative snapshot of PEI-CO_2 system after adsorption. The amount of CO_2 adsorbed in PEI with the number of monte-carlo steps is shown in Figure 7.2b. CO_2 density in PEI gradually increases and achieves saturation at around 1.2 million steps. In the similar way, equilibrated CO_2 density in PEI at pressures 1-10 bar is obtained to calculate adsorption isotherm.

Since gas pressure is a crucial factor influencing sorption capacity of sorbents, hence to further explore the effect of pressure and to determine the nature of adsorption, isotherms have been calculated. Adsorption isotherms plotted in Figure 7.3b shows that CO_2 density in PEI increases within the studied pressure range in a non-linear fashion as observed experimentally by Khader MM et al.[52] for PEI/silica sorbents. Observed adsorption isotherm is also fitted to Langmuir equation similar to experiments[52] and a correlation coefficient of ~ .90 has been obtained.

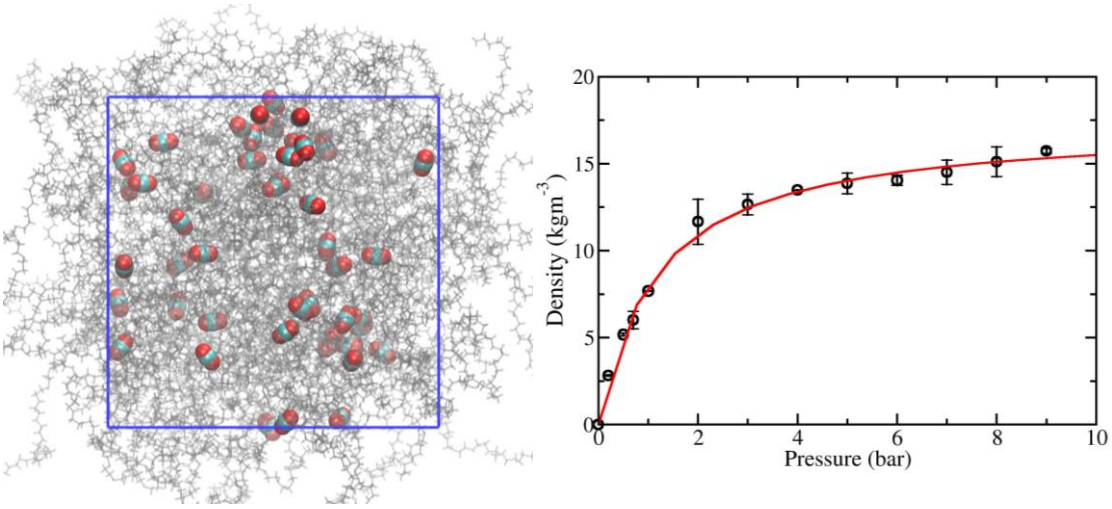

***Figure* 7.3:** (a) Representative snapshot showing adsorption of CO_2 in PEI (b) Adsorption isotherm of CO_2 in PEI (black circles, standard deviation: black bars), data fitted using Langmuir equation[52](red line).

Figure 7.3a portrays a non-homogenous distribution of CO_2 inside PEI which is an indication of structural heterogeneity in the system. To characterize this, Radial distribution functions between carbons of CO_2 in gaseous phase and in PEI melt were calculated as shown in Figure 7.4a. Higher peak intensity with the occurrence of multiple peaks for adsorbed CO_2 shows that CO_2 molecules are heterogeneously distributed in PEI which is further supported by the cluster size distribution shown in Figure 7.4b.

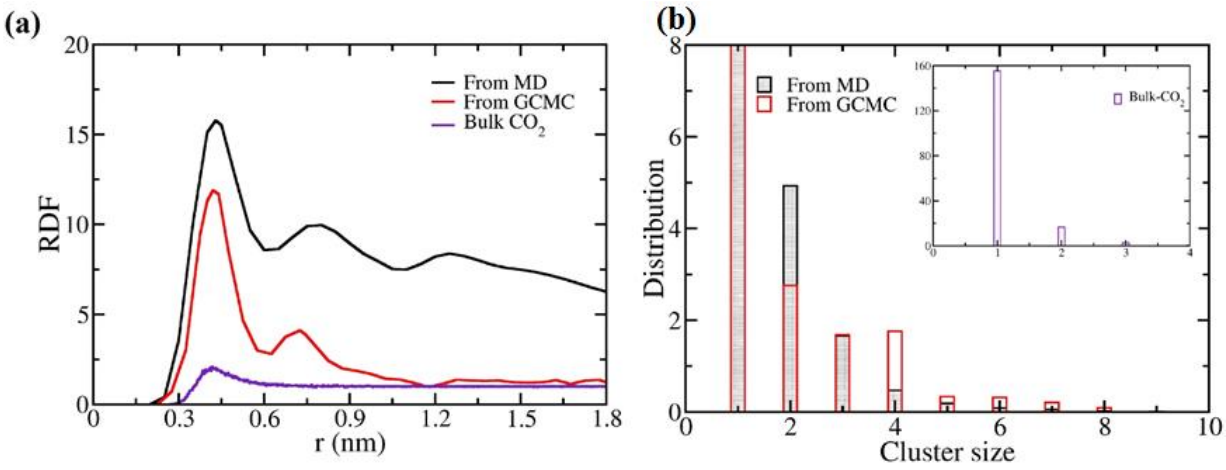

***Figure* 7.4:** (a) Radial distribution function between carbons of CO_2 (b) Cluster size distribution of CO_2 in PEI. Inset: bulk CO_2

As expected, most of the CO_2 molecules are present as monomers, a few as dimers in bulk CO_2 (Inset: Figure 7.4b) while adsorbed CO_2 shows clusters of higher sizes also. This would occur as a consequence of attractive PEI-CO_2 interactions and local arrangement of entangled PEI chains leading to trapping of CO_2 inside PEI. In that case, structural heterogeneity may lead to dynamic heterogeneity which is generally present in caged systems[53]. However, GCMC simulations do not involve time, thus dynamic/time dependent properties cannot be calculated. Besides, PEI-interfaces are also not considered in these calculations which are apparent in real systems and undeniably contribute to CO_2 solubility in PEI.

Thus to include the interfacial structural characteristics and to further investigate the interfacial/bulk adsorption kinetics, energetics, dynamical, structural properties of CO_2 in PEI, MD simulations of PEI-CO_2 systems have been performed.

7.3.2 MD simulations-CO_2 adsorptions at the interface and bulk PEI

The setup used for MD simulations is illustrated in Figure 7.5a, which includes the initial and final (after 1.5 microseconds) configurations.

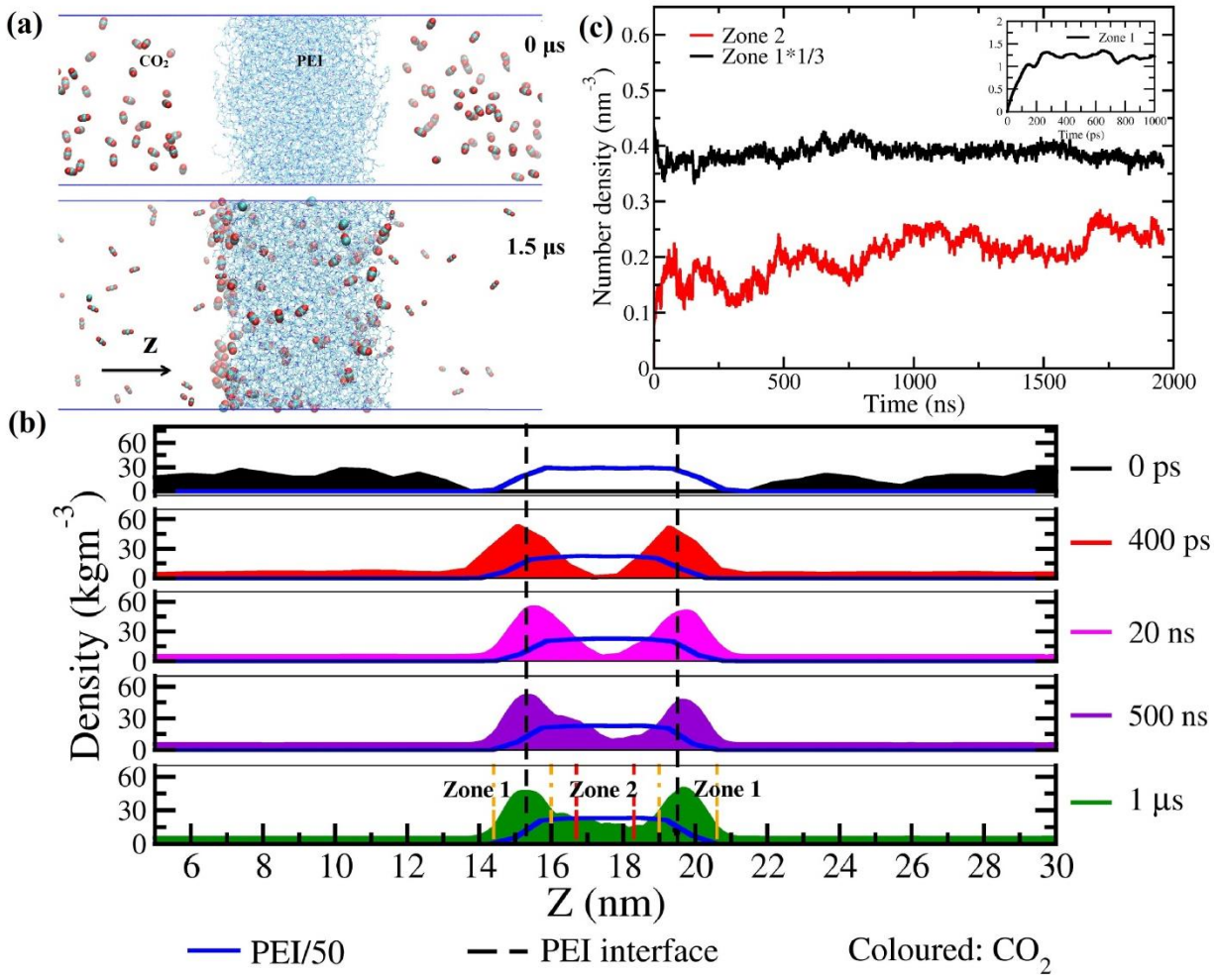

***Figure* 7.5:** (a) Representative snapshots displaying the initial simulation model and CO_2 adsorption profile with time, (b) Time evolution of the partial density profile of CO_2 along Z axis highlighting the adsorption kinetics, (c) Time evolution of CO_2 number density at the interface and in middle region of PEI throughout whole trajectory. Interfacial and middle-bulk regions of PEI are selected by dividing PEI slab into L/4 slabs where L denotes the length of box. Zone 1 denotes the interfacial region; Zone 2 corresponds to middle region of PEI. The position of Zone 1 is from 14.3 to 15.9 nm and 19.0 to 20.6 nm while that of Zone 2 is 16.6 to 18.2 nm as shown in plot 9.5b. CO_2 density in Zone 1 is scaled by 1/3 for illustration purpose. Inset shows saturation of CO_2 number density in Zone 1 during initial 1ns, with saturation observed at ~ 400 ps.

The system was initialized such that CO_2 molecules are present exclusively in the gas phase in order to investigate the kinetics of entry of CO_2 molecules into the PEI phase until equilibration.

The time evolution of the density profile (along surface normal, i.e. Z axis) of CO_2 is shown in Figure 7.5b. Interestingly, there are two distinct time-scales associated with the CO_2 uptake by the PEI membrane. First, there is a rapid growth of local density of CO_2 near the membrane interface (<1ns), followed by a much slower growth (>500ns) in the middle (bulk) region of the membrane. In Figure 7.5c, we further highlight this phenomenon by monitoring the time evolution of local density of CO_2 in an interfacial region (Zone 1) as well as the core region (Zone 2). While the interfacial region reaches saturation by 400ps (see inset of Figure 7.5c), the density in the bulk region of PEI increases in a significantly sluggish manner over hundreds of nanoseconds. Our results clearly establish a two-step mechanism of CO_2 absorption by the PEI membrane: (i) rapid adsorption of CO_2 in the membrane interface, and (ii) much slower release by diffusion of CO_2 from interface to the core (middle) region of PEI melt. Thus the overall kinetics and thermodynamics of CO_2 absorption would be governed by a weighted average of these two processes with widely varying timescales.

Once the CO_2 entry into the PEI membrane reaches a saturation point, we may use the subsequent trajectory for analyzing the equilibrium (both thermodynamic and dynamic) properties of CO_2 inside the membrane. First, we look at the convergence of average CO_2 solubility in the whole PEI membrane and compare with previous GCMC results in Figure 7.6a, where we have reasonable agreement.

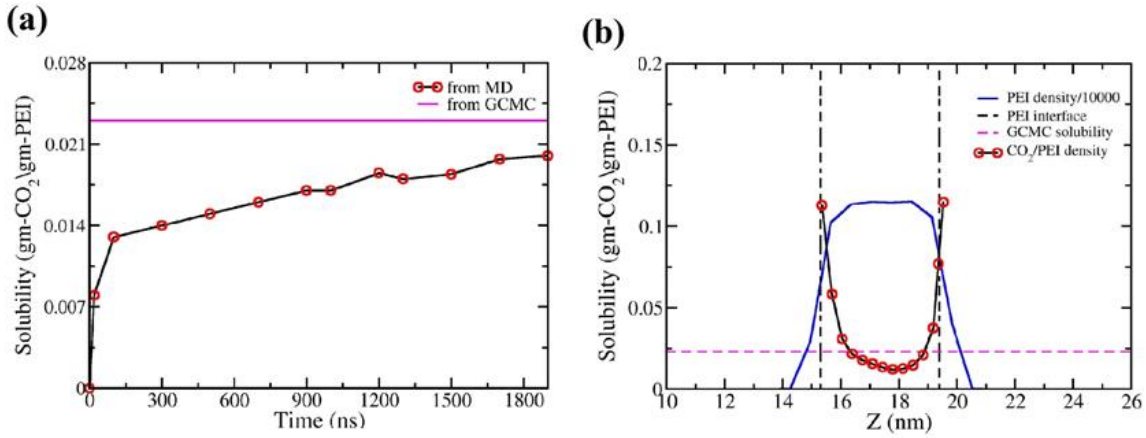

***Figure* 7.6:** (a) Time evolution of CO_2 solubility (red symbols) and its comparison to GCMC solubility (magenta line). Solubility from MD reasonably matches to GCMC at longer times. (b) CO_2 solubility profile in PEI along the surface normal, Z direction. Maximum solubility attained at interfaces of PEI, shown as dashed black lines.

The calculated average solubility in the whole PEI melt was found to be 0.034 g-CO_2/g-PEI, which is also comparable with the experimental results of Goeppert et al[11]: 0.053 g-CO_2/g-PEI at 25^{o}C. A lower solubility compared to the experimental setup is expected in our simulations, since the experimental system was L-PEI-FS (fumed silica) with an approximate CO_2 solubility of fumed silica being 0.010 g-CO_2/g-FS as described elsewhere[54] and also due to diffusion limitations in a heterogeneous system.

Subsequently, we turn our attention to the aspect of spatial heterogeneity of CO_2 solubility in different regions of the membrane, namely the interface and the bulk. Figure 7.6b shows the equilibrium solubility profile of CO_2 along the surface normal averaged over the 500ns of the trajectory after the system reached equilibrium. The solubility profile (gm of CO_2/gm of PEI) indicates the local solubility of CO_2 in PEI in a slab-wise manner, where the solubility has been computed as the ratio of mass of absorbed CO_2 and mass of PEI in a particular slab parallel to the interface. Interestingly, we find that the local solubility of CO_2 molecules is significantly higher near the interfaces as compared to the middle (bulk) region of the PEI membrane. Moreover, the density in the interior, bulk of PEI reasonably matches to the solubility obtained from GCMC simulations as expected.

7.3.3 CO_2 dynamics in PEI

To evaluate the diffusion/mobility of CO_2 in PEI, we have calculated mean square displacement (MSD) and diffusivity of CO_2 in core-PEI and interface and compared it to gaseous/bulk CO_2. Figure 7.7a shows the MSD $<\Delta r^2>$ (t) versus time plot for CO_2. While calculating MSD, CO_2 molecules can exchange between the interface, bulk CO_2 and core-PEI, thus MSD is averaged over only those times where a CO_2 molecule stays continuously in the selected region (interface or core-PEI) for the time interval of 0 to t.

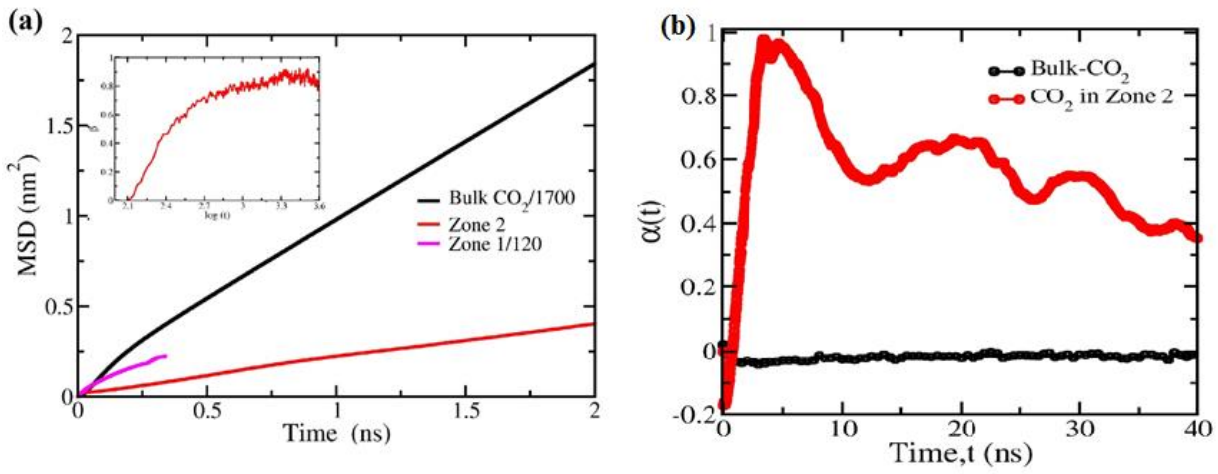

***Figure* 7.7:** (a) MSD versus time for CO_2 in bulk, core PEI. Insets shows MSD at interface and β versus time where MSD α t^{β} (b) Non-gaussian parameter (α) versus time for CO_2 in bulk, core PEI

As expected, MSD of CO_2 in core-PEI is slower (~ 4 orders of magnitude) than that in the bulk. We have also characterized that the motion of CO_2 in PEI is sub-diffusive in nature by calculating β, where MSD α t^{β}, shows the time dependence of MSD. If β =1, it shows diffusive nature while β < 1 would signify sub-diffusive regime. Inset of Figure 7.7a clearly shows that β never reaches to 1, implying that the motion of CO_2 in PEI is sub-diffusive. The diffusivities of CO_2 have been estimated using Einstein equation. For CO_2 in PEI, diffusivities are calculated at times when β saturates. Diffusion constant of bulk CO_2 is 1316 ± 101.5 X 10^{-5} cm^2/s while that inside PEI is 0.6 X 10^{-5} cm^2/s. These results clearly indicate that the attractive interaction between PEI and CO_2 leads to trapping of CO_2 in PEI which is implicated as the decrease in mobility.

Heterogeneous dynamics of CO_2 may arise as a result of trapping, which was tested by calculating non-gaussian parameter (α)[55] as given by equation 1:

$$\alpha(t) = \frac{3\langle r^4(t)\rangle}{5\langle r^2(t)\rangle^2} - 1 \qquad \textbf{(7.1)}$$

Here *r* denotes the displacement of the molecule in a time interval *t*. The value of $\alpha(t)$ is zero when the dynamics of the system is homogeneous, it increases with the increase in dynamic heterogeneity in the system. As expected, $\alpha(t)$ value fluctuates around zero (Figure 7.7b) for bulk CO_2 gas while it shows higher positive values and a peak around 4ns showing typical behavior of confined dynamics[56].

Another molecular measure to characterize sluggish dynamics and interphasial interactions between PEI-CO_2 is higher residence times of molecules. Residence time is defined as the uninterrupted time during which a particle stays in a region. Residence time probability of CO_2 molecules at interface is shown in Figure 7.8.

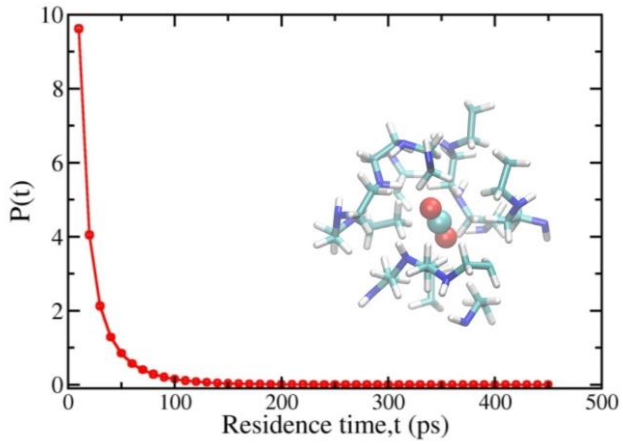

***Figure* 7.8:** Residence time probability of CO_2 molecules at the interface, CO_2 trapped in pore is also shown.

CO_2 shows average residence time of 25 ps and high residence times, up to 450 ps at the interface. This value matches with the continuous time (400 ps) for which MSD at interface was calculated. Molecules showing highest residence times were tracked in the trajectory to explore the correlation between high residence time and local structural configurations of PEI, if any. It was observed that such molecules are actually enclosed in the pores formed by the segments of PEI chain as shown in Figure 7.8. These results also conclude that CO_2 shows preferential adsorption at more free volume spaces like interfaces and pores. Klahn et al. had also pointed out the fact that solubility of CO_2 in ionic liquids also depends on the availability of unoccupied space[57].

A few CO_2 molecules showing high residence times were selected and their motion was observed throughout the trajectory to deduce if such molecules are always present at the interface or in pores. For this analysis, we calculated the distribution of average number of CO_2 molecules present around all 63 chains as shown in Figure 7.9a.

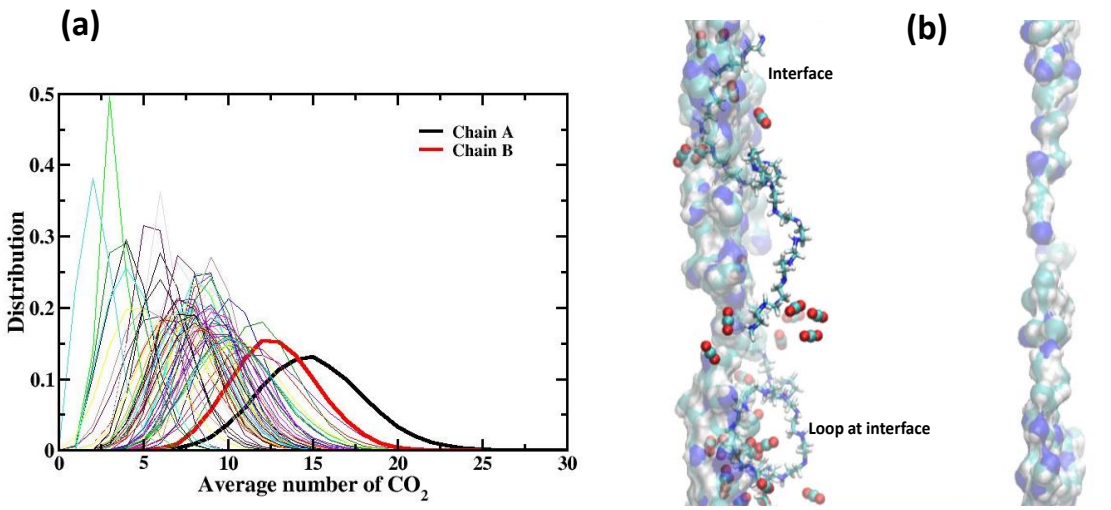

***Figure* 7.9:** (a) Distribution of average number of CO_2 present around individual 63 chains of the polymer melt. Chain A contains maximum number of surrounding CO_2 followed by chain B (b) Chain A: containing maximum number of surrounding CO_2 present at the interface, Solid lines: interface. Loops at the interface shows higher adsorption

Two chains; showing maximum number of surrounding CO_2 molecules were selected. It occurred that the chain showing maximum number of adsorbed CO_2 (Chain A) is present at the interface as shown in Figure 7.9b. However to our surprise, this is always not the case, the chain showing second highest number of adsorbed CO_2 molecules (Chain B) spans throughout the PEI matrix. At a single chain level, regions showing higher adsorption were analyzed. It happened that the loops formed by the entanglement of chains (Region1, Figure 7.10a) also shares comparable population of CO_2 as the segments touching interface. The loops formed at the interface (Region2, Figure 7.10a) actually showed highest population. Similarly for Chain A also, highest adsorption is observed for loops at interface. The population of CO_2 present in four different regions of chain B (Figure 7.10a) is presented in Figure 7.10b.

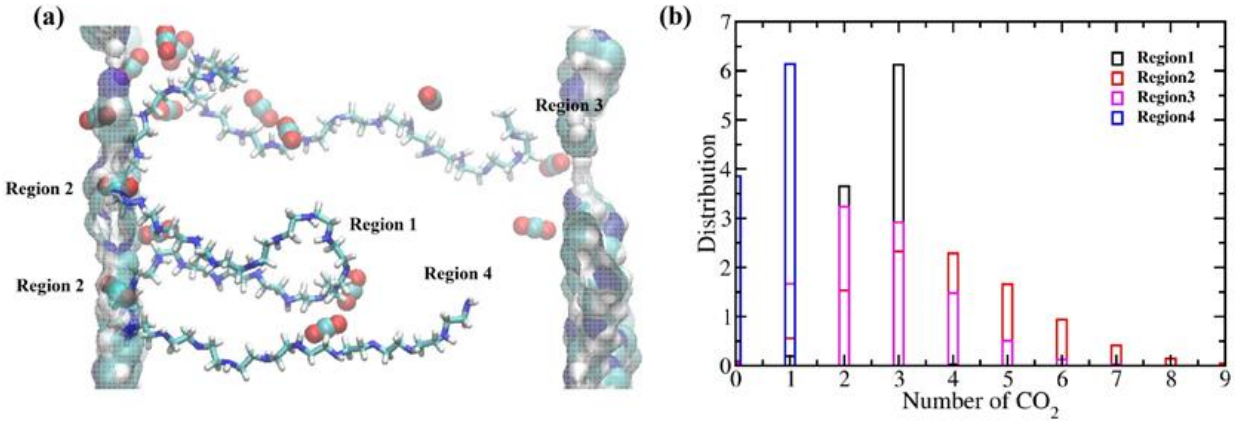

***Figure* 7.10:** (a) Chain B, showing second highest amount of adsorbed CO_2, Region1 is the loop in PEI matrix, Region 2 are the loops formed at the interface, Region 3 is the chain-end at the interface, Region 4 is the chain-start residue in PEI, Solid surfaces represents interface. (b) Time averaged distribution of number of CO_2 molecules in the four regions.

Thus population distribution of CO_2 in PEI melt (Figure 7.10b) also elucidated higher propensity of CO_2 adsorption at regions associated with interfaces.

In order to further dissect the thermodynamic origin of the preferential binding and higher solubility of CO_2 in the interfacial region, we have computed the free energy of absorption or PMF (potential of mean force) of CO_2 molecules along the surface normal of the membrane as shown in Figure 5a. The PMF ($G(z)$) is calculated by the Boltzmann inversion of the partial density profile ($\rho_{(z)}$) as defined below.

$$G(z) = -k_B T \ln \rho_{(z)} - G(z_0) \qquad \textbf{(7.2)}$$

Where reference $G(z_0)$ is choosen to be the free energy at large distance from the interface

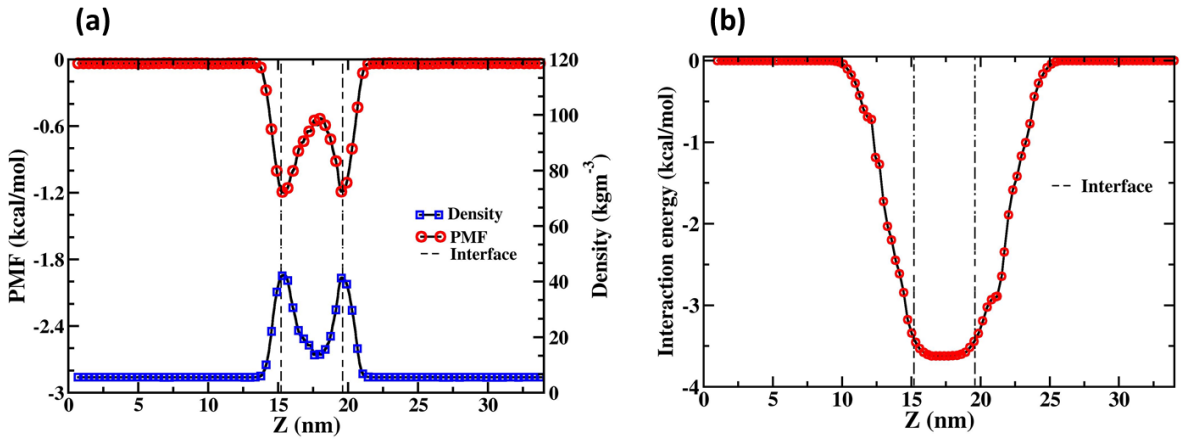

***Figure* 7.11:** (a) Partial density along z direction and PMF (b) Interaction energy along z direction

It is observed from the free energy profile that two strong minima exist at the interfaces with stabilization of 1.19 kcal/mol, which acts as the driving force for preferential adsorption of CO_2 at the interfaces. In order to dissect the role of interaction energy versus entropy towards the higher binding affinity in the interfaces, we have also calculated the average interaction energy (IE) profile between PEI and CO_2, per CO_2 molecule along Z direction as shown in Figure 7.11b. Interestingly, the average PEI-CO_2 interaction energy is more negative (favorable) near the middle (bulk) region of PEI as compared to interface due to overall higher density of PEI near the bulk region Thus, it is quite evident that the stabilization near the interfaces is predominantly entropic in origin. CO_2 adsorption is preferred at regions of higher free volume, even if with lower interaction energy. Thus while designing novel CO_2 absorbing materials it is not enough to optimize the interaction energy with individual binding sites, but maximization of free volume is particularly crucial for enhanced adsorption.

7.3.4 Structural view of PEI-CO_2 interactions

The analyses done so far have been discretely focused on PEI interface and core, however local structural interactions between CO_2 and amine sites, local chain conformations and PEI packing also affects adsorption. In order to examine local structural features, radial distribution function (RDF) between nitrogen of PEI (N) and carbon of CO_2 (C) was calculated. Figure 7.12a shows the RDF along with snapshots depicting the structural arrangement at respective peaks.

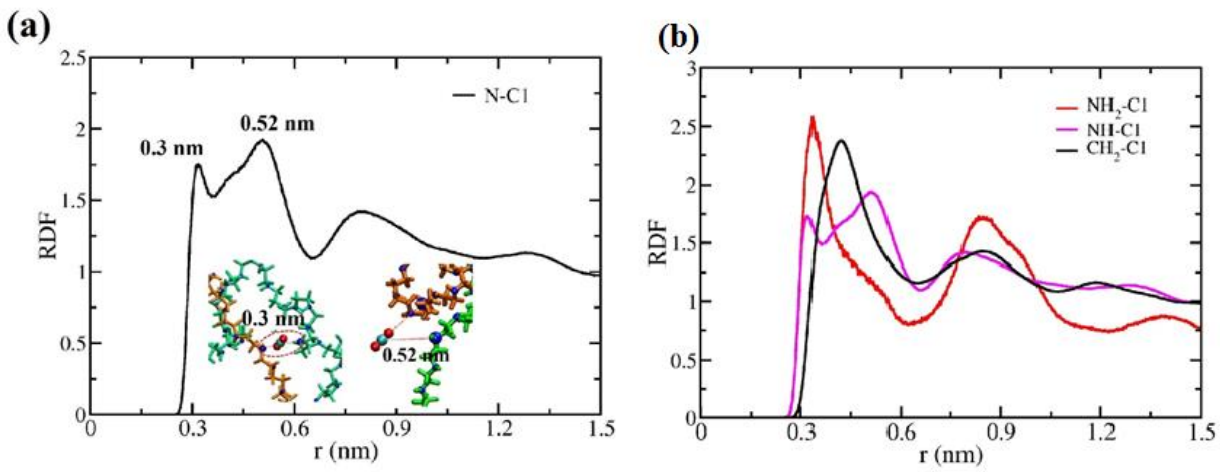

***Figure* 7.12:** (a) RDF between nitrogen (N) of PEI and carbon (C1) of CO_2. Cyan: carbon, red: oxygen, blue: Nitrogen. (b) RDF between C1 of CO_2 and different functional groups in PEI. NH_2: primary amine, NH: secondary amine, CH_2: methylene

A peak at 0.3 nm arises due to weak electrostatic interaction between CO_2 and amine. This peak may appear due to H bonding, so for checking the angle criterion, distribution of angle between N-O vector (N of PEI-oxygen of CO_2) and N-H vector was calculated. Maximum CO_2 molecules are present parallel ($\cos\theta = -1$) to the amines and minimal distribution is seen for angles less than 30^o eliminating the possibility of strong H-bonding. A peak at 0.3 nm appears due to attractive electrostatic interactions then the peak around 0.52 nm would arise due to dispersive interactions signifying physisorption. This assumption is indirectly supported by the previous experimental and simulation findings of Builes et al.[29] on PEI-silica adsorbents, where a correlation between the type of sorption and distance between two neighboring nitrogen in the sorbents was determined. They stated that chemisorption will occur for only if N-N distance is comparable to the size of CO_2 (0.23 nm). And for a N-N distance of 0.42 nm, apparently no chemisorption was observed in their study. It means the observed N-C1 peak at distance of 0.52 nm in the RDF plot would definitely signify physisorption.

On the similar grounds, we have also observed heterogeneous distribution of CO_2 in PEI with PEI density. Molecules corresponding to 0.52 nm peak (bicolored in Figure 7.13) are mostly accumulated at the interfaces (low density regions), while those at 0.3 nm (purple in Figure 7.13) are present in core-PEI (higher density region). Physisorbed CO_2 molecules form the major

population of adsorbed CO_2. Mi and Du et al.[31] have also suggested that for longer chain length PEIs, physisorption contributes more.

While most of the molecules showing peak at ~ 0.52 nm lies at interface, a few are present in the high density; core-PEI region. We found out that such molecules are actually present in the pores formed by segments of PEI (Figure 7.13). In these pores CO_2 is surrounded by amine groups on all sides, attractive interactions from all sides keep it at a distance of ~ 0.5 nm. The radius of such pores varies from 0.36 to 0.55 nm.

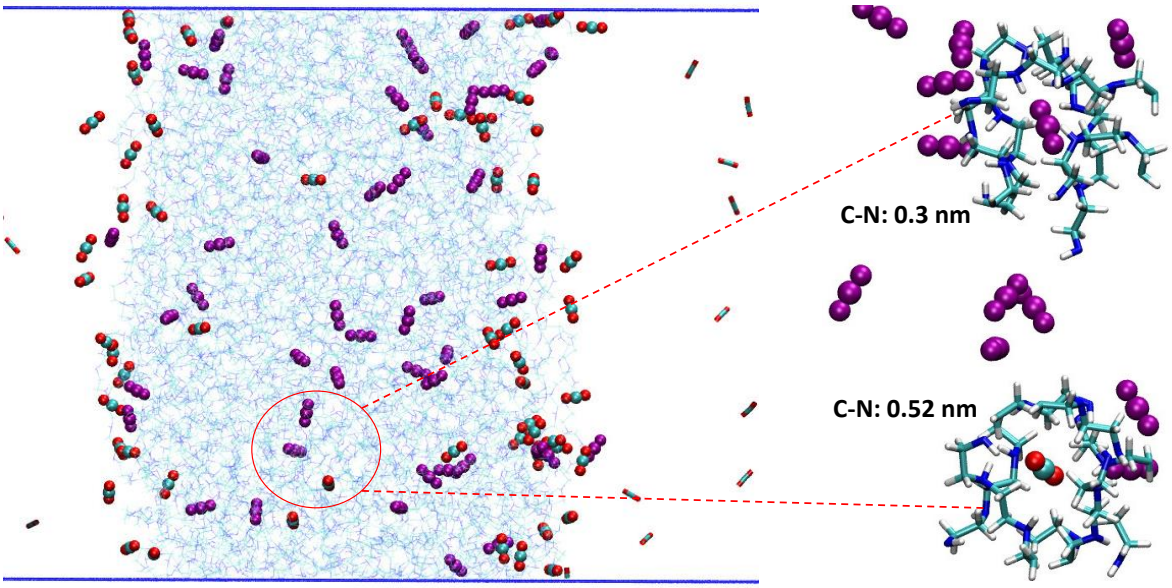

***Figure* 7.13:** Distribution of CO_2 molecules in PEI melt having N-C1 distance between 0-0.3nm (purple) and N-C1 distance between 0.4-0.55 nm (colored-cyan and red)

These instances clearly prove that local structural conformations of PEI (pores, loops, entanglements) are also an influential factor in CO_2 adsorption. We further looked into the molecular compositions of these structures and found out various possible arrangements of PEI chains as shown in Figure 7.14.

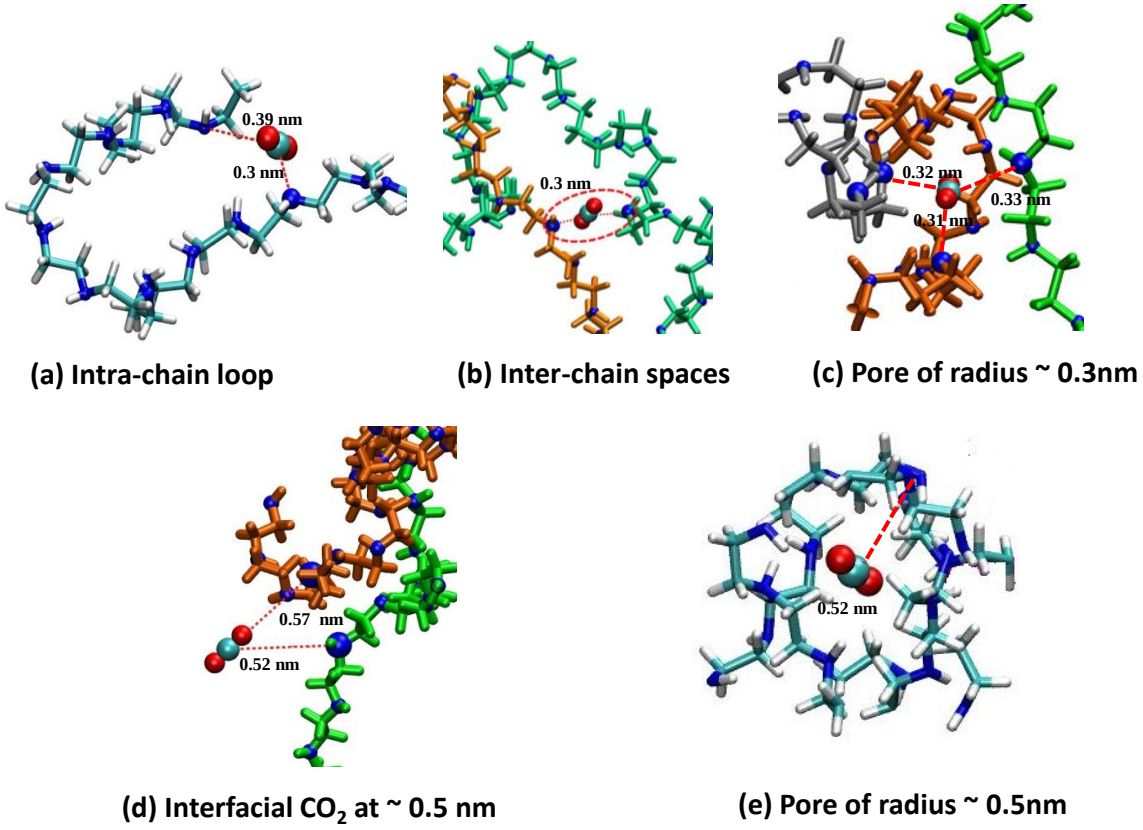

***Figure* 7.14:** Different possible structural arrangements of PEI around CO_2 corresponding to the peaks in N-C1 RDF shown in Figure 7.12.

***Table* 7.1:** Interaction energy values for different structures of Figure 7.14 (a-e) "f" denotes the pore present at interface showing highest residence time, shown in Figure 7.8

Structures	Interaction energy (LJ+CB) (kJ/mol)
a	-29.21± 1.3
b	-34.24 ± 1.6
c	-38.14 ± 0.9
d	-0.86 ± 0.0
e	-30.69 ± 1.0
f	-13.043 ± 2.1

Different compositions involve intra chain loops, inter-chain spaces, tri-coordinated inter chain pores etc. The interaction energy of CO_2 with PEI segments in these structures is also shown in Table 7.1.The tri-coordinated pores showing a radius of ~0.3 nm showed highest interaction energy followed by inter chain pores and then loops. Molecules at the interface at a distance of ~ 0.5 nm showed weakest interactions. This gives an indication on why interfacial CO_2s could not approach nearer to PEI (0.3 nm) instead having more free space. It can be inferred that the low density of PEI at interfaces leads to weaker electrostatic interactions which are insufficient to attract CO_2 as close as 0.3 nm, thus they stay at larger distance at interfaces.

At a single chain level, RDF between C1 and N of primary amine (NH_2) and secondary amine (NH) was calculated as shown in Figure 7.12b. Higher intensity peak at 0.3 nm for primary amine indicate stronger interaction with CO_2 followed by secondary amine. An only single peak around 0.5 nm for CH_2 group obviously indicates the absence of electrostatic interactions. Availability of more free volume around primary amines which are present only at chain ends also aids in the closer approach of CO_2 towards it.

Thus, either at a single chain level or in bulk PEI, free volume/spaces is the controlling factor for CO_2 adsorption in L-PEI.

7.4 Conclusions

Presence of amine centers and high charge density makes Polyethyleneimine a promising candidate for carbon dioxide capture. This work investigates the detailed mechanism of CO_2 capture in PEI through GCMC and MD simulations. Solubility predicted from the MD simulations is comparable to the experiments, thus validating the choice of model and force field. Spatial heterogeneity is observed for all the calculated properties clearly delineating different trends at interface and core-PEI. Structural heterogeneity accompanied with dynamic heterogeneity is observed as the clustering of CO_2 occurs in PEI leading to sub-diffusive behavior/caged dynamics. Higher CO_2 solubility and faster adsorption kinetics at interfaces, probed using MSD and exchange time analysis establishes the availability of free volume as the major factor affecting CO_2 adsorption in PEI. Not only interfaces, spacious regions like pores and loops, chain ends formed in core-PEI also showed higher capture capacity supporting the stated fact. The mechanism of adsorption, initially is interaction mediated till interface saturates, after that it becomes diffusion limited. Various factors *viz.* CO_2-PEI interactions, diffusion, PEI

density, conformations of PEI chain, availability of free volume etc. affects adsorption. However, in the complex interplays of all these factors, free volume/entropy, emerge out to be the dominating factor governing CO_2 adsorption in PEI.

This study provides a fundamental understanding of the mechanism, kinetics of CO_2 adsorption in PEI along with various structural and dynamical properties of CO_2 in PEI which will further aid in developing new PEI based adsorbents.

A version of this chapter has been published[58].

Sharma, P.; Chakrabarty, S.; Roy, S.; Kumar, R., Molecular View of CO_2 Capture by Polyethylenimine: Role of Structural and Dynamical Heterogeneity Langmuir 2018, 34 (17), 5138–5148

References

1. Allen, M. R.; Frame, D. J.; Huntingford, C.; Jones, C. D.; Lowe, J. A.; Meinshausen, M.; Meinshausen, N., Warming caused by cumulative carbon emissions towards the trillionth tonne. *Nature* **2009,** *458* (7242), 1163-1166.

2. Hermann, W.; Bosshard, P.; Hung, E.; Hunt, R.; Simon, A., An assessment of carbon capture technology and research opportunities. *Glob. Clim. Energy Proj. Spring* **2005**.

3. Rochelle, G. T., Amine scrubbing for CO2 capture. *Science* **2009,** *325* (5948), 1652-1654.

4. Samanta, A.; Zhao, A.; Shimizu, G. K.; Sarkar, P.; Gupta, R., Post-combustion CO2 capture using solid sorbents: a review. *Industrial & Engineering Chemistry Research* **2011,** *51* (4), 1438-1463.

5. Pera-Titus, M., Porous inorganic membranes for CO2 capture: present and prospects. *Chemical reviews* **2013,** *114* (2), 1413-1492.

6. Kentish, S. E.; Scholes, C. A.; Stevens, G. W., Carbon dioxide separation through polymeric membrane systems for flue gas applications. *Recent Patents on Chemical Engineering* **2008,** *1* (1), 52-66.

7. Lu, W.; Sculley, J. P.; Yuan, D.; Krishna, R.; Zhou, H.-C., Carbon dioxide capture from air using amine-grafted porous polymer networks. *The Journal of Physical Chemistry C* **2013,** *117* (8), 4057-4061.

8. D'Alessandro, D. M.; Smit, B.; Long, J. R., Carbon dioxide capture: prospects for new materials. *Angewandte Chemie International Edition* **2010,** *49* (35), 6058-6082.

9. Berchtold, K. A.; Singh, R. P.; Young, J. S.; Dudeck, K. W., Polybenzimidazole composite membranes for high temperature synthesis gas separations. *Journal of membrane science* **2012,** *415*, 265-270.

10. Shen, X.; Du, H.; Mullins, R. H.; Kommalapati, R. R., Polyethylenimine Applications in CO2 Capture and Separation: from Theoretical Study to Experimental work. *Energy Technology* **2017**.

11. Zhang, H.; Goeppert, A.; Prakash, G. S.; Olah, G., Applicability of linear polyethylenimine supported on nano-silica for the adsorption of CO 2 from various sources including dry air. *RSC Advances* **2015,** *5* (65), 52550-52562.

12. Wang, Q.; Luo, J.; Zhong, Z.; Borgna, A., CO2 capture by solid adsorbents and their applications: current status and new trends. *Energy & Environmental Science* **2011,** *4* (1), 42-55.

13. Lu, W.; Sculley, J. P.; Yuan, D.; Krishna, R.; Wei, Z.; Zhou, H. C., Polyamine-Tethered Porous Polymer Networks for Carbon Dioxide Capture from Flue Gas. *Angewandte Chemie International Edition* **2012,** *51* (30), 7480-7484.

14. Goeppert, A.; Czaun, M.; May, R. B.; Prakash, G. S.; Olah, G. A.; Narayanan, S., Carbon dioxide capture from the air using a polyamine based regenerable solid adsorbent. *Journal of the American Chemical Society* **2011,** *133* (50), 20164-20167.

15. Zhou, Z.; Anderson, C.; Butler, S. K.; Thompson, S.; Whitty, K.; Shen, T.-C.; Stowers, K., Stability and efficiency of CO 2 capture using linear amine polymer modified carbon nanotubes. *Journal of Materials Chemistry A* **2017**.

16. Wang, X.; Song, C., New strategy to enhance CO2 capture over a nanoporous polyethylenimine sorbent. *Energy & Fuels* **2014,** *28* (12), 7742-7745.

17. Xu, X.; Song, C.; Andresen, J. M.; Miller, B. G.; Scaroni, A. W., Novel Polyethylenimine-Modified Mesoporous Molecular Sieve of MCM-41 Type as High-Capacity Adsorbent for CO2 Capture. *Energy & Fuels* **2002,** *16* (6), 1463-1469.

18. Wang, D.; Ma, X.; Sentorun-Shalaby, C.; Song, C., Development of carbon-based "molecular basket" sorbent for CO2 capture. *Industrial & Engineering Chemistry Research* **2012,** *51* (7), 3048-3057.

19. Dillon, E. P.; Crouse, C. A.; Barron, A. R., Synthesis, characterization, and carbon dioxide adsorption of covalently attached polyethyleneimine-functionalized single-wall carbon nanotubes. *Acs Nano* **2008,** *2* (1), 156-164.

20. Lin, Y.; Yan, Q.; Kong, C.; Chen, L., Polyethyleneimine incorporated metal-organic frameworks adsorbent for highly selective CO2 capture. *Scientific reports* **2013,** *3*, 1859.

21. Xu, X.; Song, C.; Miller, B. G.; Scaroni, A. W., Influence of moisture on CO2 separation from gas mixture by a nanoporous adsorbent based on polyethylenimine-modified molecular sieve MCM-41. *Industrial & engineering chemistry research* **2005,** *44* (21), 8113-8119.

22. Heydari-Gorji, A.; Yang, Y.; Sayari, A., Effect of the pore length on CO2 adsorption over amine-modified mesoporous silicas. *Energy & Fuels* **2011,** *25* (9), 4206-4210.

23. Son, W.-J.; Choi, J.-S.; Ahn, W.-S., Adsorptive removal of carbon dioxide using polyethyleneimine-loaded mesoporous silica materials. *Microporous and Mesoporous Materials* **2008,** *113* (1), 31-40.

24. Zhang, H.; Goeppert, A.; Czaun, M.; Prakash, G. S.; Olah, G. A., CO 2 capture on easily regenerable hybrid adsorbents based on polyamines and mesocellular silica foam. Effect of pore volume of the support and polyamine molecular weight. *RSC Advances* **2014,** *4* (37), 19403-19417.

25. Heydari-Gorji, A.; Belmabkhout, Y.; Sayari, A., Polyethylenimine-impregnated mesoporous silica: effect of amine loading and surface alkyl chains on CO2 adsorption. *Langmuir* **2011,** *27* (20), 12411-12416.

26. Wang, W.; Li, J.; Wei, X.; Ding, J.; Feng, H.; Yan, J.; Yang, J., Carbon dioxide adsorption thermodynamics and mechanisms on MCM-41 supported polyethylenimine prepared by wet impregnation method. *Applied Energy* **2015,** *142*, 221-228.

27. Holewinski, A.; Sakwa-Novak, M. A.; Jones, C. W., Linking CO2 sorption performance to polymer morphology in aminopolymer/silica composites through neutron scattering. *Journal of the American Chemical Society* **2015,** *137* (36), 11749-11759.

28. Zeng, Y.; Zou, R.; Zhao, Y., Carbon Dioxide Capture: Covalent Organic Frameworks for CO2 Capture (Adv. Mater. 15/2016). *Advanced Materials* **2016,** *28* (15), 3032-3032.

29. Builes, S.; López-Aranguren, P.; Fraile, J.; Vega, L. F.; Domingo, C. n., Analysis of CO2 adsorption in amine-functionalized porous silicas by molecular simulations. *Energy & Fuels* **2015,** *29* (6), 3855-3862.

30. Chen, C.; Son, W.-J.; You, K.-S.; Ahn, J.-W.; Ahn, W.-S., Carbon dioxide capture using amine-impregnated HMS having textural mesoporosity. *Chemical Engineering Journal* **2010,** *161* (1), 46-52.

31. Zhao, Q.; Wang, Q.; Zhang, C.; Du, Z.; Tian, M.; Mi, J., Effect of chain topology of polyethylenimine on physisorption and chemisorption of carbon dioxide. *ChemPhysChem* **2015,** *16* (7), 1480-1490.

32. Andreoli, E.; Dillon, E. P.; Cullum, L.; Alemany, L. B.; Barron, A. R., Cross-linking amine-rich compounds into high performing selective CO2 absorbents. *Scientific reports* **2014,** *4*, 7304.

33. Holewinski, A.; Sakwa-Novak, M. A.; Carrillo, J.-M. Y.; Potter, M. E.; Ellebracht, N.; Rother, G.; Sumpter, B. G.; Jones, C. W., Aminopolymer Mobility and Support Interactions in Silica-PEI Composites for CO2 Capture Applications: A Quasielastic Neutron Scattering Study. *The Journal of Physical Chemistry B* **2017**.

34. Carrillo, J.-M. Y.; Sakwa-Novak, M. A.; Holewinski, A.; Potter, M. E.; Rother, G.; Jones, C. W.; Sumpter, B. G., Unraveling the dynamics of aminopolymer/silica composites. *Langmuir* **2016,** *32* (11), 2617-2625.

35. Sharma, P.; Roy, S.; Karimi-Varzaneh, H. A., Validation of Force Fields of Rubber through Glass-Transition Temperature Calculation by Microsecond Atomic-Scale Molecular Dynamics Simulation. *The Journal of Physical Chemistry B* **2016,** *120* (7), 1367-1379.

36. Prakash, P.; Venkatnathan, A., Molecular mechanism of CO 2 absorption in phosphonium amino acid ionic liquid. *RSC Advances* **2016,** *6* (60), 55438-55443.

37. Hess, B.; Kutzner, C.; Van Der Spoel, D.; Lindahl, E., GROMACS 4: algorithms for highly efficient, load-balanced, and scalable molecular simulation. *Journal of chemical theory and computation* **2008,** *4* (3), 435-447.

38. Cornell, W. D.; Cieplak, P.; Bayly, C. I.; Gould, I. R.; Merz, K. M.; Ferguson, D. M.; Spellmeyer, D. C.; Fox, T.; Caldwell, J. W.; Kollman, P. A., A second generation force field for the simulation of proteins, nucleic acids, and organic molecules. *Journal of the American Chemical Society* **1995,** *117* (19), 5179-5197.

39. Choudhury, C. K.; Roy, S., Structural and dynamical properties of polyethylenimine in explicit water at different protonation states: a molecular dynamics study. *Soft Matter* **2013,** *9* (7), 2269-2281.

40. Ziebarth, J. D.; Wang, Y., Understanding the protonation behavior of linear polyethylenimine in solutions through Monte Carlo simulations. *Biomacromolecules* **2009,** *11* (1), 29-38.

41. Aimei, Z.; Zhang, X.; Qinglin, L.; Zhang, Q., A fully flexible potential model for carbon dioxide. *Chinese Journal of Chemical Engineering* **2009,** *17* (2), 268-272.

42. Cygan, R. T.; Romanov, V. N.; Myshakin, E. M., Molecular simulation of carbon dioxide capture by montmorillonite using an accurate and flexible force field. *The Journal of Physical Chemistry C* **2012,** *116* (24), 13079-13091.

43. Babarao, R.; Dai, S.; Jiang, D.-e., Functionalizing porous aromatic frameworks with polar organic groups for high-capacity and selective CO2 separation: a molecular simulation study. *Langmuir* **2011,** *27* (7), 3451-3460.

44. Bussi, G.; Donadio, D.; Parrinello, M., Canonical sampling through velocity rescaling. *The Journal of chemical physics* **2007,** *126* (1), 014101.

45. Berendsen, H. J.; Postma, J. P. M.; van Gunsteren, W. F.; DiNola, A.; Haak, J., Molecular dynamics with coupling to an external bath. *The Journal of chemical physics* **1984,** *81* (8), 3684-3690.

46. Essmann, U.; Perera, L.; Berkowitz, M. L.; Darden, T.; Lee, H.; Pedersen, L. G., A smooth particle mesh Ewald method. *The Journal of chemical physics* **1995,** *103* (19), 8577-8593.

47. Martin, M. G.; Siepmann, J. I., Transferable potentials for phase equilibria. 1. United-atom description of n-alkanes. *The Journal of Physical Chemistry B* **1998,** *102* (14), 2569-2577.

48. Martin, M. G.; Siepmann, J. I., Novel configurational-bias Monte Carlo method for branched molecules. Transferable potentials for phase equilibria. 2. United-atom description of branched alkanes. *The Journal of Physical Chemistry B* **1999,** *103* (21), 4508-4517.

49. Widom, B., Some topics in the theory of fluids. *The Journal of Chemical Physics* **1963,** *39* (11), 2808-2812.

50. Martin, M. G.; Thompson, A. P., Industrial property prediction using Towhee and LAMMPS. *Fluid phase equilibria* **2004,** *217* (1), 105-110.

51. Martin, M. G., MCCCS Towhee: a tool for Monte Carlo molecular simulation. *Molecular Simulation* **2013,** *39* (14-15), 1212-1222.

52. Khader, M.; Al-Marri, M.; Ali, S.; Qi, G.; Giannelis, E., Adsorption of CO 2 on Polyethyleneimine 10k—Mesoporous silica Sorbent: XPS and TGA Studies. *American Journal of Analytical Chemistry* **2015,** *6* (04), 274.

53. Farmahini, A. H.; Shahtalebi, A.; Jobic, H.; Bhatia, S. K., Influence of structural heterogeneity on diffusion of CH4 and CO2 in silicon carbide-derived nanoporous carbon. *The Journal of Physical Chemistry C* **2014,** *118* (22), 11784-11798.

54. Meth, S.; Goeppert, A.; Prakash, G. S.; Olah, G. A., Silica nanoparticles as supports for regenerable CO2 sorbents. *Energy & Fuels* **2012,** *26* (5), 3082-3090.

55. Kanaya, T.; Tsukushi, I.; Kaji, K., Non-Gaussian parameter and heterogeneity of amorphous polymers. *Progress of Theoretical Physics Supplement* **1997,** *126*, 133-140.

56. Yamaguchi, T.; Kimura, Y., Non-Gaussian dynamics of a dilute hard-sphere gas. *The Journal of Chemical Physics* **2001,** *114* (7), 3029-3034.

57. Klähn, M.; Seduraman, A., What determines CO2 solubility in ionic liquids? A molecular simulation study. *The Journal of Physical Chemistry B* **2015,** *119* (31), 10066-10078.

58. Sharma, P.; Chakrabarty, S.; Roy, S.; Kumar, R., Molecular View of CO2 Capture by Polyethylenimine: Role of Structural and Dynamical Heterogeneity. *Langmuir* **2018,** *34* (17), 5138-5148.

CHAPTER – 8

Summary of the Thesis and Conclusions

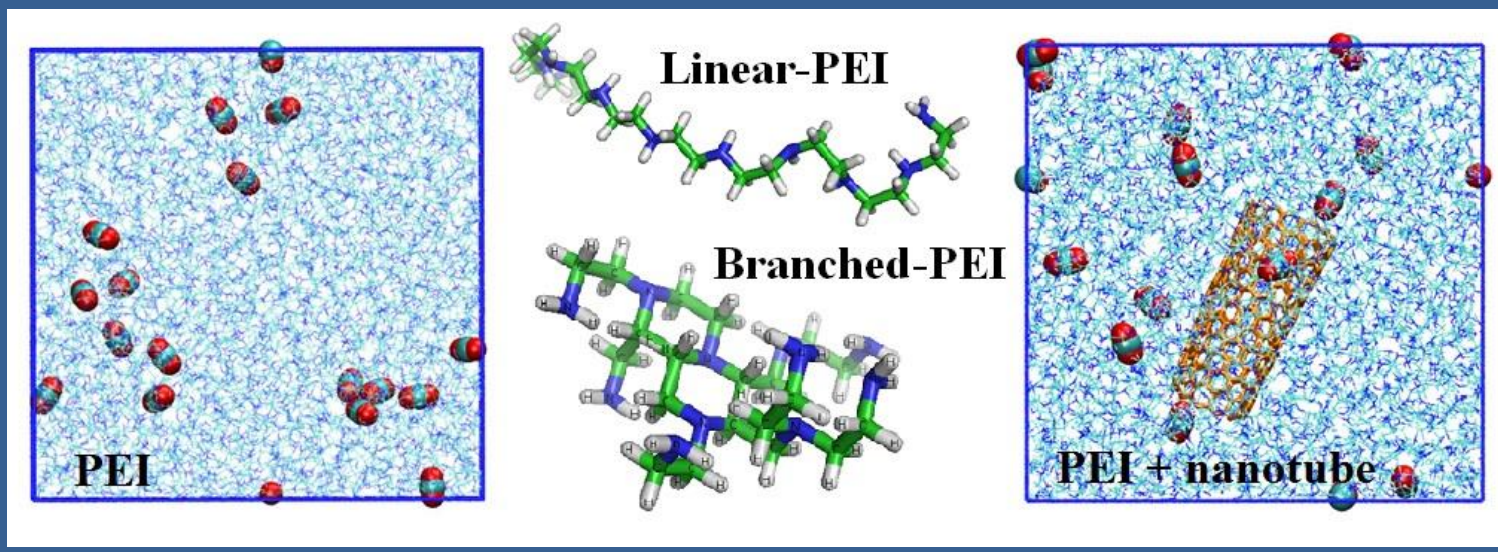

8.1 Summary of the thesis and conclusions

The current thesis explores the effect of composition and interactions on microscopic properties of polymers. Composition of the polymeric systems is modified by altering the chemical structure as well as by the incorporation of additives in a multi-component system. Change in composition modifies the inter-component interactions and subsequently alter the polymeric properties. The present thesis explores such effects on a wide range of properties, namely density, free volume, glass transition temperature (T_g), viscosity and gas adsorption properties along with local structural characteristics like end-to-end distance, radius of gyration (R_g), rigidity and mobility of polymeric chains. Detailed investigation of these properties using all-atomistic simulations provided useful insights about structure and dynamics of polymers and significant route to tailor bulk properties for specific applications.

Based on the polymer or property of interest, the thesis was divided into three parts. Part A presented all-atomistic simulations of Rubber and Rubber-plasticizer blends. The major property under investigation in this part was glass transition temperature. T_g of the rubbers under study was calculated from the change in slope of density-temperature plots and reproducibility of experimental T_g in almost all the cases established the effectiveness of atomistic simulations in predicting bulk macroscopic properties. Our simulations were also capable of capturing the change in T_g of polybutadiene blends with the addition of other polymer or plasticizer and in unraveling the molecular mechanisms responsible for T_g change. Plasticizer miscibility, free volume and chain rigidity emerged to be the major factors governing T_g change and corresponding plasticizer activity.

Emphasizing the fact that an accurate force field and proper equilibration are the major pre-requisites for a polymer simulation, validation of existing force fields of rubbers; polybutadiene and polyisoprene and plasticizers; polybutadiene and polystyrene was done by calculating and comparing T_g to experiments. Tuning of the force fields was also done in some cases to reproduce experimental T_g. A systematic procedure, based on potential energy convergence was proposed for equilibrating polymer systems. Equilibration protocol and force field validation procedure using T_g proved successful when the simulated models successfully reproduced thermodynamic properties like densities, thermal expansion coefficients and T_g. Temperature dependence of structural properties like end-to-end distance, R_g, structure factors and dynamic

properties like mean square diffusion and relaxation times were also well reproduced and showed satisfactory agreement with empirical equations. Similar claims hold true for the novel protocol proposed for T_g calculation from higher temperature correlations. We recommend that our equilibration protocol, T_g calculation protocol and properly validated force fields can be used for future simulations of rubber and its composites.

Part B dealt with the influence of substituting ionic groups on viscosity of star telechelic D, L-poly-lactide. Molecular mechanisms responsible for anomalous viscosity temperature dependence of PLA ionomer were analyzed. It is concluded that the substitution of ionic carboxylate groups to the chain ends increased the attractive interactions leading to the formation of telechelic ionic clusters. Inter-chain clustering in ionomers came out to be transient or dynamic and showed strong temperature dependence. At intermediate temperatures, formation of network, due to inter chain clustering leads to increased viscosity. While at higher temperatures, viscosity decreases owing to disruption of network due to thermal energy. Thus in this case also, atomistic molecular simulations were able to unravel the molecular mechanisms associated with macroscopic properties like viscosity.

The property investigated in part C was CO_2 capture characteristics of Polyethyleneimine (PEI). Spatial heterogeneity in the form of interfaces and cores along with local structural heterogeneities like pores, loops, aggregates etc. significantly affected CO_2 adsorption. Higher free volume areas like interface and pores showed higher adsorption of CO_2. Clustering of CO_2 is observed at various regions that lead to heterogeneous dynamics of CO_2 inside PEI. It is concluded that CO_2 adsorption in PEI is a complex interplay of selectivity and permeability and altering these properties by chemical functionalization of PEI or by introducing porous additives could be a successful strategy to increase adsorption. MD simulations can thus act as a screening technique for testing such functionalized PEIs. Thus this study will act as a benchmark for future simulation studies related to CO_2 capture using PEI or functionalized-PEIs. Knowledge of the molecular level interactions between PEI and CO_2 and associated structural and dynamic changes will further add to our understanding of the gas adsorption phenomenon. It will also open up new ideas to develop high capacity PEI-based adsorbents.

8.2 Scope of future work

The following recommendations are proposed for future work:

8.2.1 Analysis of structural and dynamic properties in High impact polystyrene, HIPS which is a blend of Polybutadiene in Polystyrene matrix, and their comparison to our studied blends (polystyrene minor phase in polybutadiene).

8.2.2 Testing of proposed method of T_g calculation from higher temperature correlations for other amorphous and semi-crystalline polymers and polymer blends.

8.2.3 Determining temperature dependence of parameters like fragility, using calculated relaxation time and T_g to measure the deviations from Arrhenius behavior for rubber and rubber blends.

8.2.4 Quantum chemical calculations to determine binding energy of functionalized PEIs with CO_2 to assess their adsorption capacity.

8.2.5 Functionalized Polyethyleneimine sorbents can be attractive candidates for CO_2 capture. Functionalization of polyethyleneimine with polar and apolar substituents can be done to enhance CO_2 sorption. Polar groups like hydroxyl, amino, carboxylates, sulphonates will further increase the interactions with CO_2. While apolar substituents like alkyl groups will aid in increasing free volume of the system.

8.2.6 In the same context, carbon nanotubes with different aspect ratio and functionalized nanoparticles with hydrophobic and hydrophilic parts can also be added in the PEI matrix for adsorption enhancement.

8.2.7 Comparison of CO_2 adsorption characteristics in linear and branched PEI and other nitrogen containing polymers.